Design Considerations for Installation of Steel Pipe using Horizontal Directional Drilling

by

Ashkan Faghih

A thesis submitted in partial fulfillment of the requirements for the degree of

Doctor of Philosophy

in

Civil (Cross-Disciplinary)

Department of Civil and Environmental Engineering
University of Alberta

Abstract

Horizontal directional drilling (HDD) technology is becoming a popular option for steel pipeline construction and replacement projects. During installation, the pipe is subject to a combination of loads and the long-term performance of a pipe installed by HDD is linked to the stresses that develop during installation. With increasing demand for steel pipeline installations using HDD, a more detailed investigation of the stress conditions that develop during installation is required to evaluate the reliability of current design guidelines. This dissertation aims to identify and address topics related to the analysis of the loads imposed on steel pipes during HDD installation. In North America, the load calculations recommended by the Pipeline Research Council International, PRCI (2015) are widely used for steel pipeline installation by HDD. Therefore, more attention is given to investigating the stress analysis method suggested in this widely accepted guideline.

Pull force estimation in HDD is essential during the planning phase. As part of current design practice, simplifications and assumptions need to be made to approximate the pull forces expected during HDD pullback. However, to date, a comprehensive assessment of the accuracy of pull force predictions has not been completed. A review of current design practice based on PRCI and industry accepted engineering assumptions for pull force calculations is presented in this work. Data from two hundred recent commercial HDD projects were collected and studied to compare actual and predicted pull forces in chapter three of this thesis. The accuracy of the pull force prediction for these crossings was investigated based on different project characteristics such as pipe size, crossing length, geotechnical conditions, and equipment size. This study indicates that the underlying assumptions for pull force estimations need to be selected based on project-specific characteristics to increase the accuracy of pull force predictions.

In some HDD applications, multiple product pipes can be bundled together and installed inside a single hole. In the absence of detailed analytical solutions for bundled pipe projects, a simple approach can be used based on current calculation methods, which involves approximating the bundled pipes by using a

single equivalent pipe to calculate the required pull force. Chapter four of this thesis reviews the concept of using a single equivalent pipe and applies it to the pull force calculation method recommended by PRCI. Five HDD case studies—including installations of bundles comprising two to six steel pipes of different sizes—were investigated to determine the accuracy of the proposed pull force estimation method. The simple method proposed in this work was found to result in pull force predictions that were close to actual loads measured during installation.

Chapters five and six of this thesis describe a strain monitoring program which was utilized for two major HDD installations over a kilometer long to analyze the axial and circumferential stresses and strains imposed on the product pipe during HDD installations. Strain measurements were presented in the form of pipe strains along the drill path during the time of the installation. The stress-strain relationships were developed for the pipe installation and installation stresses were calculated using the strain measurements. Then, the stresses calculated from the strain data were compared with the expected theoretical values determined based on current design practice. The strain monitoring and stress calculation discussed in this thesis provides some details on the expected behavior of steel pipes during HDD installations.

Finally, this thesis presents a new method to model the geometric path of the pipe inside the borehole based on Bézier curves, using drilling survey data collected while drilling the pilot hole. A large-diameter HDD project in dense soil where the actual geometry of the installed pipe was determined using an in-line inspection tool is presented as a case study. The analysis of bend radii indicates that for most locations along the bore path, the installed pipeline had a larger bend radius than the as-drilled hole. The application of the proposed geometric modeling is tested in the case study project. The smallest bending radii determined by the proposed geometric modeling method using Bézier curves was found to be closer to the actual pipe curvature as opposed to simply using the geometry of the pilot hole to determine the pipe bend radii.

Preface

This dissertation, which is presented in paper format, includes original work that I have conducted. I am the first author and responsible for the calculations, experiments, and writing of the manuscripts for each of the papers. The field data used in different chapters has been generously provided by CCI Inc. My supervisor, Dr. Bayat, has provided study objectives and technical feedback and has reviewed and monitored the research process. He is the corresponding author for all the manuscripts. Ms. Lana Gutwin of the Consortium for Engineered Trenchless Technologies (University of Alberta) provided editorial assistance to improve the quality of the papers. The individuals included as co-authors of the manuscripts listed below actively assisted me (the first author) in writing and revising the manuscripts.

Chapter 3 of this thesis has been approved by the *Journal of Pipeline Systems Engineering and Practice* as Faghih, A., and Bayat, A. "Accuracy of Pull Force Estimation in Horizontal Directional Drilling Pipe Installations – A Review of Two Hundred Case Studies".

Chapter 4 of this thesis has been submitted to the *Canadian Journal of Civil Engineering* as Faghih, A., and Bayat, A. "Pull Force Estimation for Installation of Bundled Steel Pipes using Horizontal Directional Drilling".

Chapter 5 of this thesis has been submitted to the *Journal of Tunnelling and Underground Space Technology* as Faghih, A., Bayat, A., and Goerz., B. "Stress Analysis of Steel Pipe Installation in Horizontal Directional Drilling based on Strain Monitoring".

Chapter 6 of this thesis has been published in the *International No-Dig 2019, 37th International Conference and Exhibition*, Florence, Italy as Faghih, A., Bayat, A., and Wilson, S. "Experimental Study on Pullback Loads for Steel Pipelines Installed by Horizontal Directional Drilling.".

Chapter 7 of this thesis has been published in the *NASTT No Dig North 2021 Conference*, Vancouver, Canada as Faghih, A., Collins, R. and Bayat, A. "As-Built Modeling of Pipes Installed by Horizontal Directional Drilling".

Chapter 8 of this thesis has been submitted to the *Journal of Pipeline Systems Engineering and Practice* as Faghih, A., Bayat, A., and Collins, R. “Evaluation of Product Pipe Bend Radius for Large-Diameter HDD Applications in a Case Study”.

Dedicated to

my Family,

who encouraged me to go on this adventure,

for their love, support, and patience.

Acknowledgements

I wish to express my sincere gratitude to my supervisor, Dr. Alireza Bayat, for his technical and financial support, guidance, and friendship during my PhD program at the University of Alberta. Without his supports, this journey would not have been possible.

I would like to express my gratitude to the members of my supervisory committee, Dr. Farook Hamzeh and Dr. Leila Hashemian, for their guidance and insightful comments to improve my dissertation.

I would also like to thank Ms. Lana Gutwin, M.Sc., our Research Coordinator, for assisting in the editorial review of this study.

I would like to express my deepest gratitude to my colleagues at CCI Inc., particularly, Mr. Ralph Collins for his expertise and technical supports as well as Mr. Brent Goerz, P.Eng., for his mentorship, engineering feedback, and financial support for this research.

I would like to acknowledge the Natural Sciences and Engineering Research Council of Canada for providing financial support for this research.

Finally, I would like to extend my deepest appreciation to my family, for their continuous support, encouragement, and unconditional love.

Table of Contents

List of Tables

List of Figures

1 Chapter 1: Introduction

1.1 Background

Traditionally, pipelines are installed by digging an open trench along the pipeline alignment and placing the pipe in line and grade. However, open-cut trenching is increasingly overshadowed by the improved efficiency and cost effectiveness associated with new trenchless technologies. These techniques are known as trenchless technology (TT) because their key feature is minimal excavation or digging. The rapid growth in demand for new pipeline installations requires faster and less expensive construction methods. Some of the advantages of TT are significant reductions in environmental impacts, ground disturbance, traffic delays, and public frustration, while at the same time realizing considerable savings due to the high costs associated with pavement, soil removal, and site restoration. TT methods have gained popularity based on their wide range of applications—including installation, replacement, rehabilitation, renovation, repair, inspection, and leak detection for underground utilities (Najafi, 2010). The availability of various equipment, methods, and materials has made TT a feasible option for pipeline construction (Allouche et al., 2000).

Among TT techniques, horizontal directional drilling (HDD) is one of the most rapidly growing technologies due to its environmentally friendly procedure and wide range of applications. HDD is a directionally controlled drilling method used to create boreholes to install utilities and pipelines under surface obstacles. For deep installations or crossings beneath rivers, lakes and highways, HDD is typically a more economical and viable alternative than any other trenchless method (Atalah et al., 2009).

HDD first originated in the oil industry during the 1970s to install utilities under obstacles such as rivers, lakes, roads, railways, and airport runways. With advances in steering and navigation tools and the integration of modern technologies from the oil industry, HDD received increasing attention from utility companies as a feasible and cost-effective alternative to open cut methods. In a relatively short period (15 years), HDD developed from a method offered by only a few contractors into a multibillion-dollar industry

(Allouche et al., 2003). In 1990's, the expansion of the HDD industry was mostly due to the rapid growth in telecommunications and high demands for installation of fiber optics. In more recent years, the major focus of the HDD market has become pipeline installation (Trenchless Technology, 2011). At the same time, HDD has developed from being a simple utility boring technology to what is now a sophisticated method capable of installing pipes over 127 cm (50 in) in diameter (Najafi, 2014). HDD can be employed for a wide range of applications: from the installation of oil and gas distribution networks, water mains, gravity sewers, telecommunications, and electrical conduits, to geotechnical investigation and environmental applications such as remediation of contaminated underground areas (Conroy et al., 2002; Gokhale et al., 1999; Kirby et al., 1996; Khan et al., 1994; Latorre et al., 2002; Lubrecht, 2012). HDD technology is also becoming a popular option in the oil and gas industry for construction and replacement of steel pipelines due to improved efficiency and reduced cost (Trenchlesspedia, 2021).

There are three essential stages to the HDD process as shown in Figure 1.1: drilling the pilot hole, reaming, and pipe pullback (Gokhale et al., 1999; Gelinas et al., 2000). The process begins with drilling a small diameter borehole, referred to as a pilot hole, along the planned drill path, which has straight and curved sections. A bottom hole assembly (BHA)—which includes a drill bit and a steering tool—is used to advance the pilot hole along the drill path. Once the drill bit emerges from the exit point and the pilot hole is complete, a reaming sequence is used to enlarge the borehole to a final size adequate for pipeline installation. Drilling fluid is used in each phase of the HDD construction, which assists with stabilizing the borehole and transporting the cuttings to the surface, among other functions. The final step is pullback, when the product pipe is pulled inside the borehole. The drilling rig is connected to the product pipe through a series of drill stem, reamer, and swivel, and pullhead. The rig then pulls the drill stem—joint by joint—to install the product pipe.

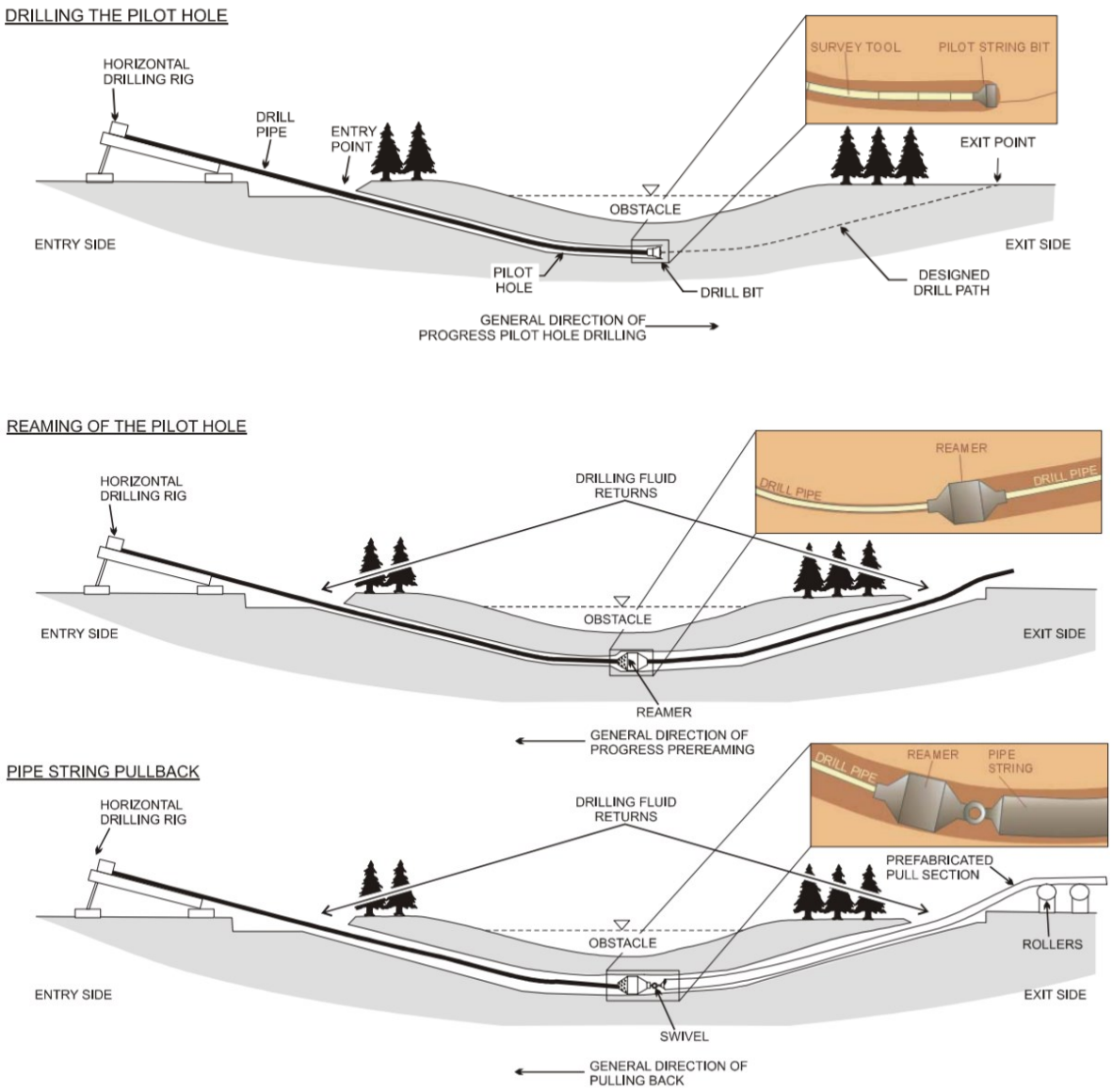

Figure 1.1. Schematic of a typical HDD operation (CAPP, 2004)

Pipes installed by HDD are subject to two types of loading: installation and operational loads (ASCE, 2014). Evaluation of magnitude of stress on the product pipe during installation is essential to the successful operation of the pipeline. Since the loads developed during installation are sometimes greater than long-term operational loads on the product pipe, the installation loads can in some cases govern the design requirements. For steel pipes, the installation loads include pull force (tension), bending and circumferential (hoop) stresses.

The load required to pull the product pipe must be high enough to overcome several resisting forces inside the borehole, including the net buoyant weight of the pipe, the friction between the borehole and the pipe sections, and the fluidic drag resulting from the drilling fluid surrounding the pipe within the annulus below ground, as well as the friction between the pipe and the support equipment above ground (Chehab & Moore, 2007). Since the pullback load must overcome these resistance forces, pull force estimation is key to choosing the appropriate drilling rig and evaluating pipe stress during pullback (Chehab, 2008). In addition to the axial tensile force, the pipeline is exposed to bending stress due to the curvature of the borehole and hoop stress resulting from external drilling fluid pressure and earth loads. Typically, the most critical stress condition for the pipe wall will be located in the areas where the greatest tensile, bending and external hoop stresses converge.

The bending stress component of the HDD installation is one of the most critical limiting factors when it comes to design of the crossing geometry. Curvature-induced bending stress is imposed on the pipe cross-section as the pipeline is pulled through the curved drill path. Excessive bending can overstress the product pipe and increase the risk of damage to the coating and the pipe. Since bending stress is directly related to the curvature of the bore path, the HDD borehole must be constructed such that pipe stress limits are met at all locations along the profile. Verification of the bend radius of the product pipe based on the as-built drill path is necessary for pipeline owners to approve as-drilled bore and allow the contractor to install the product pipe. To date, minimal research has been done to assess the curvature of large-diameter pipes installed by HDD.

There are currently design guidelines for pipe stress analysis—including Canadian Association of Petroleum Procedures (CAPP 2004-0022, 2004) and Pipeline Research Council International (PRCI, 2015) which are widely used and these are referenced as the applicable HDD guidelines by the Canadian Standard Association (CSA) for Oil and Gas Pipeline Systems (CSA Z662, 2019). However, within these guidelines, many of the design recommendations are solely based on constructability experience, without any detailed studies to support the recommendations. Moreover, many of the design inputs are undefined and depend on the judgement and experience of the engineers or contractors involved. During the pullback phase of HDD,

the product pipe is subjected to a complex combination of stresses that requires further investigation and a better understanding. However, as for the design inputs, relatively little research has been done towards the development of rational design guidelines for HDD and the current design methodology relies mostly on the experience and judgment of contractors, manufacturers and engineers (Polak and Lasheen, 2001). A limited number of studies and some experiments have been done to evaluate the stress condition of plastic pipe during HDD installation, based on actual case studies (Baumert et al., 2004; Polak et al., 2004; Petroff, 1997; PPI Handbook of Polyethylene Pipe, 2009). However, no similar detailed study or field measurements have been completed for evaluation of the stress condition for steel pipeline installation by HDD. With increasing demand for steel pipeline installations using HDD methodology, a more detailed investigation of the stress and strain condition of the pipe during installation is required to develop rational design guidelines. The development of new design procedures that can be more accurately applied to HDD projects is necessary to ensure safety, avoid damage to the product pipe, and keep up with the rapid growth in the HDD industry.

1.2 Research Objectives

Several existing gaps related to the design and engineering of steel pipe installations by HDD will be investigated in depth in this thesis. The overall objective of this research is to evaluate the installation stress conditions for HDD installed steel pipes using the current guideline developed by PRCI (2015) and improve the accuracy of the design assessments. To achieve this goal, this thesis sets the following objectives:

1- Identify the accuracy of current pull force prediction method (Chapter 3).

2- Evaluate the required pull force for bundled pipe installations (e.g., simultaneous installation of multiple pipes inside a single HDD bore) (Chapter 4).

3- Develop a strain monitoring program and calculate the actual stress conditions imposed on the pipe during installation (Chapter 5 and 6).

4- Develop and verify a predictive model to evaluate pipe bend radius inside the borehole which defines the magnitude of bending stress (Chapter 7 and 8).

1.3 Expected Contributions

The expected contributions of this research are as follows:

1- Assessment of the commonly used engineering assumptions in pull force estimation and evaluation of the prediction's accuracy based on the scope of the HDD crossings.

2- Identification of the appropriate safety factors for pull force calculation during design phases of the HDD projects.

3- Expand applicability of PRCI pull force prediction method to bundle pipe installations based on the concept of an equivalent single pipe.

4- Assess the expected strain and stress behavior of steel pipes during HDD installations and evaluate different installation loads imposed on the pipe using strain gauges during different stages of the pullback operation.

5- Development and incorporation of a geometric modeling technique to predict pipe position within the reamed borehole which can be used for as-built stress analysis and identifying any sections within the drilled path that may require steering corrections or re-drill.

1.4 Methodology

This research was conducted based on the methodologies outlined in the following sections.

1.4.1 Accuracy of Pull Force Analysis

To compare pull force estimates with the actual maximum loads supplied by the drilling rig during pullback, a database are created comprising 200 commercial HDD projects completed throughout Canada between 2012 and 2021. These projects involved installation of single steel pipes ranging in diameter from 60 mm (NPS 2) to 1067 mm (NPS 42) with crossing lengths from 60 m to 2,000 m. The HDD rigs utilized for these projects had thrust/pull capacities ranging from 16 tonnes to 500 tonnes. The maximum recorded pull loads at the rig (observed pull forces) are compared with the predicted maximum pull forces (predicted pull force) for each project. For better comparison between predicted and observed pull force, the HDD crossings are

categorized based on various factors, thus group projects with similar execution methodologies. These include pipe size (considering the application of buoyancy control), HDD crossing length, HDD equipment size (mini, midi, and maxi) and ground formation (e.g., soft soil vs. hard soil and rock). Within each project category, the pull forces are assessed using mean prediction error (ME) as a measure of bias and root mean squared error (RMSE) as a measure of the precision of the predictions. The data are summarized and the prediction error distribution for different project categories are analyzed.

1.4.2 Pull Force Estimation for Bundled Steel Pipes

The concept of using parameters associated with a single equivalent pipe to represent the pipe bundle is examined. The parameters based on the single equivalent pipe concept are combined with the PRCI method to predict pull forces for bundled installations. Data from five medium to large scope bundled HDD crossings—including installations of bundles comprising two to six steel pipes of different sizes—were studied to check the accuracy of the proposed method. The results of the proposed method are compared with actual loads.

1.4.3 Strain Monitoring Program and Stress Calculation

A more detailed investigation of the HDD installation is done by evaluating axial and circumferential stresses, as well as the strain imposed on the pipe section, considering that the pipe is forced to conform to the borehole geometry. To assess the strains during installation of the product pipe, strain gauges are placed inside steel pipes to record longitudinal and circumferential strains throughout the pipe installation process for large-scale HDD installations. Strain measurements are presented in the form of pipe strains along the drill path over installation time. Stress-strain relationships for pipe installation are developed and installation stresses are calculated based on the strain measurements. Then, the stresses calculated from strain data are compared with expected theoretical values based on current design practice as developed by PRCI (PRCI, 2015).

1.4.4 Pipe Curvature Analysis

Since the bending stress imposed on the product pipe depends on as-built drill path and pipe curvature inside the borehole, the bending radius is calculated based on geometric modeling of the product pipe within the borehole. A Bézier curve algorithm is used to model the pipe geometry and curvature inside the borehole. 3D geometry modeling software (Civil 3D) is also used to illustrate possible pipe deformation scenarios within the borehole and compare the results with the proposed method.

To gain an understanding of the actual pipe deformation within the borehole, in-line inspection (ILI) data is acquired using smart pig in a case study of an HDD installation. This data is used to investigate the geometry of the installed pipeline and compare it with the as-built profile of the pilot hole. Application of the proposed geometric modeling method is tested using the data for the case study.

1.5 Outline

This dissertation is composed of five articles which were integrated in a paper-based format. The content of each chapter is summarized as follows:

Chapter 1: In this chapter, some background on HDD was presented and the importance of better understanding the installation loads imposed on steel pipes during pullback was highlighted. The thesis objectives, methodology and outline are included.

Chapter 2: In this chapter, a review of current design models to calculate installation loads in HDD is presented. Individual and combined stresses on product pipes during pullback are discussed. The allowable limits defined by pipeline codes are included for both individual and combined stress conditions.

Chapter 3: A review of the current design practice and industry-accepted engineering assumptions for pull force calculations for steel pipes is presented in this chapter. A comprehensive assessment of pull force prediction accuracy has been completed by using the data for 200 recent commercial HDD projects to compare actual and predicted pull forces. The accuracy of the predicted pull forces is investigated by categorizing the HDD crossings based on pipe size, crossing length, geotechnical conditions, and rig size.

Chapter 4: In this chapter, pull force estimation for bundled pipe installation is discussed. In the absence of detailed analytical solutions for bundled pipe projects, the concept of using the parameters associated with a single equivalent pipe to represent the pipe bundle is examined. The single equivalent pipe concept is combined with the PRCI method to predict pull forces for bundled installations. Data from several bundled HDD installations in Alberta, Canada were studied to check the accuracy of the proposed method. The equivalent pipe method suggested by NEN 3650 is also used to compare pull force prediction models for the case studies.

Chapter 5: This chapter focuses on evaluation of the stresses on the product pipe during installation by HDD, through development and calibration of a strain gauge monitoring tool. The strain gauges were utilized in two major HDD crossings of steel pipe (762 mm O.D.) over a kilometer long. The stresses calculated based on strain data were compared with expected theoretical values determined based on current design practice.

Chapter 6: This chapter focuses on evaluation of the axial force transferred to product pipe during installation by HDD, using the strain monitoring program explained in Chapter 5. The axial force is calculated and compared with the recorded rig force. The impact of applying buoyancy control to reduce pull forces during pipe installation is discussed. Theoretical calculations completed with and without internal water are presented and the results compared with actual force imposed on the product pipe.

Chapter 7: A review of radius of curvature and bending stress calculations for the product pipe based on downhole survey measurements is presented in this chapter. The shortcomings of current industry practice related to the as-built pipe stress check practice are discussed. Geometric modeling of the pipe inside the borehole based on Bézier curves is explained and applied to a case study. To better compare potential pipe curvatures, 3D modeling using Civil 3D software was done to evaluate the best pipe-curve fitting scenario. The bend radii determined using the Bézier method can be used as a theoretical representation of the realized bending radii imposed on the pipe along the bore path.

Chapter 8: A large-diameter HDD project was used as a case study for determination of the geometry of the installed pipe using an ILI tool and comparison with the as-drilled pilot hole geometry. The bend radius

analysis was completed to compare the curvature of the as-drilled pilot hole with the curvature of the installed pipe inside the borehole. In addition, using the concept of geometric modeling, the Bézier method was utilized to calculate the bend radii of the pipe based on as-drilled survey data. The proposed method was tested based on the case study and verified against the actual geometry of the installed pipe.

Chapter 9: In this chapter, the research approaches are summarized, and the results and findings of this thesis are highlighted. Future research areas are also proposed to further develop the potential of this research in the trenchless industry.

2. Chapter 2: Literature Review

Pipes installed using horizontal directional drilling (HDD) are exposed to high tensile forces, bending, and external pressures during installation compared to conventional cut and cover pipeline installation. For longer and deeper crossings, loads on the pipe during installation may be larger than the service loads during the long-term operation of the pipeline. Designers need to select pipe properties and operational conditions to ensure that the selected pipe has the strength to withstand installation loads as well as operational loads. The parameters to be considered for stress assessment calculations should include the pipe diameter, wall thickness, grade, depth, and geometric design of the crossing.

The load conditions imposed on the pipe during installation primarily include an axial tensile pulling force, external hoop pressure, and bending as the pipe is pulled through the borehole. Assessment of each of these individual components of the load and their combinational interaction is required for pipe stress analysis and potential for failure (Fowler, 1991; Loh, 1990). As part of the stress analysis, an estimate of the pull force is required to calculate the tension from these loads.

2.1 Tension from Pull Force

The mechanics of pipe installation in HDD involves multiple factors, due to the interactions between the product pipe and the surrounding environment, which includes the ground surface, drilling fluid, soil, and bedrock within the borehole. The pullback operation begins with the entire length of the pipeline supported above ground by rollers and lifting equipment. During the initial stages of the pullback process, there is frictional resistance due to the movement of the pipe against the surface of the rollers and lifting devices. Depending on the above-ground topography and the borehole profile, the weight of the pipe can contribute to the resisting force or act in the same direction as the pullback.

The main resistance to the movement of the pipe inside the borehole during installation is due to friction, which is directly proportional to the friction factor and normal force due to the pipe-soil interaction. Pipe weight is an important factor in the calculation of the normal forces and the resulting friction forces. Since

during installation the pipe is being pulled into a borehole that is filled with drilling fluid, an upward buoyant force is present on the pipe due to the weight of the drilling fluid displaced by the pipe. The effective weight or submerged weight of the pipe is equal to the pipe weight minus the upward buoyant force. In addition to the pipe weight, the magnitude of the contact force at the soil-pipe interface (along the curved sections of the borehole) depends on the bending stiffness of the pipe, the radial displacement of the soil at pipe-soil contact points, and the stiffness of the soil (Kruse and Hergarden 2010). The load used to pull the product line inside the borehole must also overcome the fluidic drag resulting from the drilling fluid surrounding the product pipe (Faghih et al, 2015). Some designers apply an additional frictional component due to moving the drill rods and the BHA following the pull section to estimate the total required pull force.

The resulting tension is assumed to act at the centroid of the pipe cross-section, resulting in a uniform axial tensile stress on the cross-section of the pipe. The tensile stress is calculated by dividing the tension by the pipe cross sectional area. The maximum allowable tensile stress during installation should be limited to 90% of the specified minimum yield strength (SMYS) of the pipe (PRCI, 2015).

Various numerical methods have been proposed to estimate the pull force (Driscopipe, 1993; Drillpath, 1996; Huey et al., 1996; ASTM F1962, 1999; Polak et al., 2002; Baumert, 2002; Cheng and Polak 2007; Rabiei, 2016; Cai and Polak 2019; NEN 3650 2020). A similar approach to estimate the pull force was followed in most literature methods: this involves dividing the bore path into a series of straight and curved sections and calculating the resistive forces based on equations provided for each method. The major differences between these models were the assumptions related to fluidic drag and friction calculation within the curved sections. In the end, the total pull force is calculated by adding the loads within each segment.

In North America, the pull force method proposed by Huey et al. (1996) and adapted by PRCI is widely used for steel pipe installation using HDD. The designed drill path is divided into a series of straight and curved sections within a vertical 2D plane, and the maximum pull force occurs at the end of pullback as the pipe exits the ground (Figure 2.1).

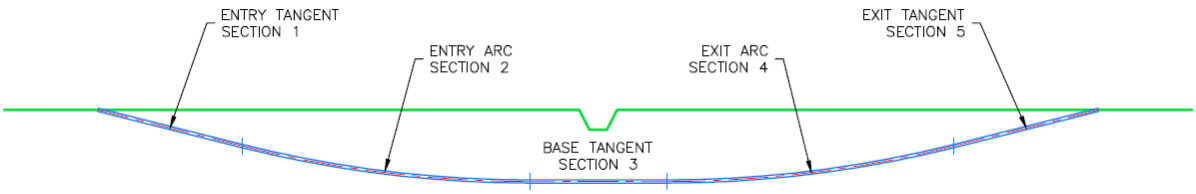

Figure 2.1. Typical PRCI Section Diagram

The process of pull force calculation requires that the drill path be divided into a minimum of five sections, separating the straight and curved sections of the bore path. The first section (section one) is located at the entry where the drill rig is set up, and the last section (section five) is at the exit where the product pipe is. For straight sections, the tension results from the frictional force between the pipe and the borehole, the effective buoyant weight of pipe, and the fluidic drag from the drilling fluid surrounding the pipe. For curved sections, a more complicated approach is used to account for the radial forces resulting from bending. The PRCI method involves modeling the pipe within the curved sections as a beam with three points of contact with the borehole and calculating the normal force acting on the pipe based on the known geometry of the curved segment (Figure 2.2).

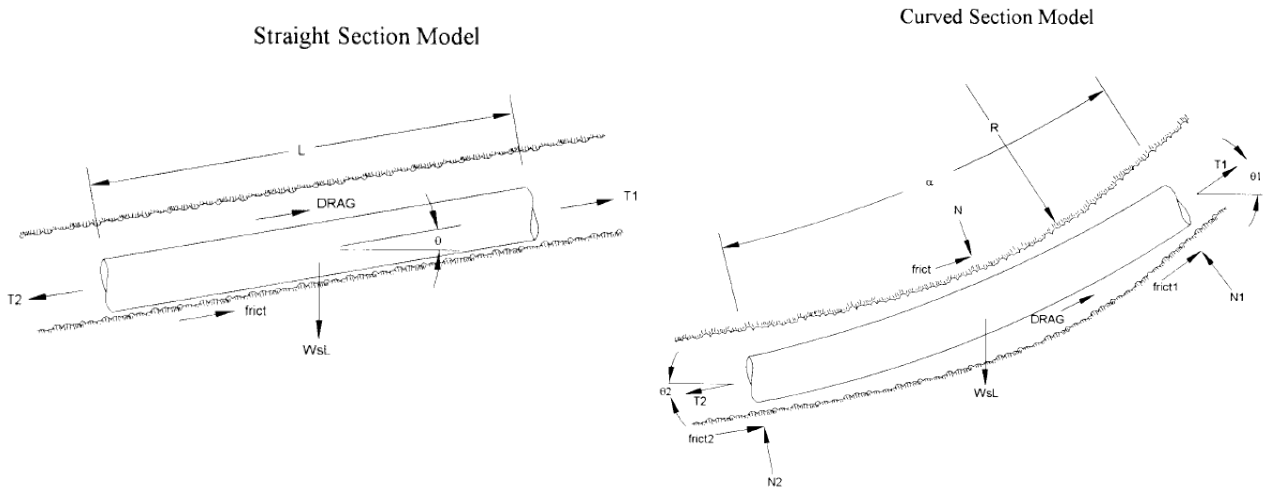

Figure 2.2. Straight and Curved Section Models (Huey et al., 1996)

The incremental tension for each section is calculated as follows (Equation 2-1):

$$T_2 = T_1 + F_f + 12\pi DL\mu_{mud} \pm WL\sin\theta \qquad (2\text{-}1)$$

where T_1 and T_2 are the tensions at each end of the section (lb); F_f is the frictional force between pipe and borehole wall (lb); W is the weight of the pipe segment (lb); L is segment length (ft), μ_{mud} is the coefficient of friction for the mud (i.e., drilling fluid); D is the pipe diameter (in); and θ is the angle of the segment with the horizontal.

For straight sections, the friction is simply determined as in Equation 2-2:

$$F_f = WL\cos\theta \times \mu_{soil} \quad (2\text{-}2)$$

where μ_{soil} is the average coefficient of friction between the pipe and soil.

The friction calculation for curved sections requires an iterative solution by first assuming an average tension to calculate the normal force (N) and associated reactions ($N/2$) and then calculating the tension on the leading end of the section (see Figure 2.2). For bends in the horizontal plane, a similar calculation is used without considering the weight component of the segment. The following equations (Equations 2-3 through 2-9) are for friction force calculations for curved sections:

$$F_f = N \times \mu_{soil} \quad (2\text{-}3)$$

$$N = (Th - W\cos\theta\,(\mathrm{Y}/144))/(\mathrm{X}/12) \quad (2\text{-}4)$$

$$h = R(1 - \cos(\alpha/2)) \quad (2\text{-}5)$$

$$Y = 18L^2 - j^2(1 - 1/\cosh(U/2)) \quad (2\text{-}6)$$

$$U = 12L/j \quad (2\text{-}7)$$

$$j = (EI/T)^{1/2} \quad (2\text{-}8)$$

$$X = 3L - (j/2)\tanh(U/2) \quad (2\text{-}9)$$

where T is the average tension over the segment, $T = (T_1+T_2)/2$ (lb); N is the normal force (lb); E is Young's modulus; I is the bending moment inertia (in^4); h is the center displacement of the segment (ft); R is the radius of curvature for the segment (ft); α is the deflection angle of the segment; and θ is the average angle of the segment with horizontal, $(\theta_1+\theta_2)/2$, in degrees.

2.1.1 Pullback Parameters

The installation force during pullback depends on many factors, such as the pipe properties, drilling fluid properties, buoyancy control, number of pipe segments to be welded during pullback, execution plan, pipe handling above ground, etc. Among these parameters, some (such as the friction coefficients) may vary significantly along the borehole path, due to differences in geological conditions and mud properties at different locations. Therefore, considering the numerous variables and uncertainties involved, the accurate prediction of pull force is difficult,. In practice, assumptions are required to simplify calculations. The following is a summary of the main parameters used in pullback force predictions:

2.1.1.1 Borehole Friction Coefficient

The friction coefficient between the pipe and borehole is an important parameter that significantly affects calculations of pullback force. Many studies have been completed to determine the value of the friction coefficient for oil and gas applications (Maidla and Wojtanowicz 1990, Johancsik et al. 1984). Although most of these studies focused on the friction between the casing and drilling rod in oil and gas drilling, recent works by El Chazli et al. (2005) and Hassan et al. (2014) have attempted to address HDD-specific applications, taking into account different pipe materials and soil types, presence of a drilling fluid filter cake, and magnitude of the applied normal force. In addition, the age of the drilling fluid (measured from when the bentonite is first mixed with water) was discussed by El Chazli—the results showed a reduction in friction coefficient as the age of the drilling fluid increased. In general, a value within the range of 0.20 and 0.45 is recommended for the borehole friction coefficient.

2.1.1.2 Above-Ground Friction Coefficient

The friction coefficient between the pipe and ground surface depends on the roughness of the pipe coating, the ground roughness, and the type of roller and lifting device used to support the pipe during installation. This friction coefficient (referred to in this work as the above-ground friction coefficient) can range from 0.1-0.8 (Chehab 2008). The Netherlands Standardization Organization (NEN 3650 2020) recommends a value of 0.3 and 0.1 for the case when the pipe is placed on the ground or supported by rollers, respectively. ASTM F1962 (2020), which is a standard for polyethylene pipe or conduit installation using HDD, included

values of 0.5 and 0.1 for similar cases. In recent years, rollers have been commonly used for handling pipes during HDD installations, therefore, a value of 0.1 is generally used for the above-ground friction coefficient.

2.1.1.3 Fluidic Drag Coefficient

Fluidic drag is the resistance of the pipe to movement due to the flow of drilling fluid in the borehole. It results from the viscous shear stress on the outer surface of the pipe, which is created by the interaction between the viscous fluid and the pipe. In the PRCI guideline (2015), fluidic drag is treated as the friction force between the drilling fluid and the pipe, and is estimated by the coefficient of friction between the drilling fluid and the pipe, multiplied by the external area of the pipe. The fluidic drag coefficient can be determined using a typical value for the viscous shear stress on a steel pipe pulled through a bentonite fluid. A value of 345 Pa (0.05 psi) was originally recommended in NEN 3650. Further comparisons between the predicted pullback loads and actual field data based on two case studies conducted by Puckett (2003) suggested a lower drag coefficient of 172 Pa (0.025 psi), which is also currently adopted in the PRCI guideline. However, adopting a constant value for fluidic drag coefficient in all projects may cause errors in calculations, since the fluidic drag coefficient is a function of drilling fluid rheology, annular geometry (pipe and bore diameter), flow rate, and rate of installation.

2.1.1.4 Drilling Fluid Density

The drilling fluid density is another important parameter that significantly affects estimates of pullback force, since the net buoyant weight of the pipe depends on the weight of drilling fluid. The density of the drilling fluid, which varies with the mud properties and the amount of cuttings suspended within the fluid, can range from 1060 to 1320 kg/m^3 (NASTT, 2017). Higher values are sometimes recommended to account for heavier drilling fluids carrying soil cuttings. For instance, mud densities up to 1440 kg/m^3 are recommended in PRCI, while ASTM F1962 suggested a value of 1500 kg/m^3 for drilling fluid density to give a conservative analysis.

2.1.2 Verification of Pull force Calculation

Serval studies have been completed to verify theoretical models against measurements of actual drilling rig forces (Baumert and Allouche 2002; Baumert et al. 2004; Duyvestyn 2009). In these studies, a limited number of case studies were used to show that there may be a significant variation between the trend in the pull force and the location of maximum force during pullback compared to theoretical estimations. In a more comprehensive study by Baumert et al. (2004), monitoring cells were utilized for measuring actual pull loads during 19 commercial small size crossings. The study pointed out that most theoretical models assume an ideal open borehole whereas actual site conditions play an important role in the required pull force. The authors observed that the presence of hole obstructions, as well as changes of curvature within the drill path, influenced the amount of pull force. While the PRCI method attempts to account for less-than-ideal borehole conditions by adding a mud drag component, this method does not provide a range for viscous drag based on different site conditions. Another study by Puckett (2003) showed that reducing the fluidic drag coefficient by half (to 175 Pa from the original proposed value of 350 Pa by PRCI) gave estimated forces that matched well with measured values. This suggestion was later accepted by PRCI and is referenced in the guideline.

2.2 Bending

As the pipe is pulled through the curved sections of the drill path, the curvature imposes an axial bending strain on the pipe cross-section. The curvature-induced bending results in an axial compressive strain on top of the pipe section and an axial tensile strain on the bottom. The bending stress during HDD installation is calculated and should be within the allowable limits established for tubular members in offshore structures as recommended by the American Petroleum Institute (API) due to the similarity in the loading conditions (API RP 2A-WSD). The bending stress can be calculated as in Equation 2-10 (Timoshenko and Gere, 1972):

$$f_b = (ED)/(2R) \quad (2\text{-}10)$$

where f_b is the longitudinal stress resulting from bending; E is the modulus of elasticity; D is the outer diameter of the pipe, and R is the radius of curvature of the borehole.

The allowable bending stress, F_b, is determined as recommended by API (API RP 2A-WSD) as in Equation 2-11 through 2-13:

$$F_b = 0.75\,F_y \quad \text{for} \quad D/t \leq 1500/F_y \tag{2-11}$$

$$F_b = [0.84 - 1.74(F_y D/(Et)]F_y \quad \text{for} \quad 1500/F_y \leq D/t \leq 3000/F_y \tag{2-12}$$

$$F_b = [0.72 - 0.58(F_y D/(Et)]F_y \quad \text{for} \quad 3000/F_y \leq D/t \leq 300 \tag{2-13}$$

where F_y is the SMYS of the pipe (lb/in^2), and t is the wall thickness of the pipe (in).

For any directional drill using magnetic or gyro steering tools, three components are measured at any given point in the drill path to determine the drill bit position. The measured depth (distance from the rig along the drill path), inclination or pitch, and azimuth are measured, and these values are used to calculate the position at intervals while drilling. The technique for the measurement of these three components is termed a survey, and a single measurement during the survey is termed a survey shot. At a minimum, a survey shot is taken when drilling has progressed a full drill pipe joint, before adding the next joint. The inclination (I) describes the pipe tilt with respect to the horizontal plane, and the azimuth (A) specifies the angle between the pipe direction and the local magnetic field of the earth. The as-drilled HDD profile proceeds along a three-dimensional path, with incremental directional drilling occurring in both the vertical and horizontal planes, due to the continuous steering required to conform to the designed drill path. The horizontal component of the bend radius (R_H) is a function of changes in azimuth, while the vertical component of the radius of curvature (R_V) depends on changes in inclination over the measured distance.

The following equations (Equation 2-14 to 2-16) based on angular measurements are used to calculate the total combined radius of curvature:

$$R_H = \frac{L}{(\Delta A)}\frac{360}{2\pi} \tag{2-14}$$

$$R_V = \frac{L}{(\Delta I)}\frac{360}{2\pi} \tag{2-15}$$

$$R_C = \sqrt{\frac{R_V^2 \times R_H^2}{R_V^2 + R_H^2}} \quad (2\text{-}16)$$

where L is the distance measured along the bore path; ΔA is the change in the azimuth angle over the distance between the two survey points; ΔI is the change in the inclination angle over the distance between the two survey points; and R_C is the total combined radius of curvature. All angle measurements are in degrees.

The as-drilled bend radii are calculated based on drilling survey information using Equation 2-14, 2-15, and 2-16 and compared with the minimum allowable bend radius. The goal is that the realized bending radii imposed on the pipe should be equal to or greater than the minimum allowable bending radius throughout the entire bore path. In the directional drilling industry, it is common practice to take the average over 30 m (100 ft) to determine the radius of curvature of the drill path at any location (API, 1985).

2.3 Circumferential (Hoop) Stress

A net external pressure is imposed on the pipe during the installation process. This external pressure is a function of the hydrostatic pressure due to the weight of the drilling fluid surrounding the pipe, the hydrokinetic pressure due to the flow of the drilling fluid, the hydrokinetic pressure resulting from the surge or plunger action produced by moving the pipe into the borehole, and the earth pressure or bearing pressure of the pipe against the borehole wall (PRCI, 2015). In cases where water is present in the pipe for buoyancy control (typically for larger pipes to reduce the amount of pull force), the net external pressure is calculated from the combined effects of the external pressure and the internal water pressure. The hoop stress due to hydrostatic pressure (f_h) can be calculated as:

$$f_h = (\Delta p \times D)/(2t) \quad (2\text{-}17)$$

where Δp is the difference (at a given depth) in hydrostatic pressure due to drilling fluid exerted on the outside of the pipe and the pressure due to water acting on the inside of the pipe (in case of internal buoyancy water).

At any point within the borehole, the hydrostatic pressure is a function of the height and density of the drilling fluid. For HDD applications, the density of the drilling fluid depends on the mud properties and amount of cuttings suspended within the slurry (as discussed in Section 2.3.1.4).

For HDD installed pipelines, the earth pressure is generally treated as a tunnel load, including a reduction factor (arching factor, k) on the geostatic soil pressure. ASTM F1962 recommends using arching when dynamic live loads are insignificant, the soil has sufficient internal friction, and the depth of cover exceed five pipe diameters, which is the case for most HDD installations. ASTM F1962 recommends using Terzaghi's equation with a reduced friction angle (50% lower) as referenced by Stein et al. (1989). The arching factor is calculated using an earth pressure coefficient, which in turn is calculated using the silo width (reamed borehole diameter) angle of wall friction, and the internal friction angle soil. The following equations are used for external earth pressure calculation (Equation 2-18 to 2-20):

$$K = tan^2(45 - \varphi_{soil}/2) \tag{2-18}$$

$$\kappa = \frac{1 - e^{-2\frac{KH}{B}\times\tan(\delta_{soil}/2)}}{(2KH/B)\tan(\delta_{soil}/2)} \tag{2-19}$$

$$p_e = \kappa * \gamma * H \tag{2-20}$$

where K is the earth pressure coefficient; κ is the arching factor; H is the depth of cover; B is the silo width or reamed borehole diameter; φ_{soil} is the internal friction angle of the soil; δ_{soil} is the angle of wall friction in degrees (which is assumed to be equal to φ_{soil}) ; γ is the soil weight; and p_e is the external earth pressure. Hydrokinetic pressure arises from the pressure required for the flow of the drilling fluid and can be calculated using annular pressure loss formulas. Mud properties, fluid rheology, flow rates, and annular space configurations are required for the analysis (Baroid, 1998). Due to low fluid velocity and pump rate during pipe installation, the contribution of hydrokinetic pressure to total hoop stress is very low.

The criteria established for tubular members in offshore structures (API RP 2A-WSD) are recommended by PRCI for use as allowable limits for hoop stress for HDD installations. Due to pipe ovality during installation as well pipe bending and dynamic loading, a conservative factor of safety should be applied

when designing the pipe wall thickness. The hoop stress should be less than the critical hoop bucking stress which is calculated for different cases as follows (API, 2014) in Equation 2-21 to 2-25:

$F_{he} = 0.88E(t/D)^2$ for long unstiffened cylinders (2-21)

$F_{hc} = F_{he}$ for $F_{he} \leq 0.55F_y$ (2-22)

$F_{hc} = 0.45F_y + 0.18F_{he}$ for $0.55F_y \leq F_{he} \leq 1.6F_y$ (2-23)

$F_{hc} = 1.31F_y/(1.15 + F_y/F_{he})$ for $1.6F_y \leq F_{he} \leq 6.2F_y$ (2-24)

$F_{hc} = F_y$ for $F_{he} > 6.2F_y$ (2-25)

where F_{he} is elastic hoop buckling stress (lb/in^2) and F_{hc} is the critical hoop buckling stress (lb/in^2).

2.4 Combined Stress

After all single load scenarios are checked, and it is confirmed that the loading on the pipe wall does not cause overstress or buckling, the combination of loading conditions is checked. The pipe is expected to be under the most stress in cases where tensile, bending, and external hoop forces occur at the same time. Typically, the highest combined stresses will occur in zones where there is high bending due to tight radii, high tension, and high hydrostatic drilling fluid pressure (e.g., at the deepest point of the borehole).

The combined stress analysis calculations based on PRCI recommendations are first completed incorporating only the tensile and bending stress values, which is consistent with the established design practice for the tubular members of offshore structures (API RP 2A-WSD) with modifications to allowable tensile proportion. This is a unity check which limits the sum of the ratio of tensile and bending stress divided by their allowable values to one, as shown in Equation 2-26:

$f_t/0.9F_y + f_b/F_b \leq 1$ 2-(26)

where f_t and f_b are the tensile and bending stress, respectively; F_y is the pipe SMYS; and F_b is the allowable bending stress.

When the pipe is under longitudinal tension (due to tensile and bending stress) as well as compressive pressure due to hoop stress, a full interaction load unity check must be satisfied, which involves combining

the stress ratios representing the allowable total longitudinal tensile stress and the allowable hoop compressive stress based on Von Mises equivalent stress combination as in Equation 2-27 to 2-29:

$$A^2 + B^2 + 2\upsilon|A|B \leq 1 \quad (2\text{-}27)$$

$$A = ((f_t + f_b - 0.5f_h)1.25)/F_y \quad (2\text{-}28)$$

$$B = (1.5f_h)/F_{hc} \quad (2\text{-}29)$$

where υ is Poisson's ratio for steel pipe and 1.25 and 1.5 are the safety factors for axial tension and hoop compression, respectively (according to API RP 2A-WSD).

3. Chapter 3: Accuracy of Pull Force Estimation for Steel Pipe Installations using Horizontal Directional Drilling– A Review of Two Hundred Case Studies[1]

3.1 Introduction

Horizontal directional drilling (HDD) is among the most practical trenchless methods to install pipelines, with minimal ground disruption compared to open-cut construction. There are three essential stages in the HDD process: pilot hole, reaming, and pipe pullback. A schematic of the pullback process is shown in Figure 3.1. The pull force supplied by the HDD rig during pipe pullback must overcome the resistive forces against the product pipe motion. During the planning phase, estimation of the maximum expected pull force is a key factor in pipe stress analysis and selection of a drilling rig with adequate pull capacity (Chehab, 2008). The loads that develop during the installation are sometimes greater than the long-term operational loads on the pipeline, and thus can govern the design requirements. The product pipe should be designed to have the capacity to avoid damage during installation, while the HDD rig used for the installation should be capable of successfully pulling the pipe into the borehole (Baumert and Allouche, 2002).

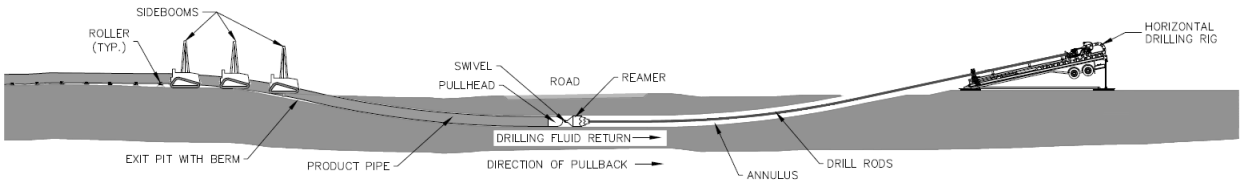

Figure 3.1. HDD pullback process

Many studies have been completed to provide different pull force calculation models (Huey et al. 1996; ASTM F1962 2020; Baumert and Allouche 2002; Cai and Polak 2019; NEN 3650 2020). However, these

[1] A version of this chapter is under final revision for acceptance to ASCE Journal of Pipeline Systems Engineering and Practice.

analytical calculations only have been evaluated using a limited number of case studies. Moreover, there are many factors that affect the pullback force which are heavily dependent on execution of the HDD crossing. In addition, pull force calculations can be relatively complicated when considering variations during the HDD construction process compared to design phase. These variations include but are not limited to the as-drilled bore geometry, subsurface geotechnical conditions, drilling fluid properties, pipe buoyancy, amount of cuttings inside the bore, and borehole condition. Simplifications and assumptions need to be made during design to approximate the pull forces expected during pullback operations.

To date, a comprehensive assessment of pull force prediction accuracy based on actual case studies has not been completed. This paper includes a review of 200 engineered HDD projects. The pull force calculation method based on the current state of practice as outlined by the Pipeline Research Council International (PRCI 2015) and North American Society for Trenchless Technology (NASTT 2017) was used for pull force estimation in these case studies. The accuracy of pull force calculations was investigated for the 200 crossings by comparing the maximum predicted pull force with the maximum rig pull load measured during pullback.

3.2 Components of Pull Force

The mechanics of pipe installation during pullback involve multiple factors, due to the interaction between the product pipe and the surrounding environment—including the ground surface, drilling fluid, soil, and bedrock within the borehole. The pullback operation begins with the entire length of the pipeline supported by ground rollers and rollie cradles attached to lifting devices. During the initial stages of the pullback process, there is frictional resistance due to the movement of the pipe against the surface of the rollers and rollie cradles.

The main resistance to pipe installation inside the borehole is friction, which is a function of the pipe-borehole contact force and friction coefficient between the pipe and the formation. The pipe weight is an important factor in the calculation of the friction. Because the pipe is pulled into a borehole that is filled with drilling fluid, an upward buoyant force acts on the pipe due to the weight of drilling fluid displaced by

the pipe. In a borehole full of drilling fluid, the top of pipe can be pushed against the crown of the borehole. The pipe may be less buoyant in sections of the borehole that are not completely full of drilling fluid, and therefore, the invert of the pipe may be in contact with the formation. The effective weight or submerged weight of the pipe is equal to the weight of the empty pipe minus the upward buoyant force. An upward submerged weight indicates that the pipe bears on the crown of the borehole, and a negative submerged weight indicates that the pipe bears on the bottom of the borehole.

The buoyancy uplift can be substantial for larger diameter pipes. Generally, buoyancy control (BC) measures may be necessary to reduce pullback loads for pipes equal to or larger than 610 mm (24 in) in diameter. BC is the practice of adding weight to the pipe to balance some or all of the upward buoyant force, usually by filling the pipe with water. The product pipe can be filled with water as it is pulled into the borehole. An alternative method is to use an internal line (known as ballast) inside the product pipe. In this case, weight is added by either filling the ballast pipe or filling the annular space between the product pipe and the ballast.

In addition to the pipe weight, the magnitude of the contact force at the borehole-pipe interface (along the curved sections) depends on the bending stiffness of the pipe, the radial displacement of the borehole wall at the contact points, and the stiffness of the formation (Kruse and Hergarden, 2010). The load used to pull the product line inside the borehole must also overcome fluidic drag forces resulting from the drilling fluid surrounding the product pipe. Fluidic drag can play a large part on pulling loads and can be estimated by modeling axial flow of fluid through an annulus and determining the viscous shear stress acting on the outside of the product pipe assuming a laminar flow (Baumert et al 2005, Duyvestyn 2009, Faghih et al 2015, Rabiei et al 2017). Rheological parameters of drilling fluid, drilling fluid density, flow rate, size of annular space (i.e., pipe and borehole sizes), and speed of pullback are parameters affecting the magnitude of fluidic drag on the pipe. Since rheological parameters of drilling fluid are critical in the magnitude of the resulting fluidic drag, with appropriate additives and mud management, the fluidic drag can be reduced.

3.3 Pull Force Calculation Method for the Case Studies

In North America, the method for pull force calculation recommended by PRCI (2015) is widely used for steel pipeline installation by HDD and is referenced in American and Canadian steel pipeline codes (ASME B31.4 2019, CSA Z662 2019). For the pull force calculations used in the case studies discussed in the next section, the PRCI model was used as a basis, with the addition of above-ground friction. The following outlines the calculation steps completed for pull force estimation for each case study.

The PRCI method is an empirical method, and it requires the drill path to be divided into a minimum of five separate straight and curved sections. The five sections considered in the pull force calculation are indicated in the crossing profile shown in Figure 2. The pull force calculation starts at Point A (where the product pipe is located and the location from where it is pulled into the ground) and ends at Point F (where the drill rig is set up).

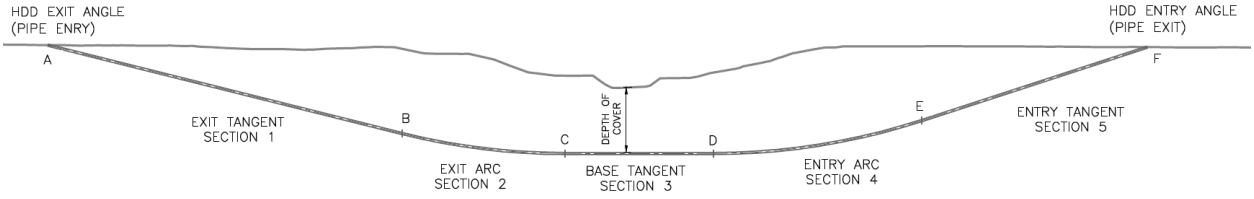

Figure 3.2. Typical HDD profile for PRCI method

The above-ground frictional component is calculated using Equation 3-1 for the start of pullback (at Point A in Figure 2):

$$T_A = w_d \times L_p \times \mu_r \tag{3-1}$$

where T_A is the above-ground friction force; w_d is the weight of the empty pipe per unit length; L_p is the total length of pipe; μ_r is the friction coefficient between the pipe and rollers.

The tension in the straight sections (Section 1, 3 and 5 in Figure 2) results from the frictional force between the pipe and borehole, the effective weight of the pipe, and the fluidic drag due to the drilling fluid surrounding the pipe. As the leading portion of the pipe is pulled through each section, the above-ground component of the friction corresponding to the length of the section above ground is subtracted from the

pull force at the end of the section. For each straight section, the incremental tension is calculated using Equation 3-2, 3-3 and 3-4:

$$T_2 = T_1 + |F_s| + DRAG \pm w_e L \sin\theta - w_d \times L \times \mu_r \quad (3\text{-}2)$$

$$F_s = w_e L \cos\theta \, \mu_b \quad (3\text{-}3)$$

$$DRAG = \pi D L \mu_{mud} \quad (3\text{-}4)$$

where T_1 and T_2 are the tension at the beginning and end of the section; F_s is the frictional force between the pipe and the borehole wall within the straight sections; w_e is the effective weight of the product pipe per unit length; L is the length of the pipe segment; θ is the angle of the segment with the horizontal plane; μ_b is the average coefficient of friction between the pipe and borehole wall; $DRAG$ is the fluidic drag between the pipe and the drilling fluid; D is the outer diameter of the pipe; and μ_{mud} is the fluidic drag coefficient.

In the curved sections, the stiffness of the product pipe and additional normal forces are calculated using beam equations with an imposed deflection based on the geometry of the curved segment (Huey et al. 1996), as in Equation 3-5 and 3-6.

$$T_2 = T_1 + |F_c| + DRAG \pm w L_{arc} \sin\theta - w_d \times L_{arc} \times \mu_r \quad (3\text{-}5)$$

$$F_c = 2N\mu_b \quad (3\text{-}6)$$

where L_{arc} is the length of the curved section of the borehole; F_c is the frictional force between the pipe and the borehole wall within the curved sections; and N is the normal contact force between the pipe and soil at the center of the pipe section.

The above equations for pull force analysis are based on the assumption that the borehole is full of drilling fluid up to the elevation of the HDD equipment used to pump the drilling fluid downhole (static elevation of the drilling fluid). For sections of the bore path located above the static elevation of the drilling fluid, the weight of the empty pipe is used in the pull force calculations. For installations where buoyancy control is applied, it is assumed that all portions of the pipe submerged within the drilling fluid are completely filled with water, whereas the pipe above the static elevation of the drilling fluid is assumed to be empty.

3.4 Case Study Database and Description of HDD Projects

To compare pull force estimates with the maximum loads actually supplied by the drilling rig during pullback, a database was created comprising 200 commercial HDD projects completed throughout Canada between 2012 and 2021. CCI Inc. was involved in the design, inspection, or monitoring during construction for these projects. The crossings involved installation of single steel pipes ranging in diameter from 60 mm (NPS 2) to 1067 mm (NPS 42), with crossing lengths from 60 m to 2,000 m. The HDD rigs utilized for these projects had between 17 tonnes to 500 tonnes of thrust/pull capacity. The maximum pull loads recorded at the rig (observed pull forces) were used for comparison with the maximum pull forces predicted (predicted pull force) for each project.

The subsurface geological materials encountered during these HDD projects included clay, silt, or sand overburden soils, underlain by clay shale, mudstone, sandstone, or siltstone bedrock. HDD crossings shorter than 300 m were designed to stay within the overburden soils. Most of the projects with lengths ranging from 300 m to 700 m included a significant portion through overburden soils and some sections within the lower bedrock. Crossings that exceeded 700 m occurred mostly within bedrock.

The tooling required to successfully progress through the formation is different for soft or loose soil as opposed to hard or dense soils and rocks. Jetting assemblies were used for installations in soft or loose soil, where mechanical displacement of soil particles is possible. Mud motors were used for drilling in harder formations. In a mud motor assembly, the hydraulic pressure from pumping drilling fluid downhole is utilized to generate the energy required to rotate the bit to break the formation and cut the material. Standard Penetration Tests (SPT) are completed on nearly all geotechnical drilling programs and provide a good indication of relative density or consistency of granular and cohesive soils (ASTM D1586, 2018). The SPT N-Value is the number obtained from the test that indicates the relative density or consistency of the soil. SPT N-Values up to 30 generally indicate soft and loose formations suitable for a jetting assembly while N-Values greater than 30 correlate with denser and harder formations which generally require a mud-motor to progress the bore through. This classification is used in this paper to differentiate soft vs. hard formations. The 200 case studies are summarized in Appendix A.

3.4.1 Pullback Parameters

Industry accepted values for pull force parameters were used in Equations 3-1 to 3-6 to estimate pull forces for each case study. Since PRCI method does not consider all resistance components (e.g., pipe-soil friction due to the Capstan effect, the radial displacement of the borehole wall at the contact points, and the stiffness of the formation), it is an accepted engineering practice to use input parameters that will result in larger pull forces to improve the prediction accuracy and account for worst case scenarios. The density of clean drilling fluid utilized during HDD typically ranges between 1080 kg/m3 and 1200 kg/m3. To ensure a conservative analysis and account for heavier fluids due to accumulation of cuttings, a density of 1438 kg/m3 was utilized in the analysis as recommended by PRCI. In buoyancy control applications where the pipe is filled with water, lower drilling fluid densities lead to heavier effective pipe weight, thus greater pull forces. For these projects, a low mud density of 1080 kg/m3 was used in the analysis for a conservative approach. Fluidic drag is treated as the friction force between the drilling fluid and the pipe in the PRCI method with a recommended fluidic drag coefficient of 172 Pa (0.025 psi), as Puckett (2003) suggested. Although more studies based on drilling fluid rheology and annular flow equations showed that the viscous shear stresses (friction) acting on the pipe are less than the fluidic drag coefficient of 172 Pa (Faghih et al. 2015; Baumert et al. 2005; Haciislamoglu and Langlinais 1990), this value was used in the pull force calculation for conservative analysis.

The friction coefficient between steel pipe and borehole is dependent on pipe coating type, formation type, and presence and age of mud filter cake El Chazli et al. (2005). Due to differences in geological conditions and mud properties at different locations, friction coefficients may vary along the borehole path. Friction coefficients between 0.2 and 0.3 are generally used in HDD applications, adopted from Maidla and Wojtanowicz (1990). A value of 0.3 was used in these case studies, as recommended by PRCI, to represent the friction coefficient between fusion bonded epoxy coated steel pipes and the borehole in the presence of drilling fluid and filter cake. A value of 0.1 is used for the friction coefficient between the pipe and rollers as recommended by the Netherlands Standardization Organization (NEN 3650 2020) and ASTM F1962 (2020). Table 1 summarizes the parameters used in the pull force calculations.

Table 3.1. Input parameters for pull force calculations

Parameters	Values
Pipe modulus of elasticity, MPa (ksi)	207,000 (30,023)
Density of steel pipe, kg/m^3 (lb/ft^3)	7,800 (487.0)
Density of water, kg/m^3 (lb/ft^3)	1,000 (62.4)
Density of drilling fluid, kg/m^3 (lb/ft^3)	1,438 (89.8)
Density of drilling fluid for buoyancy control, kg/m^3 (lb/ft^3)	1,080 (67.4)
Fluidic drag coefficient, Pa (psi)	172 (0.025)
Friction coefficient between pipe & borehole wall	0.3
Friction coefficient between pipe & rollers	0.1

3.4.2 Typical Pull Force Calculation

In this section, two sample HDD crossings as part of the 200 case studies were discussed to calculate the pull force based on Equations 1 through 6. Case 1 involved a 324 mm outside diameter (NPS 12) pipe grade 359 steel pipe with a 9.5 mm wall thickness which was installed in an 847 m long river crossing in Alberta, Canada. Case 2 included a 610 mm outside diameter (NPS 24) pipe grade 483 steel pipe with a 12.7 mm wall thickness that was installed in a 515 m long river crossing in Alberta, Canada. Figures 3.3 and 3.4 show the profile of the HDD crossings for Case 1 and Case 2, respectively. In addition to the parameters listed in Table 3.1, other design parameters for Case 1 and Case 2 are presented in Table 3.2. Table 3.3 lists a summary of the resultant pull forces for each section of the drill path and the final maximum pull force at the end of the pullback for Case 1 and Case 2.

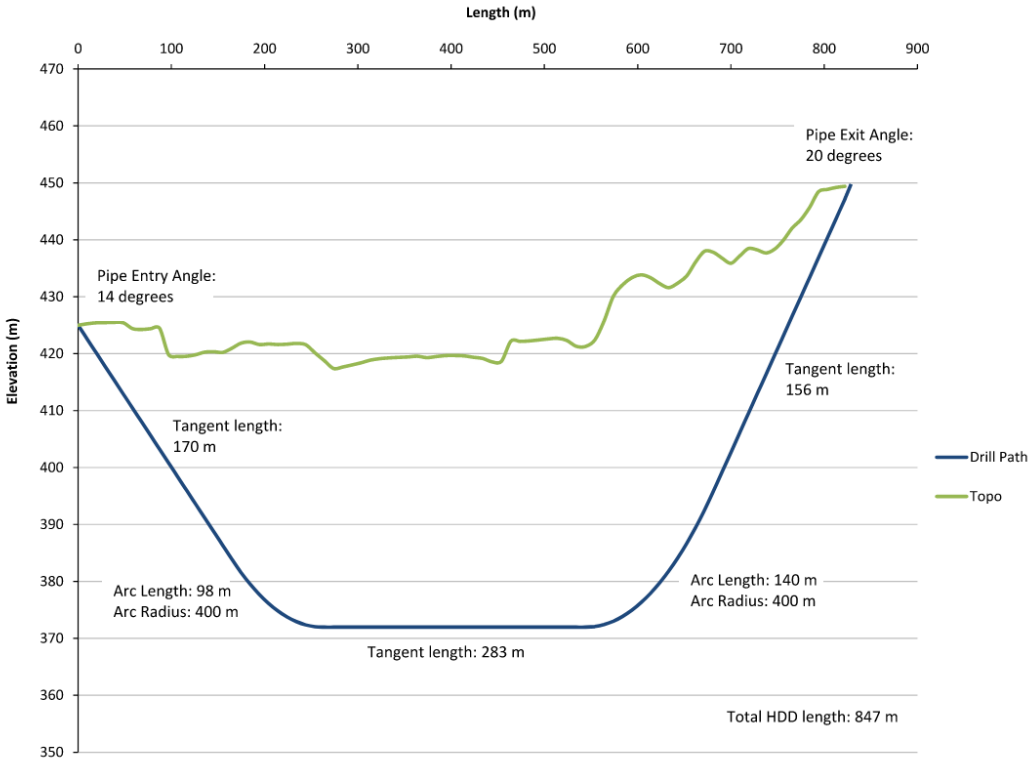

Figure 3.3. Drill path geometry for Case 1 HDD crossing

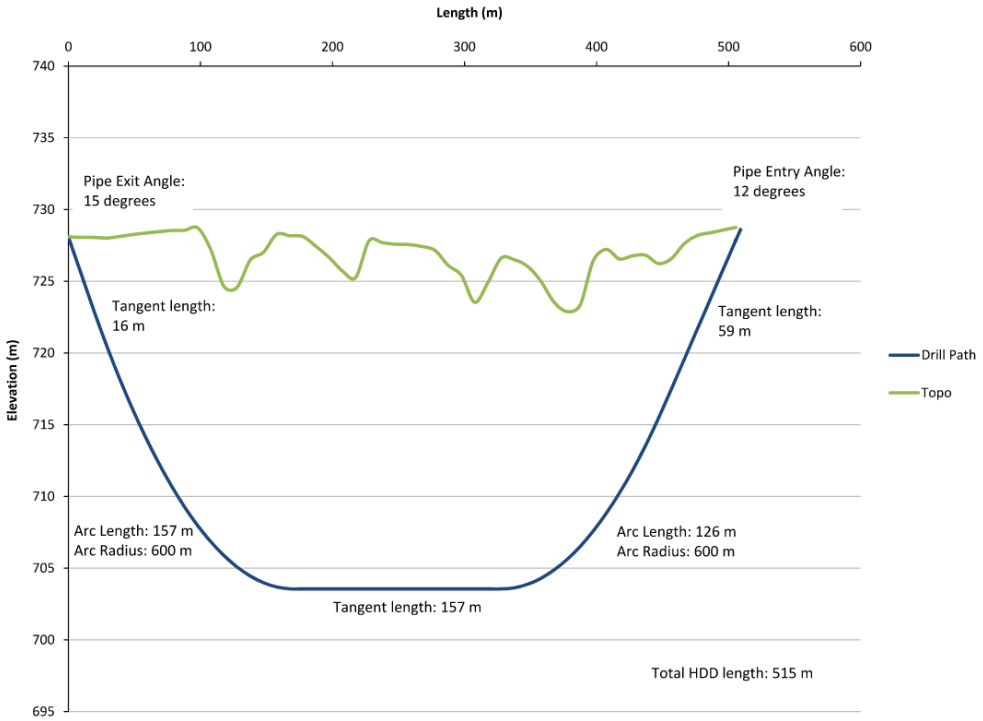

Figure 3.4. Drill path geometry for Case 2 HDD crossing

Table 3.2. Design parameters for Case 1 and Case 2 HDD installations

Design Parameters	Case 1	Case 2
Outside Diameter of Pipe (mm)	323	610
Wall Thickness of Pipe (mm)	9.5	12.7
Pipe Weight - Dry (kg/m)	73.2	185.7
Pipe Weight - Submerged (kg/m)	-45.3*	-233.8*
Application of Buoyancy Control	No	No
Specified Minimum Yield Strength of Pipe (MPa)	359	483
Radius of Curvature (m)	400	600
HDD Entry / Pipe Exit Angle	20°	15°
HDD Exit / Pipe Entry Angle	14°	12°
Total Crossing Length (m)	847	515
Depth of Cover under Waterbody (m)	45	18
Borehole Diameter (mm)	457	914
Drilling Rig Size (kg-force)	200,000	200,000
Formation	Hard Clay Till	Soft Clay

* Negative sign means upward direction.

Table 3.3. Summary of Pull force Calculation for Case 1 and Case 2

Drill Path Section (See Fig. 2)	Case 1		Case 2	
	Resultant Force at Start of Section (kN)	Resultant Force at End of Section (kN)	Resultant Force at Start of Section (kN)	Resultant Force at End of Section (kN)
5 (AB)	62.0	120.0	95.0	166.0
4 (BC)	120.0	164.5	166.0	348.5
3 (CD)	164.5	231.5	348.5	480.0
2 (DE)	231.5	287.0	480.0	640.0
1 (EF)	287.0	**329.2**	640.0	**646.5**

3.5 Comparison of Predicted and Measured Pull Forces

The case studies reviewed and discussed in this paper comprise a full range of project sizes and execution strategies. To allow better comparison between the predicted and observed pull force (maximum rig pull load), projects with similar execution methodologies were grouped. Case studies were categorized based on various factors, including pipe size, HDD crossing length, buoyancy control, HDD equipment used in the installation (mini, midi, and maxi) and soft vs. hard formation.

Within each project category, pull forces were assessed using mean prediction error (ME) as a measure of bias and root mean squared error (RMSE) as a measure of the precision of the predictions (Sheiner and Beal 1981). ME and RMSE are determined using Equation 3-7 and 3-8, respectively:

$$\mathrm{ME} = \frac{1}{N}\sum_{i=1}^{N}(P_i - O_i) \tag{3-7}$$

$$\mathrm{RMSE} = \sqrt{\frac{1}{N}\sum_{i=1}^{N}(P_i - O_i)^2} \tag{3-8}$$

where N is the number of case studies in each category; P_i is the predicted value for case study i; and O_i is the observed (measured) value for case study i.

Negative and positive mean prediction error can relate to the overall underestimating and overestimating of values by the prediction model, respectively, while greater absolute values can indicate the magnitude of the systematic component of the error. The RMSE is a measure of how well the model predicts pull force: smaller RMSE values indicate more precise predictions.

Scatter charts (Figure 3.5 through 3.8) for observed vs. predicted pull forces per meter length based on various project factors were generated. A dashed line representing equal observed and predicted pullback forces is included in the figures to indicate overestimation (points under the line) or underestimation (points over the line) of the design predictions. Another line was also added to the charts to indicate the predicted pullback force including a safety factor (SF). An SF of 1.5 or 2 are commonly included in pull force calculations during the design phase to account for project uncertainties and enable proper rig selection and stress analysis to be performed. In these charts, a safety factor of 1.5 was shown as an example safety margin.

Figure 3.5 shows the pull forces per meter for pipe outer diameters grouped in four categories: 60 mm to 324 mm (small pipes), 355 mm to 559 mm (medium pipes), 610 mm to 914 mm with no buoyancy control (large pipes w/o BC), and 610 mm to 1067 mm with buoyancy control applied (large pipes w/ BC).

Table 3.4 lists the mean predicted and observed pull forces, ME, and RMSE; as well as the percentage of cases for which actual pull forces were underestimated based on the different pipe size categories.

The average predicted and observed pull forces (Table 3.4) for small pipes are 0.264 kN/m and 0.394 kN/m, respectively, indicating an average underestimation (*ME* = -0.130 kN/m). The mean pull force values increase as the pipes increase in diameter. The average predicted and observed pull force for medium pipes are 0.730 kN/m and 0.720 kN/m, respectively. For large pipes without BC, the mean predicted pull force (1.400 kN/m) is greater than the mean observed pull force (1.205 kN/m). The increase in average pull force from small to large pipes is mostly the result of higher frictions due to an increase in effective weight of the pipe in the bore and higher fluidic drag forces due to increase in pipe outer area.

The mean prediction (1.247 kN/m) for large pipes with BC is smaller than the mean observed pull forces (1.434 kN/m). Based on site observations, it was noted that contractors may first attempt to pull the pipe without adding any water, and only add water once pull forces increase. Therefore, in the field there were sections during pullback with no water inside the pipe, whereas pull force estimates included the weight of water added for BC and consequently involved a reduction in the effective weight of the pipe. Thus, for some projects with BC, higher values of measured pull force than predicted could be due to a partially filled pipe rather than a pipe that is full.

The values of RMSE (Table 3.4) show that the precision of the pull force prediction model decreases as the pipe size increases (which is also seen in Figure 3.5). In 52% of installations involving small pipes, the observed pull forces are greater than the values predicted (including a factor of safety). As the pipe diameters increase, overprediction becomes more frequent, e.g., for medium and large pipes (without BC). For large pipes with no BC applied, only 7.3% have measured pull forces greater than the predicted values (with a factor of safety).

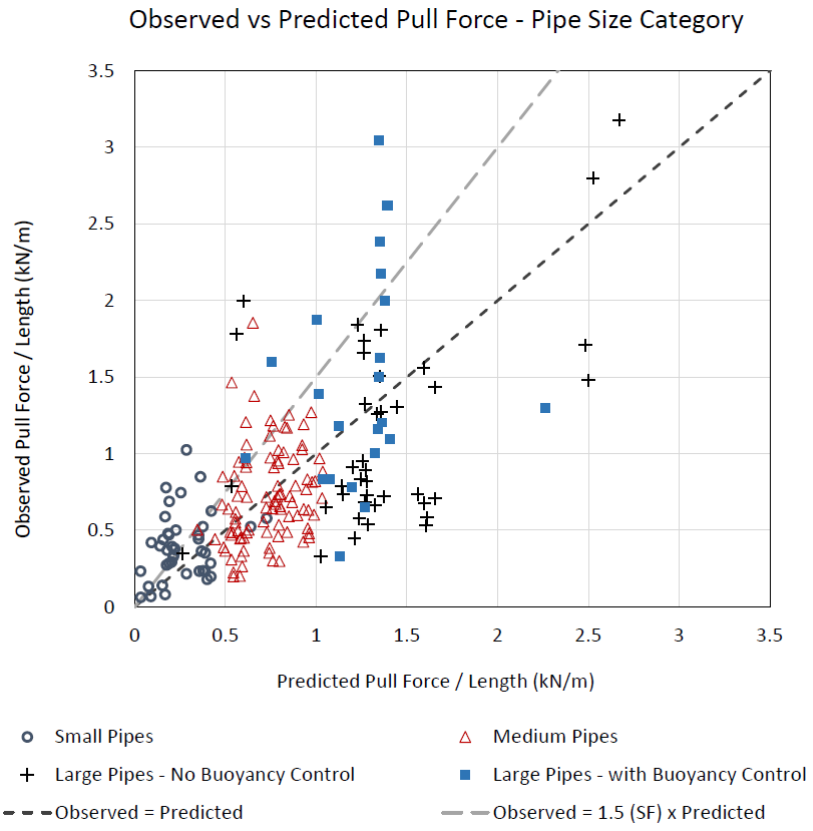

Figure 3.5. Observed vs. predicted pull forces based on based on pipe size and buoyancy control

Table 3.4. Pull force prediction performance categorized based on pipe size

Category	Mean predicted pull force (kN/m)	Mean observed pull force (kN/m)	ME (kN/m)	RMSE (kN/m)	Percentage of cases with underestimation (%)	Percentage of cases with underestimation including SF (%)
Small pipes (60-324 mm)	0.264	0.394	-0.130	0.259	66.7	52.4
Medium pipes (355-559 mm)	0.730	0.720	0.010	0.313	38.9	12.6
Large pipes w/o BC (610-914 mm)	1.400	1.205	0.195	0.672	31.7	7.3
Large pipes w/ BC (610-1067 mm)	1.247	1.434	-0.187	0.702	54.5	31.8

Figure 3.6 shows the scatter chart for data categorized based on HDD length for groups with crossing lengths shorter than 300 m, from 300 m to 700 m, and longer than 700 m. Table 3.5 summarizes the performance of the prediction model for crossing categorized based on length.

Pull forces were underestimated for nearly half of the crossings with lengths shorter than 700 m. For lengths shorter than 300 m, 53.7% of pull force predictions were underestimations, and for lengths between 300 m and 700 m, 46.1% were underestimations. Including a safety factor of 1.5 during design reduces the number of these projects for which pull forces are underestimated by over half, indicating that the magnitude of underestimation is within fifty percent of the predicted values for these crossings. Mean prediction errors (Table 3.5) suggest that predictions based on the current calculation model tend to overestimate actual pull forces as crossings lengths increase above 700 m. The prediction errors for pull force are highest for crossings with lengths less than 300 m (RMSE = 0.562 kN/m).

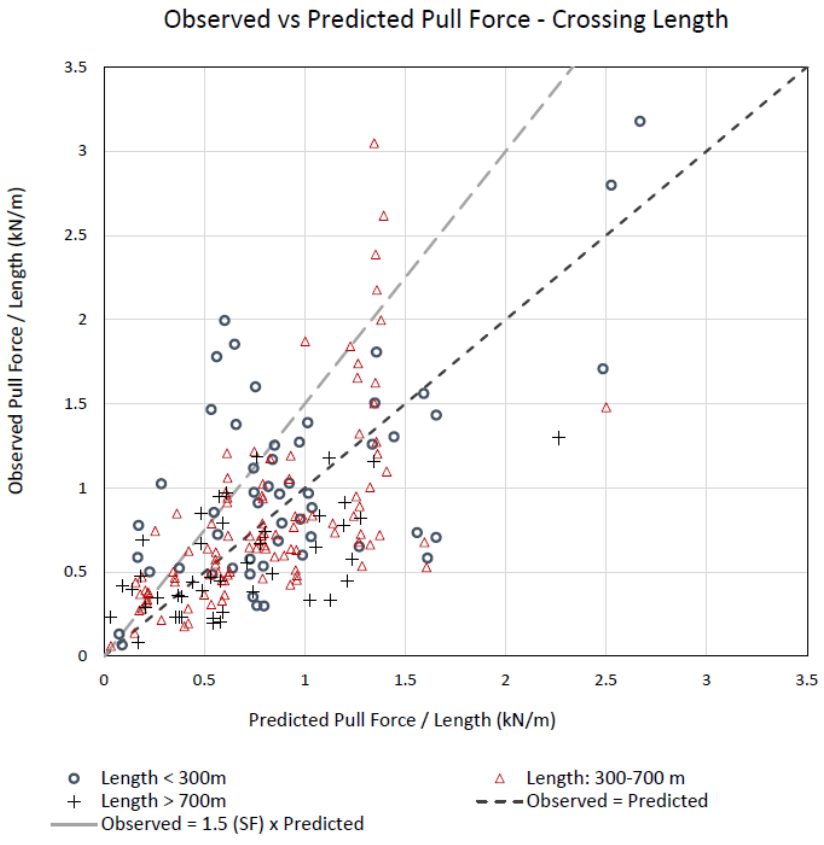

Figure 3.6. Observed vs. predicted pull forces based on crossing length

Table 3.5. Pull force prediction performance categorized based on HDD length

Category	ME (kN/m)	RMSE (kN/m)	Crossings with underestimation (%)	Crossings (including SF) with underestimation (%)
Crossing length < 300 m	-0.117	0.562	53.7	24.1
Crossing length: 300-700 m	0.003	0.427	46.1	21.6
Crossing length > 700 m	0.124	0.365	31.8	20.5

Figure 3.7 depicts observed versus predicted pull forces for HDD crossings drilled through soft formations (soft or loose soils with SPT N-Values less than 30) vs. hard formation (hard or dense soils with SPT N-Values greater than 30 and rock). Table 3.6 lists the prediction performance based on geotechnical conditions.

For these projects, both over- and underestimations can be seen in the predicted pull forces for HDD crossings advanced through soft or hard formations; however, underestimation of actual pull forces is more common in soft formations (*ME* = -0.128 kN/m). In 54.3% of the crossings in soft formations, pull forces were underestimated, compared to underestimation for 38.7% of cases involving hard formations. When a safety factor of 1.5 is included in the predicted pull forces, the percentage of cases for which the pull force is underestimated is reduced to 24.7% and 20.2% for soft and hard formations, respectively. The prediction error is higher in soft formations, with an RMSE of 0.538 kN/m compared to an RMSE of 0.390 kN/m in hard formations. The higher deviation in predicted pull force values from measured values for soft formations indicates the potential for more variation during pullback due to less ideal borehole conditions. Less idea borehole condition can involve more cuttings downhole or greater likelihood that portions of the borehole have partially or fully collapsed.

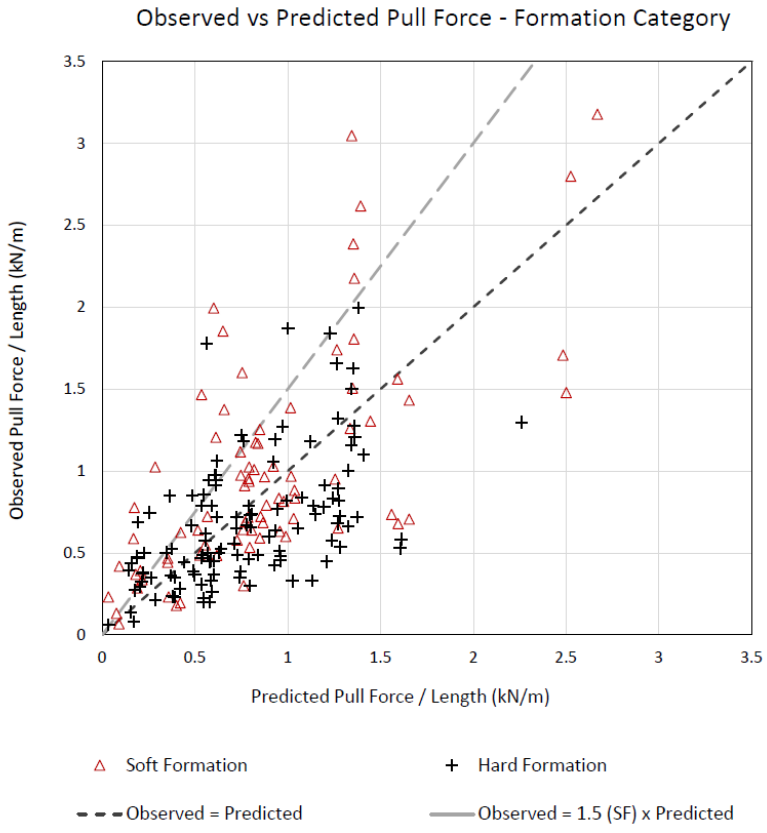

Figure 3.7. Observed vs. predicted pull force based on subsurface formation

Table 3.6. Performance of pull force predictions categorized based on soft vs hard formations

Category	ME (kN/m)	RMSE (kN/m)	Cases with underestimation (%)	Cases (including SF) with underestimation (%)
Soft formation	-0.128	0.538	54.3	24.7
Hard formation	0.082	0.390	38.7	20.2

Figure 3.8 shows the pull force values categorized based on equipment size, including crossings employing mini-HDD rigs (17 tonnes to 50 tonnes), midi-HDD rigs (63 tonnes to 181 tonnes), and maxi-HDD rigs (200 tonnes to 500 tonnes). Table 3.7 shows the prediction performance categorized based on HDD equipment.

Pull force estimates, which are based on ideal bore conditions, should be independent of the drill rig equipment used for a crossing. However, ideal bore conditions can be more easily achieved using better

equipment, better drilling fluid management (higher pump capacity and recycling systems such as shakers and centrifuges), and better project execution (generally implemented for larger HDD operations with midi- and maxi-rigs). In contrast, a lower level of construction effort may be expended for lower-budget HDD projects using mini-rigs, and there is the potential for poor hole cleaning which may lead to additional force being expended to displace soil cuttings during pullback. This was shown by a mean prediction error of -0.128 kN/m for mini-HDD operations, with predictions tending to underestimate the actual pull forces. 68.8% of predictions for projects involving mini-HDD rigs underestimated actual values of pull force. The number of projects for which pull force is underestimated decreases for larger equipment sizes (as in Table 3.7). The precision of predictions is less for midi-HDD rigs (RMSE = 0.502 kN/m) and maxi-HDD rigs (RMSE = 0.437 kN/m) compared with mini-HDD operations (RMSE = 0.297 kN/m).

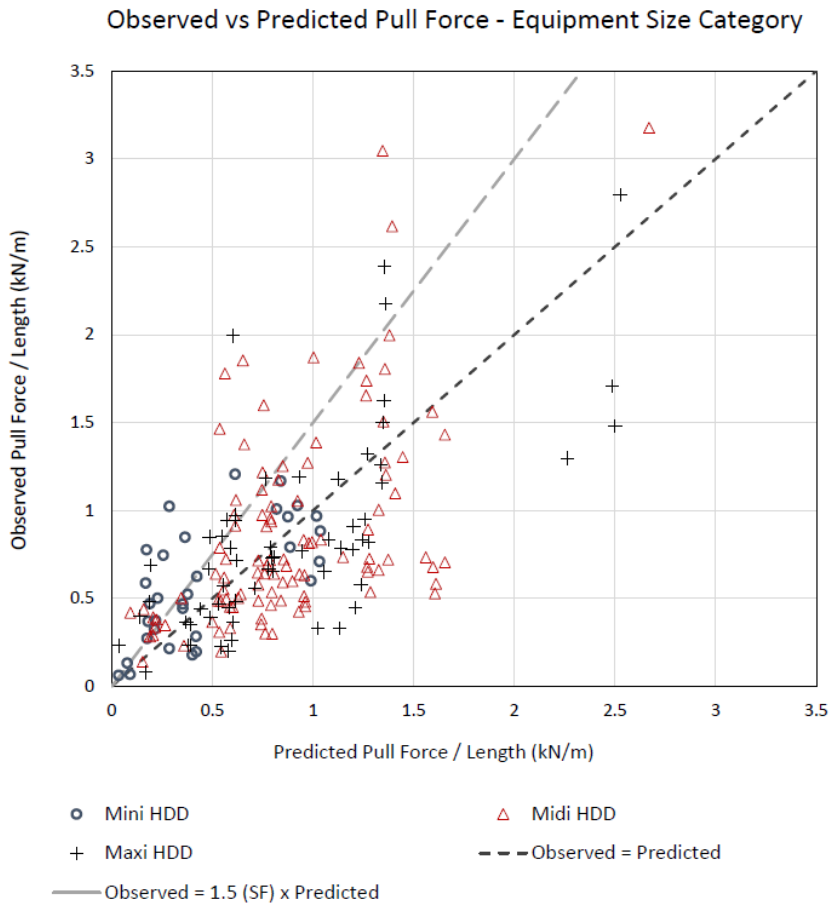

Figure 3.8. Observed vs. predicted pull forces based on HDD equipment size

Table 3.7. Pull force prediction performance categorized based on HDD equipment

Category	ME (kN/m)	RMSE (kN/m)	Crossings with underestimation of pull force (%)	Crossings involving SF with underestimation of pull force (%)
Mini HDD (17-50 tonnes)	-0.128	0.297	68.8	43.8
Midi HDD (63-181 tonnes)	0.001	0.502	41.1	15.9
Maxi HDD (200-500 tonnes)	0.056	0.437	39.3	21.3

Figure 3.9 shows observed vs. predicted loads (not normalized by length) for all 200 case studies. The pull force prediction model does not perform well (underestimation) in for predicted values less than 250 kN. As the predicted values increase, there is a general shift towards overestimation of pull forces. This trend is illustrated by the linear regression line shown in the chart. The regression yields a slope of 0.59, far from the slope of one for the case of observed pull forces equal to predicted pull forces. The regression gives an intercept of 137.3 kN and R^2 of 0.52, indicating an average fit for the linear regression. A correlation coefficient, r, of 0.7 was determined, showing a moderate positive linear relationship between predicted and actual values of pull force.

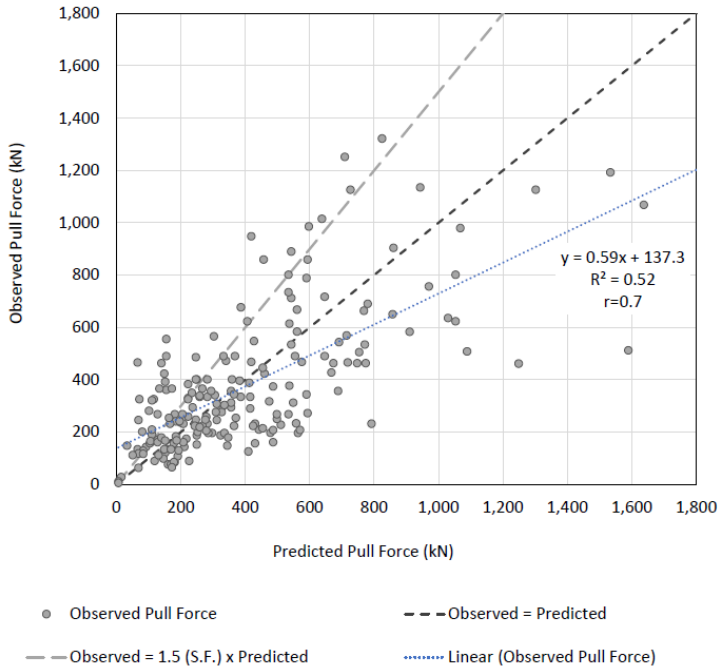

Figure 3.9. Observed vs. predicted pull forces for 200 HDD crossings (not normalized by length)

3.6 Data Distribution

Box plots of the data categorized by pipe diameter, crossing length, formation type, and HDD equipment size are presented in Figure 3.10 to summarize the data. Prediction errors were calculated by taking the difference between predicted and observed pull forces and displayed for each category. The whiskers in each chart show the extent of the variation, indicating the lower and upper extremes, excluding any outliers, which are plotted as individual data points. The top and bottom box boundaries indicate the upper and lower quartiles—the lower quartile, or first quartile (Q_1), includes one quarter of the ordered data set. This means that there are exactly 25% of cases with values less than the first quartile, while 75% of data points are greater. Similarly, the upper quartile, or third quartile (Q_3), includes three quarters of the ordered set, with 25% of the data points being greater. The box spans the interquartile range (IQR), which is a measure of the data spread and includes 50% of the data set. The median of the data in each group is indicated by a horizontal line inside the box, and the mean value (ME) of each data set is shown by a cross marker inside the box. Finally, a mean line connecting the mean values is shown to illustrate the average trend between categories.

A box plot of the prediction error based on pipe size categories is shown in Figure 3.10a. The mean prediction error is -0.130 kN/m for small pipes, 0.010 kN/m for medium pipes, 0.195 kN/m for large pipes w/o BC, and -0.187 kN/m for large pipes w/ BC. A general trend from underprediction to overprediction can be seen as the pipe size increases, excluding HDD crossings with BC, where the distribution is skewed towards underprediction. Among all categories, the greatest magnitude of error and highest data spread is observed for large pipes with application of BC, with lower and upper quartile values of -0.768 kN/m and 0.292 kN/m, respectively (Table 3.8). Figure 3.10b shows a box plot of the prediction error for HDD crossings with different lengths. The median pull force prediction errors are -0.098 kN/m, 0.052 kN/m, and 0.116 kN/m for crossings less than 300 m, from 300 m and 700 m, and greater than 700 m, respectively. Several outliers were seen for crossings shorter than 300 m and crossings between 300 m and 700 m; however, the mean line (trend) and the interquartile range show how the pull force predictions generally tend from underestimations for short crossings (less than 300 m) to overestimations for crossings longer

than 700 m. Figure 3.10c shows the box plot for pull force prediction errors for projects in soft and hard formations. The median pull force prediction errors are -0.095 kN/m and 0.089 kN/m for soft and hard formations, respectively. The IQR for prediction error is -0.348 kN/m to 0.153 kN/m for crossings advanced through soft formations and -0.159 kN/m to 0.329 kN/m for hard formations. The IQR values and the mean line (Figure 3.10c) indicate that underestimation of pull force is more common for soft formations, while a slight tendency towards overprediction is seen in crossings drilled in hard formations. Prediction errors grouped according to the size of HDD equipment used are shown in Figure 3.10d. The median pull force prediction error is -0.109 kN/m, 0.081 kN/m, and 0.077 kN/m for mini-HDD rigs, midi-HDD rigs, and maxi-HDD rigs, respectively. The interquartile range of the prediction errors is from -0.276 kN/m to 0.055 kN/m for crossings executed with mini-HDD rigs, from -0.243 kN/m to 0.304 kN/m for midi-HDD rigs, and -0.199 kN/m to 0.305 kN/m for maxi-HDD rigs. The distribution of the pull force prediction errors across HDD crossings in different categories is summarized in Table 3.8.

Table 3.8. Distribution of pull force prediction errors for HDD crossings in different categories

Category	Prediction Errors (Predicted Value minus Observed Value)				
	Median (kN/m)	Mean (ME) (kN/m)	Q_1 (kN/m)	Q_3 (kN/m)	IQR ($Q_3 - Q_1$) (kN/m)
Small Pipes (60-324 mm)	-0.114	-0.130	-0.269	0.033	0.302
Medium Pipes (355-559 mm)	0.071	0.010	-0.176	0.230	0.406
Large Pipes w/o BC (610-914 mm)	0.350	0.195	-0.156	0.663	0.819
Large Pipes w/ BC (610-1067 mm)	-0.107	-0.187	-0.768	0.292	1.060
Length < 300 m	-0.098	-0.117	-0.372	0.178	0.550
Length: 300-700 m	0.052	0.003	-0.188	0.232	0.420
Length > 700 m	0.116	0.124	-0.112	0.347	0.460
Soft Formation	-0.095	-0.128	-0.348	0.153	0.501
Hard Formation	0.089	0.082	-0.159	0.329	0.488
Mini HDD (17-50 tonnes)	-0.109	-0.128	-0.276	0.055	0.331
Midi HDD (63-181 tonnes)	0.081	0.001	-0.243	0.304	0.547
Maxi HDD (200-500 tonnes)	0.077	0.056	-0.199	0.305	0.504

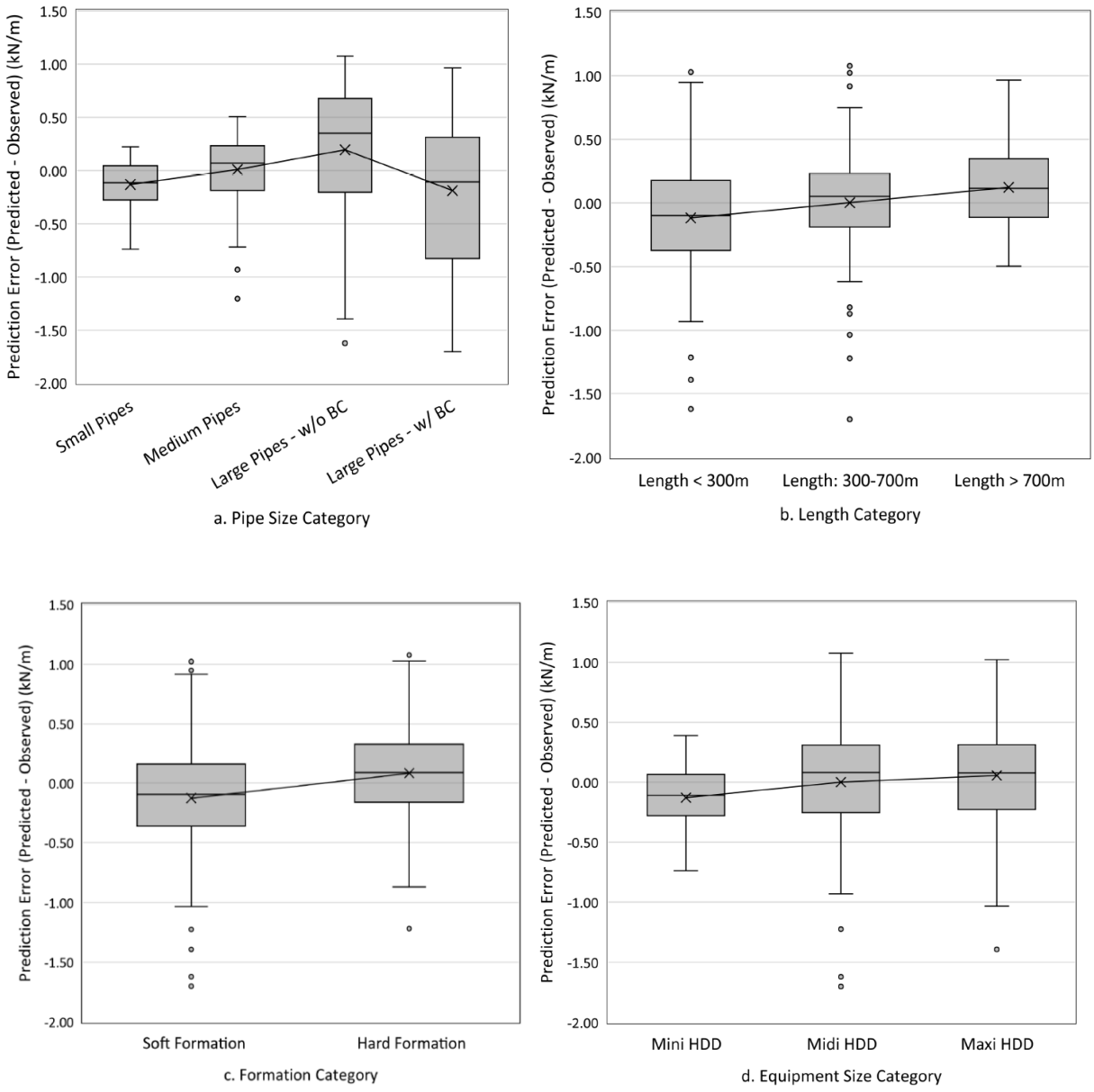

Figure 3.10. Distribution of differences between observed and predicted pull force for four groupings: a. pipe size, b. crossing length, c. subsurface formation, and d. HDD equipment size

3.7 Discussion and Summary

Pull force underprediction is common for HDD crossings involving a lower level of construction effort, resulting in the potential of poor hole cleaning and borehole conditions far from ideal. A combination of the accumulation of cuttings in the borehole, borehole instability, and mechanical displacement of soils within the borehole during line pull can result in observed pull forces that are higher than predicted for this

type of HDD crossing. In the case of pullback where there is an accumulation of cuttings, a large portion of the pull force is required to compress the cuttings and overcome the axial shear between the displaced cuttings and the pipe. The possibility of less ideal bores is higher in projects involving mini-HDD operations through soft formations, for small pipe sizes, and for short crossing lengths. More attention must be given to pull force estimations for this type of crossing because the current design model does not consider any additional resistance to the pipe pull inside a less-than-ideal bores.

As the pipe diameter increases, overprediction of pull force becomes more frequent for the installation of large pipes without BC. A large spread in prediction errors of large pipes (IQR values of 0.819 kN/m and 1.060 kN/m for large pipes without and with BC, respectively, as in Table 3.8) indicates poor estimations of pull force as the pipe size increases. One reason for significant overestimations in larger pipes may be due to the assumptions of submerged pipe weight for the portion of pipe within the borehole. For larger pipes the increase in predicted pull force is directly related to the increase in the effective weight of the submerged pipe in the bore, the assumption of a pipe being fully buoyant within a heavy drilling fluid throughout the entire borehole (up to the static level) may not be true for all crossings. For large pipes with diameters greater than 610 mm, the weight of the empty pipe is less than the submerged weight. Therefore, the resistance to pipe movement inside the borehole decreases if the pipe is not fully submerged in the drilling fluid. Such discrepancies were also reported in experimental investigations by Baumert et al. (2004). When buoyancy water is included in estimations of pull force for large pipes, significant underpredictions were observed due to pipes being partially filled during pullback, in contrast to a pipe full of water, which is the basis for pull force estimations. Significant overestimation in pull force was also observed for large pipes with BC, which may be due to the assumption of the pipe not being fully buoyant, as discussed above.

Pull force prediction errors show that predictions generally vary from underestimation for short crossings (i.e., with lengths less than 300 m) to overestimation for crossings longer than 700 m. Conservatism in the design assumptions contributes to a general trend towards overprediction of pull force for longer HDD crossings. Also, analysis of pull force estimations and measured values for the case studies suggests that

prediction accuracy is lower in soft formations, with a higher probability of underestimating the pull force than for crossings completed in hard formations. The assumption of ideal borehole conditions, which forms part of current design practice for HDD, is more likely to be achieved for crossings in hard formations. In softer soil formations, achieving a clean and stable borehole is not always possible and a combination of accumulation of cuttings, mechanical displacement of soils within the borehole, and borehole instability may account for the higher observed pull forces.

A comparison of predicted and observed pull forces based on HDD equipment size shows an increase in the percentage of HDD crossings with underestimated pull force in projects involving mini-HDD rigs. For smaller-scale HDD projects where mini-rigs are used, poor borehole cleaning as a result of lower construction effort (e.g., inadequate equipment, lack of an effective engineered drilling fluid plan, and omission of cleaning passes) may lead to additional forces being required to displace soil cuttings during pullback. Generally, better equipment, better drilling fluid management and better project execution are implemented for large HDD installations to account for the higher costs and risks associated with these projects. In addition, for large HDD operations, proper conditioning of the borehole and slow pull rates eliminate excessive friction during pullback.

Despite using conservative pullback parameters accepted by industry as summarized in Table 3.1, significant underestimations were observed, especially for some crossings with pull force predictions less than 250 kN (see Figure 3.9). As the pull force values increase above 250 kN, most data points are located close to or under the equity line (observed pull force equal to predicted pull force), with a safety factor of 1.5 included in the predicted pull force (except some of the cases with buoyancy control application). This highlights the importance of including safety factors during the design phase when selecting the product pipe specification and drilling rig capacity to allow for variation during construction. The observed deviation between predicted and observed pull forces suggest that appropriate safety factors may range from an upper value of 2.5 to 3 for smaller projects with poor borehole conditions and a lower limit of 1.25 to 1.5 for large projects involving proper conditioning of the borehole and effective removal of cuttings, which assists in reducing excessive mechanical work during pullback.

In the absence of a modeling method for pull force that accounts for actual borehole conditions, the pull force prediction errors tabulated in Table 3.8 may be used as a measure of potential adjustments to pull force estimations. For instance, the negative mean predictions errors listed in Table 3.8 for different project categories may be taken as a reference for a typical value for resistance to add to the pull force estimation for crossings with a similar scope (pipe size, length, formation type and HDD operation size). A simple approach to account for pull force underestimation is to consider higher values for the design inputs (including borehole friction coefficient, mud density and buoyancy assumption resulting in heavier pipe weight) listed in Table 3.1 for smaller HDD projects for which less ideal bore conditions may exist. Similarly, using values of input parameters towards the low end of the range (including borehole friction coefficient, fluidic drag coefficient, mud density and buoyancy assumption resulting in lighter pipe weight) may lead to more accurate pullback force predictions for larger projects with clean, stable boreholes.

3.8 Conclusions

Pull force estimation was reviewed in this paper for the installation of steel pipes in HDD crossings based on current design practice guidelines. A comparison of predicted and actual drill rig pull forces was completed using data from 200 HDD crossings constructed between 2012 and 2021. The predicted pullback forces were calculated using a set of constant assumptions based on ideal bore conditions and parameters (including friction factor, fluidic drag, and mud properties) accepted by industry to evaluate the accuracy of pull force estimations. In most cases, for small pipes with diameters of 64 mm to 324 mm, the data indicates that pull forces were underestimated. As the pipe diameters increase, a clear trend is visible, showing a shift in the distribution towards higher predicted values of pull force compared to measurements of pull force during pullback. For large pipe diameters (610 mm to 914 mm) without buoyancy control, most measured pull forces are below the predicted values. When buoyancy control was utilized on larger installations, both overprediction and underprediction were observed. Underestimations may be attributable to the application of partial buoyancy control during construction (i.e., installation of a pipe partially filled with water), whereas pull force estimations are based on a pipe that is filled completely. Comparison

between measured and predicted pull force for the HDD crossings indicate that predictions generally vary from underestimation for short crossings (with lengths less than 300 m) to overestimation for crossings longer than 700 m. Analysis of data from the case studies suggests that underestimation of actual loads is more common for crossings through soft formations than for crossings in hard formations. A comparison of predicted and observed pull forces based on HDD equipment size shows an increase in the number of cases with underestimated pull force in projects involving mini-HDD rigs.

A review of these case studies showed significant underestimations, especially in some crossings with pull force predictions less than 250 kN, despite the conservative assumptions for calculation of pullback used in the paper. Among the projects studied, pull forces were underpredicted for most crossings that could possibly have less ideal bore conditions, including projects with small pipe diameters, short crossings, crossings in soft formations, and mini-HDD rigs. The underestimations in these projects could be due to current design models that do not consider the additional resistances to the pipe pull present in less-than-ideal bores. A general shift towards overestimation is clear as the predicted values of pull force become greater. Overestimations of measured pull forces were more common in crossings completed by midi- and maxi-HDD rigs involving pipe diameters larger than 610 mm, lengths over 700 m, and hard formations. The increase in overestimation for many crossings as the pipe diameters increase may indicate that the assumption of full buoyancy control (e.g., a completely filled pipe) for the pipe within the drilling fluid may not be valid for all sections of the drill path, resulting in a lower submerged weight than for assumptions based on current design practice.

To account for actual borehole conditions, the deviations in predicted values from actual pull forces per meter length obtained in this work (such as negative mean prediction errors) may be taken as a measure of the resistance that should be added to the estimated pull force for a crossing of similar scope (e.g., length, pipe diameter, etc.). Moreover, pull force estimations should allow for contingencies based on the project scope, geotechnical conditions, and the expected execution plan. A simple approach is to consider more conservative values for borehole friction coefficient, mud density and buoyancy assumptions resulting in heavier pipe weights for smaller HDD projects with less ideal bore conditions. Similarly, lower values of

borehole friction coefficient, fluidic drag coefficient, mud density and buoyancy assumptions resulting in lighter pipe weight could be considered for larger projects with more ideal construction conditions. Finally, the inclusion of safety factors during the planning phases is critical to allow for sufficient HDD designs and site variations during construction. A review of pull force calculations for 200 case studies suggests that safety factors can range from a lower limit of 1.25 to 1.5 for large projects with a high level of construction effort to an upper limit of 2.5 to 3 for small projects for which poor bore conditions may exist.

4. Chapter 4: Pull Force Estimation for Installation of Bundled Steel Pipes using Horizontal Directional Drilling[1]

4.1 Introduction

Horizontal Directional Drilling (HDD) is a method that is widely used to install pipelines while minimizing ground disruption. HDD involves three primary stages, including drilling the pilot hole, reaming, and pullback (Gelinas et al., 2000), where the product pipe is pulled through the borehole. During pullback, the drilling rig is connected to the product pipe through a series of drill rods (drill pipes), a reamer, a swivel, and a pullhead. The rig pulls the drill rods, joint by joint, to install the product pipe. During product pipe installation, the pull force supplied by the rig must overcome the forces resisting the motion of the product pipe.

During the planning phase, pull force estimation is important in choosing the appropriate rig equipment (i.e., with adequate capacity) and evaluating the pipe stress during pullback (Chehab, 2008). The loads imposed on the pipe during installation are sometimes greater than the long-term operational loads and may govern the design requirements. The product pipe should be designed to avoid any damage during installation, while the HDD rig should be capable of pulling the pipeline through the borehole (Baumert and Allouche, 2002).

The load required to pull the product line inside the borehole must be high enough to overcome several resisting forces, including the net buoyant weight of the pipe, the friction between the borehole and the pipe sections, the fluidic drag arising from the drilling fluid that surrounds the pipe in the annulus, and the friction between the pipe and the above-ground support equipment (Chehab and Moore, 2007). The forces due to interactions between the pipe and soil in curved sections of the borehole, as well as the forces due to

[1] A version of this chapter has been submitted to the Canadian Journal of Civil Engineering.

the drill rods in the hole and the reamer and swivel (following the pull section) also contribute to resisting forces during pullback.

For some HDD applications, multiple product pipes of different sizes are bundled together and installed in a single bore. This technique is more commonly utilized where a series of small conduits such as polyethylene pipes carrying fiber optic, communication or electrical cables are to be placed together. With advancements in HDD equipment and tooling, bundled installation has also been applied for larger steel pipes. For bundled installations, bindings are placed along the length of the bundled pipelines, so that the pipes move as a single unit. During pullback, all pipes in the bundle are connected to a common pullhead and pulled into the borehole simultaneously. Figure 4.1 shows an example of a pipe bundle and its arrangement inside the hole.

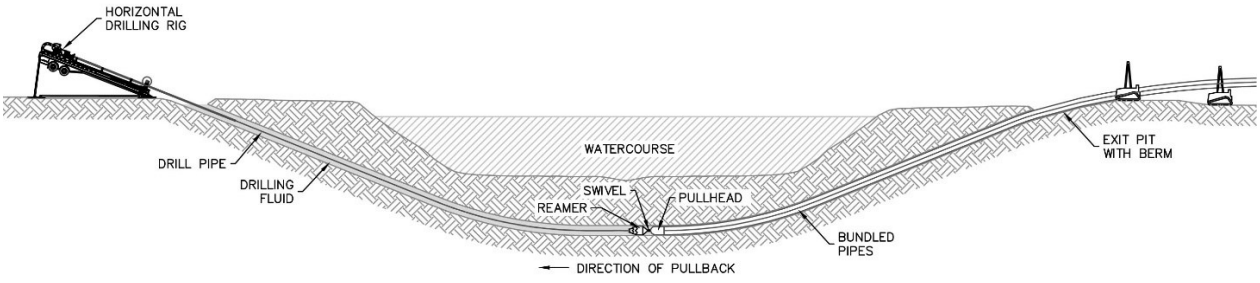

(a)

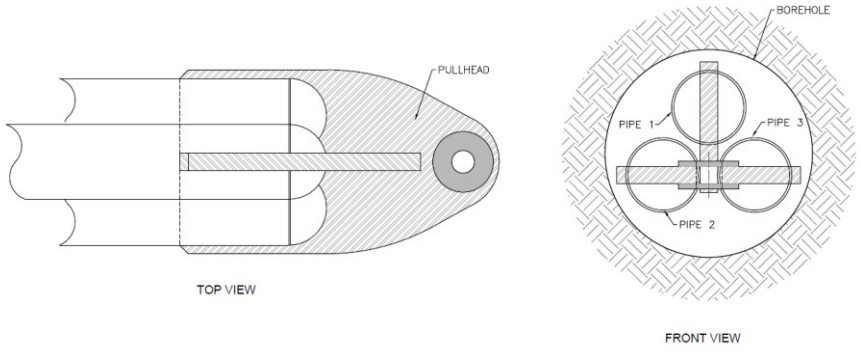

(b)

Figure 4.1. Schematic of a bundled three-pipe installation: (a) pullback process and (b) pullhead assembly.

Various analytical methods have been proposed in the literature to estimate the pull force for single pipe installation using HDD (Huey et al., 1996; ASTM F1962, 2020; Polak et al., 2002; Cheng and Polak, 2007; Cai and Polak, 2019; NEN 3650, 2020). Most of these methods employ a similar approach to estimate the pull force, including dividing the bore path into a series of straight and curved sections and calculating the resistive forces for each individual section, based on the equations recommended in each method. However, insufficient attention has been given to pull force analysis for bundled HDD crossings using any of the theoretical pull force models. In the absence of a detailed analytical solution, a conservative determination of pull force for bundled installations can be done by summing the individual pull forces for each single pipe in the bundle. This approach is conservative because it accounts for frictions and fluidic drag forces acting on each individual pipe as if each single pipe is in full contact with borehole and drilling fluid. However, in a bundled pipe configuration, pipes' contacts with borehole and drilling fluid are limited to the exposed and external surfaces of the pipes in the bundle.

Among the theoretical models available, the method recommended by the Royal Netherlands Standardization Institute (NEN 3650) is the only guideline that currently has a provision for calculating pull force for bundled installation based on the concept of a single equivalent pipe. In North America, the method presented by PRCI is widely used as the recommended guideline for HDD design involving steel pipelines and the PRCI method is referenced in American and Canadian pipeline codes (ASME B31.4, 2019; CSA Z662, 2019). In this paper, the concept of using the parameters associated with a single equivalent pipe to represent the pipe bundle is examined; and the concept of a single equivalent pipe is combined with the PRCI method to predict pull forces for bundled installations. Data from several bundled HDD installations completed in Alberta, Canada between 2013 and 2019 were studied to check the accuracy of the proposed method. The details of these projects are included in the case study section. The equivalent pipe method suggested in NEN 3650 is also used to compare pull force prediction models based on the case studies. The following section (Section 4.2) provides a summary of the two pull force calculation methods.

4.2 Guidelines for Pullback Load Estimation

4.2.1 PRCI Method

The PCRI method requires that the drill path be divided into a minimum of five sections (to separate straight and curved sections). The pull force calculation starts at section one (where the product pipe is located and pulled into the hole) and ends at the HDD entry point (where the drill rig is set up). The five sections considered in the PRCI method are indicated in the crossing profile shown in Figure 4.2. After calculations are done for each separate section, the total pull force is calculated by adding the loads determined for each segment.

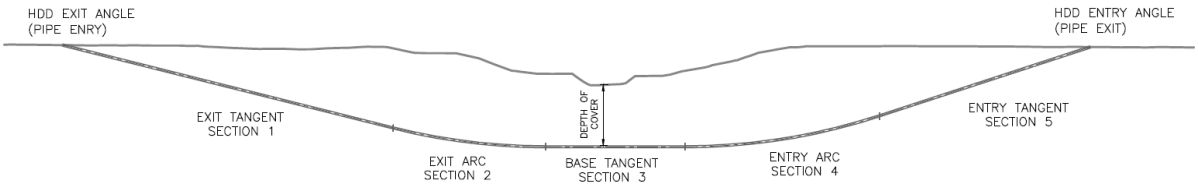

Figure 4.2. Typical HDD profile for PRCI method

In the straight sections, the tension results from the frictional force between the pipe and the borehole, the effective buoyant weight of pipe, and the fluidic drag from the drilling fluid surrounding the pipe. In the curved sections, the pipe is modelled as a beam with three points of contact with the borehole, and the normal force acting on the pipe is calculated based on the known geometry of the curved segment (Huey et al., 1996).

For the straight sections, the incremental tension is calculated using Equations 4-1 through 4-3:

$$T_2 = T_1 + |F_1| + DRAG \pm wL \sin\theta \quad (4\text{-}1)$$

$$F_1 = wL \cos\theta \, \mu_{soil} \quad (4\text{-}2)$$

$$DRAG = \pi DL\mu_{mud} \quad (4\text{-}3)$$

where T_1 and T_2 are the tension at the beginning and end of each section, respectively; F_1 is the frictional force between the pipe and the borehole wall within the straight sections; w is the submerged weight of the product pipe per unit length; L is the segment length; θ is the angle of the segment with the horizontal; μ_{soil}

is the average coefficient of friction between the pipe and soil, (with recommended values between 0.21 and 0.30); *DRAG* is the fluidic drag between the pipe and the drilling fluid; *D* is the pipe diameter; and μ_{mud} is the fluidic drag coefficient (with a recommended value of 175 Pa (0.025 psi)).

Equations 4-4 and 4-5 are used for the curved sections:

$$T_2 = T_1 + 2 \times |F_2| + DRAG \pm wL_{arc} \sin\theta \quad (4\text{-}4)$$

$$F_2 = N\mu_{soil} \quad (4\text{-}5)$$

where L_{arc} is the length of the curved section of the borehole; F_2 is the frictional force between the pipe and the borehole wall within the curved sections; and *N* is the normal contact force between the pipe and soil at the center of the pipe section.

4.3 NEN 3650 Method

In the NEN 3650 method, the total pull force comprises five different components: the resistance due to friction between the pipe and roller (T_1); the resistance due to borehole and drilling fluid friction in the straight section of the pipe (T_2); the resistance due to borehole and drilling fluid friction in the curved section of pipe (T_{3a}); the resistance due to pipe-soil interactions in the curved section of pipe (T_{3b}); and the friction due to forces in the curved section (T_{3c}). Equations 4-6 through 4-11 are used to calculate the total resistance, based on these five components:

$$T_{total} = T_1 + T_2 + T_{3a} + T_{3b} + T_{3c} \quad (4\text{-}6)$$

$$T_1 = f_{install} \times L_{roller} \times Q \times f_1 \quad (4\text{-}7)$$

$$T_2 = f_{install} \times L_2 \times (\pi D_0 \times f_2 + Q_{eff} \times f_3) \quad (4\text{-}8)$$

$$T_{3a} = f_{install} \times L_{arc} \times (\pi D_0 \times f_2 + Q_{eff} \times f_3) \quad (4\text{-}9)$$

$$T_{3b} = f_{install} \times 2 \times q_r \times D_0 \times \pi/\lambda \times f_3 \quad (4\text{-}10)$$

$$T_{3c} = f_{install} \times L_{arc} \times g_t \times f_3 \quad (4\text{-}11)$$

where $f_{install}$ is a load factor to account for stochastic variation and model uncertainty, with a value of 1.4 in the case of a normal crossing and 2.0 in cases with a gravel layer; L_{roller} is the length of pipe on rollers above ground; *Q* is the weight of pipe per unit length; f_1 is the friction coefficient between the pipe and rollers or

the pipe and the ground surface (for rollers, a value of 0.1 is recommended); L_2 is the length of pipe in the straight section of the borehole; D_0 is the outer diameter of the pipe; f_2 is the friction coefficient between the pipe and the drilling fluid (50 Pa is recommended); Q_{eff} is the effective weight of the pipe; f_3 is the friction coefficient between the pipe and the borehole wall (with a recommended value of 0.2); L_{arc} is the length of the curved section; q_r is the maximum soil reaction; and g_t is the thrust force (in N/m).

4.4 Concept of Equivalent Single Pipe for Bundled Pull Force Estimation

A review of pullback models indicates that friction forces account for most of the resistance during the pipe installation (Cai et al., 2017). Pipe weight is an important factor in the calculation of the normal forces and the resulting frictions. Therefore, pipe weight, for either dry or submerged pipe (i.e., the buoyant weight of pipe when submerged in drilling fluid), is a significant parameter in the pull force estimation. An equivalent single pipe can be defined with a weight that is the same as the total weight of the individual pipes in the bundle. Similarly, the stiffness of the equivalent pipe should also equal the total stiffness of the bundle pipes. The equivalent single pipe parameters (diameter and wall thickness) are then used in the pull force calculations to represent the parameters of the bundled pipes.

Equations 4-12 and 4-13 can be used for calculation of the weight of the bundled pipes in dry and submerged conditions:

$$W_{\ bundle,dry} = \sum_{i=1}^{n} \frac{\pi}{4}\left(D_i^2 - (D_i - 2t_i)^2\right)\gamma_s \tag{4-12}$$

$$W_{\ bundle,sub} = W_{\ bundle,dry} - W_{\ bundle,uplift} \tag{4-13}$$

$$W_{\ bundle,uplift} = \sum_{i=1}^{n} \frac{\pi}{4} D_i^2\, \gamma_{mud} \tag{4-14}$$

where $W_{bundle,dry}$ is the total dry weight of the bundled pipes; D_i and t_i are the outside diameter and wall thickness, respectively, of pipe *I* of the bundle; n is the total number of pipes in the bundle; γ_s is the density of the steel pipe; $W_{bundle,\ sub}$ is the total submerged weight of the bundled pipes within a borehole filled with

drilling fluid; $W_{bundle,uplift}$ is the upward buoyancy force from drilling fluid acting on the bundled pipes; and γ_{mud} is the density of the drilling fluid (or drilling mud).

The equivalent single pipe should have both a dry weight and submerged weight equal to those of the bundled pipes. Therefore, the upward buoyancy force on the equivalent pipe should be equal to that of the bundle. This means that the equivalent pipe should displace the same volume of fluid as the total of the bundled pipes. Therefore, the volume of the equivalent pipe should be the same as the total volume of the bundled pipes. Given a similar length, the equivalent pipe diameter can be defined as in Equation 4-15:

$$\frac{\pi}{4}D_{eq}^2 = \sum_{i=1}^{n}\frac{\pi}{4}D_i^2 \rightarrow D_{eq} = \sqrt{\sum_{i=1}^{n}D_i^2} \tag{4-15}$$

where D_{eq} is the outer diameter of the equivalent pipe.

After determining the equivalent diameter, an equivalent wall thickness can be defined by equating the equivalent pipe dry weight (from Equation 4-16) with the right-hand side of Equation 4-12. This results in the equivalent wall thickness (t_{eq}), as given in Equation 4-17:

$$W_{\ eq,dry} = \frac{\pi}{4}\left(D_{eq}^2 - \left(D_{eq} - 2t_{eq}\right)^2\right)\gamma_s \tag{4-16}$$

$$t_{eq} = \frac{1}{2}\left[\sqrt{\sum_{i=1}^{n}D_i^2} - \sqrt{\sum_{i=1}^{n}D_i^2 - \sum_{i=1}^{n}(D_i^2 - (D_i - 2t_i)^2)}\right] \tag{4-17}$$

The stiffness of the equivalent pipe is assumed to be the total stiffness of the individual pipes in the bundle:

$$(EI)_{\ eq} = \sum_{i=1}^{n}(EI)_i \tag{4-18}$$

where $(EI)_{\ eq}$ is equivalent pipe stiffness and $(EI)_i$ is the pipe stiffness for pipe *I* of the bundle.

Once the parameters associated with the equivalent pipe have been determined, they are used as inputs for the PRCI pull force method to estimate the pullback load required for bundled steel pipe HDD installations. When the total pullback load has been determined, the pull force applied on an individual pipe in the bundle

can be calculated based on a ratio of the total pullback force. This ratio can be determined by taking the net weight of the single pipe and dividing it by the total net weight of the bundled pipes.

The concept of equivalent pipe was first introduced in NEN 3650. However, NEN 3650 recommends different equations (rather than Equation 4-15 and 4-17) to determine the equivalent outer diameter and wall thickness, as in Equation 4-19 and 4-20:

$$D_{eq} = \frac{1}{n^{0.3}} \times \sum_{i=1}^{n} D_i \tag{4-19}$$

$$t_{eq} = \frac{1}{2}\left[\frac{1}{n^{0.3}} \times \sum_{i=1}^{n} D_i - \sqrt{(\frac{1}{n^{0.3}} \times \sum_{i=1}^{n} D_i)^2 - \sum_{i=1}^{n}(D_i^2 - (D_i - 2t_i)^2)}\right] \tag{4-20}$$

where n is the number of pipes in the bundle. NEN 3650 also includes a load factor ($f_{install}$) of 1.8 for bundled installations to increase the contingency factor and account for the risk of higher pull forces than calculated.

4.5 Bundled HDD Installation Case Studies

Five bundled HDD crossings were reviewed to investigate the accuracy of the proposed method of pull force estimation. These installations were completed in Alberta, Canada between 2013 and 2019, and were designed, inspected, or monitored during construction by CCI Inc. The HDD crossings ranged from 882 m to 1840 m in length, with final borehole diameters ranging from 762 mm to 1067 mm. These projects include crossings that are medium to large in scope, where pull force estimation and selection of the proper drilling rig are vital to project success. The projects involved installation of steel pipelines of various size and different numbers of pipes in the bundle. For each of the case studies, the majority of the crossing was drilled through bedrock. Table 4.1 and Table 4.2 summarizes the main characteristics of the case studies.

Table 4.1. Case studies description

Case Study	Crossing Feature	HDD Length (m)	HDD Depth Under Crossing Feature (m)	Drill Rig Size (Tonnes)	Crossing Location Topography	Geotechnical Condition
A	Road	882	32	200	relatively flat, entry point elevation slightly higher than exit	Sand overlaying Mudstone
B	Watercourse	1068	65	200	steep slopes at both sides of the river, entry and exit at same elevation	Clay and Clay Till overlaying Shale
C	Watercourse	1113	71	500	steep slopes at both sides of the river, entry and exit at same elevation	Clay and Clay Till overlaying Shale
D	Watercourse	1840	72	500 (entry side) 380 (exit side)	relatively wide section of the river valley, exit elevation 12 m higher than entry	Intermittent Clay and Sand overlaying Clay shale, Mudstone and Sandstone
E	Watercourse	1137	45	380	steep slopes at both sides of the river, exit elevation 33 m higher than entry	Clay Till overlaying Clayshale, Mudstone and Sandstone

Table 4.2. Case studies geometries

Case Study	Pipe Entry Angle	Pipe Exit Angle	Radius of Curvature (m)	Section 1* (m)	Section 2* (m)	Section 3* (m)	Section 4* (m)	Section 5* (m)	HDD Length (m)
A	14	18	400	65	98	548	126	45	882
B	20	24	400	425	140	10	169	324	1068
C	24	23	400	360	168	53	164	368	1113
D	20	18	1200	294	419	427	377	323	1840
E	18	18	1100	271	346	10	346	164	1137

* HDD path sections are defined as Figure 2

For each project, the maximum pull forces measured at the drilling rig were compared with the estimated pull forces. Prediction of the pullback force was determined using the conservative method of adding the individual pull forces for each pipe in the bundle, based on the PRCI method (PRCI, 2015). The pull force calculation was repeated using the proposed equivalent pipe method, and the equivalent pipe parameters were used as inputs for the PRCI method to estimate the pull forces for each case study. In addition, calculations were completed using the equivalent pipe method and pull force calculation recommended in NEN 3650 to compare both estimation methods. Table 4.3 lists the bundled pipe sizes and equivalent pipe

parameters determined based on the proposed method (Equation 4-15 and 4-17) and NEN 3650 (Equation 4-19 and 4-20).

Table 4.3. Bundled pipe and equivalent pipe sizes for five bundled pipe installations

Case Study	# Of Pipes in Bundle	Pipe Size	Pipe Outside Diameter (mm)	Pipe Wall Thickness (mm)	Borehole Diameter (mm)	Equivalent Pipe			
						Proposed method		NEN 3650	
						D_{eq} (mm)	t_{eq} (mm)	D_{eq} (mm)	t_{eq} (mm)
A	2	NPS 12 NPS 8	323.9 219.1	9.5 6.4	762	391.0	11.5	441.1	10.1
B	6	NPS 8 NPS 6 (x 4) NPS 3	219.1 168.3 (x 4) 88.9	5.6 4.8 (x 2) - 6.4 (x 2) 4.8	762	411.2	13.0	573.2	9.2
C	6	NPS 8 NPS 6 (x 4) NPS 4	219.1 168.3 (x 4) 114.3	5.6 4.8 (x 2) - 6.4 (x 2) 4.8	762	417.5	13.3	588.1	9.3
D	4	NPS 16 NPS 8 (x 3)	406.4 219.1	9.5 6.4	914	556.0	14.5	701.8	11.4
E	5	NPS 16 NPS 12 NPS 8 (x 2) NPS 6	406.4 323.9 219.1 168.3	9.5 9.5 6.4 5.6	1067	628.0	17.0	824.9	12.8

The density of clean drilling fluid (i.e., no cuttings) utilized during pullback for the various case studies ranged between 1060 kg/m^3 and 1200 kg/m^3. To ensure a conservative analysis and account for heavier fluids due to the accumulation of cuttings, a density of 1300 kg/m^3 was utilized in the analysis. Table 4 lists the input parameters for the PRCI and NEN 3650 methods.

Table 4.4. Input parameters for pull force calculations

Design Parameters	PRCI Method	NEN 3650 Method
Modulus of Elasticity – Pipe (MPa)	207,000	207,000
Poisson's Ratio – Pipe	0.3	0.3
Steel Pipe Density (kg/m^3)	7800	7800
Drilling Fluid Density (kg/m^3)	1300	1300
Fluidic Drag Coefficient (Pa)	173 [1]	50 [2]
Friction Coefficient – Pipe and Borehole Wall	0.3 [1]	0.2 [2]
Friction Coefficient – Pipe and Rollers	0.1	0.1
Modulus of Elasticity – Soil (MPa)	N/A	30
Modulus of Elasticity – Bedrock (GPa)	N/A	5

[1]- Recommended values as suggested by the PRCI method
[2]- Recommended values as suggested by the NEN 3650 method

Figure 4.3 shows the maximum measured pull force at the rig and the forces predicted using the above calculations. The conservative approach, based on the sum of individual pull forces, overestimated the total pull forces for each case study compared to measured maximum rig loads. For all five case studies, the proposed equivalent pipe parameters utilized in the PRCI method resulted in closer estimates of the maximum measured rig loads during pullback. Overestimation was more significant for pull forces calculated using the recommendations in NEN 3650.

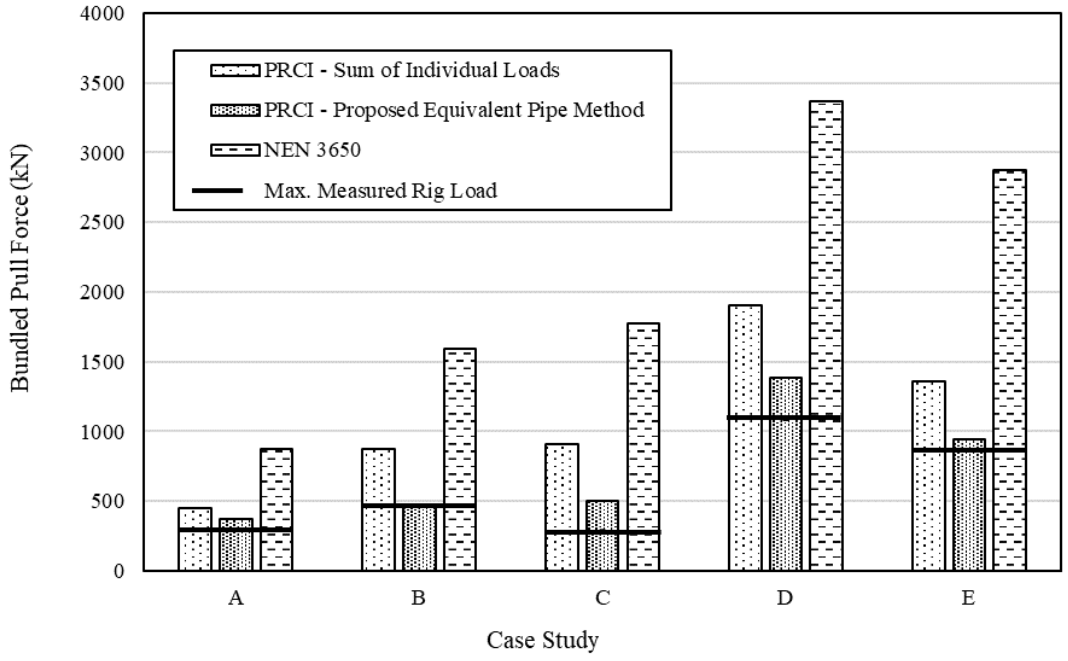

Figure 4.3. Comparison of theoretical pull force predictions with measured rig load for bundled installations

Table 4.5 summarizes the results of the pull force predictions for each of the case studies and presents the accuracy (as a percentage) between the predicted pull forces and pull forces measured at the rig during HDD operations. Comparisons show that the accuracy of the predicted pull forces ranges from +187% to +513% and +48% to +215% for the method described in NEN 3650 and the sum of individual pull forces determined by PRCI, respectively. Different contingency factors embedded in the pull force equations

suggested in NEN 3650 contribute to the high degree of conservatism of the predictions made using this method. It should be noted that while the PRCI method does not include contingency factors in the pull force equations, engineers commonly utilize safety factors ranging from 1.5 to 2 times the calculated pullback load. The inclusion of safety factors in these case studies would result in even more overestimation using the PRCI method.

The accuracy of the pull force estimations based on the proposed equivalent pipe parameters utilized in PRCI method ranges from +1% to +73%. Bundled pull force calculations based on the proposed equivalent pipe method led to closer estimations of the measured rig loads for all five case studies, demonstrating an improved accuracy for this approach compared to the other methods.

Table 4.5. Accuracy of pull force estimations compared to measured rig loads

Case Study	Sum of Individual Pull Forces - PRCI (kN)	Proposed Equivalent Pipe Method – PRCI (kN)	NEN 3650	Max. Measured Rig Load (kN)	Accuracy (%) *		
					Sum of Individual Pull Forces - PRCI	New Method	NEN 3650
A	450	369.6	871	303	+48	+22	+187
B	872	468.0	1592	463	+88	+1	+244
C	910	499.5	1774	289	+215	+73	+513
D	1900	1385.6	3367	1090	+74	+27	+209
E	1357	939.5	2871	861	+58	+9	+234
				Average	+97	+26	+277

*Calculated using (Predicted Value – Measured Value) / Measured Value × 100%

4.6 Conclusions

The concept of an equivalent single pipe to calculate the pull force required for bundled steel pipe installations by HDD was investigated in this paper. In the proposed method for pull force estimation, an equivalent pipe is defined to represent the bundled pipe group for the pullback analysis. The equivalent pipe is defined to have properties (e.g., dry weight, submerged weight, and stiffness) equivalent to those of all individual pipes in the bundle. A review of five case studies involving bundled HDD installations of two to six pipes in a bundle, including steel pipes from NPS 3 to NPS 16, showed that pull force predictions

based on the sum of individual pull forces determined by PRCI gave conservative results which overestimated the pull forces measured at the rig during installation. Overestimation was also observed for pull forces calculated for all case studies using the equivalent pipe method in NEN 3650.

The accuracy of pull force predictions improved significantly compared to actual recorded pull forces when calculations were based on the modified PRCI method using the proposed equivalent pipe parameters. The simple equivalent pipe method can be used to extend the PRCI method for pull force estimation of steel bundled pipes in medium to large HDD crossings.

5. Chapter 5: Stress Analysis of Steel Pipe Installation in Horizontal Directional Drilling based on Strain Monitoring[1]

5.1 Introduction

Trenchless technologies have become increasingly common for pipeline installation beneath waterbodies, roads, and other obstacles at the surface where traditional open-cut construction is not feasible. Horizontal directional drilling (HDD) is a trenchless method for pipe installation initially adopted by the oil and gas industry (Yan et al., 2018). Through continuous advancement of steering and navigation tools and integration of modern technologies utilized in the oil and gas sector, HDD gained increasing attention from utility companies as a feasible, cost-effective alternative to open-cut methods. Since the first HDD crossing completed in northern California in 1971, HDD has expanded from a few contractors to a multibillion-dollar industry worldwide (Bueno, 2021). Initially a simple utility boring technology, HDD has progressed to a sophisticated method with the capacity to install pipes over 127 cm (50 in) in diameter (Najafi, 2014). During installation, the product pipe is subject to a complex combination of stresses and strains. The long-term performance of a pipeline installed by HDD pipe is affected by the loads on the pipe during installation. The loads developed during installation are sometimes greater than the long-term operational loads, and may govern the design requirements. There is a combination of axial and circumferential stresses and strains imposed on the product pipe during HDD installations. However, to date limited research has been done to analyze the stresses and strains on the product pipe during installation. Gelinas et al. (2000) conducted one of the first field tests using two instrumented high-density polyethylene (HDPE) pipes installed using HDD. The method involved collecting readings from a pressure transducer attached to the drill rig hydraulic system and strain gauges from instrumented test sections inside the pipe. Data were recorded during pullback operations and for several hours after the installations were complete. The recorded strains were

[1] A version of this chapter has been submitted to Journal of Tunneling and Underground Space Technology.

depicted over time and associated with the approximate location in the bore path. Polak et al. (2004) continued previous experimental work by conducting five field tests on instrumented HDPE pipes installed by HDD and examined the mechanical behavior of the pipes, their stiffness, strength, and deformation. The results showed the variation in pipe strain with time along the bore path, including both flexural and axial deformations. Cholewa et al. (2010) conducted physical experiments on HDPE pipe responses during and after installation in a laboratory setting. The axial stress and strains inside the pipe were quantified during simulated installation, strain recovery, and stress redevelopment after the pipe was restrained.

While the above-mentioned studies investigated the stresses and strains developed in polyethylene pipe during HDD installation, there is a lack of detailed stress and strain analysis for the loads imposed on steel pipe during pullback. Steel pipelines account for a critical part of oil and gas installations as well as municipal infrastructure. Steel pipe is predominately used to transport hazardous liquids, including crude oil and refined petroleum products (Pipeline & Hazardous Materials Safety Administration, PHMSA, 2015). HDD is becoming a popular option for steel pipeline construction and replacement in oil and gas industry due to improved efficiency and reduced cost compared to open cut method (Trenchlesspedia, 2021). Therefore, a more detailed investigation is required to evaluate the stresses and strains developed during installation of steel pipe by HDD to ensure the long-term structural safety of pipelines while identifying areas for design improvement.

This paper presents a strain measurement system that was developed and utilized on several major HDD crossings to record the strains imposed on steel pipes during the pullback phase of HDD projects. The load conditions and corresponding strains on the pipe cross-section change as the pipe progresses through the borehole. An assessment of the structural integrity of the installed pipe is completed by analyzing each load component and the combined effect of these loads on the pipe throughout the installation process. Comparison of theoretical predictions with the data measured during pullback is undertaken to ensure that current design standards are reliable.

5.2 Expected Installation Loads

In North America, the analysis method developed by Pipeline Research Council International (PRCI, 2015) remains the most common industry-wide standard to model the stresses imposed on steel pipelines and allowable limits for stresses during installation. The basis for this model is a theoretical profile comprising straight and curved sections within the HDD alignment. The load conditions imposed on the pipe during installation include the axial tensile pulling force, net external hoop pressure, and curvature-induced bending.

During pullback, a pulling force supplied by an HDD drilling rig is required to install the product pipe in the borehole. The applied pulling force must overcome all resistive forces encountered during the product pipe installation (Cai and Polak, 2019). The resulting tension is assumed to act at the centroid of the pipe cross-section, resulting in a uniform axial tensile stress on the cross-section of the pipe. An external circumferential (hoop) stress from the external pressure is also imposed on the pipe during the installation process. The external pressure is mainly a function of the hydrostatic pressure due to the weight of the drilling fluid surrounding the pipe and the earth pressure, with some contribution from the hydrokinetic pressure due to the flow of drilling fluid and the surge or plunger action produced by moving the pipe into the borehole (PRCI, 2015). For larger pipe installations, when water is present inside the pipe due to the application of buoyancy control, the internal hydrostatic pressure of the water is considered when calculating the net pressure applied on the pipe. As the pipe is pulled through the curved sections of the drill path, the curvature imposes an axial bending strain on the cross-section of the pipe (Silva et al., 2009). The curvature-induced bending results in an axial compressive strain at the top of the pipe section and an axial tensile strain on the bottom.

The stress imposed on the pipe cross-section during installation is assumed to result in a biaxial stress state, including axial tensile stress from the pulling force, circumferential compressive stress from the net external hoop pressure, and axial bending stress along the curved sections. For the curved sections of the bore path, a linearly varying axial strain is expected on the pipe cross-section, as a result of the combined tensile and bending forces. The circumferential strain is also expected to vary linearly over the cross-section in curved

sections due to Poisson's ratio effect of the axial stress. A detailed investigation of the forces present during the pullback process is completed in the next sections by evaluating the axial and circumferential stresses, as well as the strain imposed on the pipe as it is forced to conform to the borehole geometry.

5.3 Strain Testing Methodology

The determination of strain components from strain gauge measurements is necessary to measure the maximum longitudinal and circumferential strains and stresses on the pipe during installation. Due to the simultaneous application of axial load and bending moments on the pipe, at least three strain measuring points on the pipeline circumferential are required at the selected cross section to differentiate between the axial strain due to bending along axes x and y and the axial load strain along axis z (Figure 5.1). Based on the analysis done by Gawedzki (2015), the smallest error in determining the longitudinal strain components is achieved by measuring the strain at four equally distributed points along the pipe circumference (strain measured every 90º). The principal stresses on the pipe during installation are in the longitudinal and circumferential directions. The strain gauges should be oriented so that one grid measures the principal strain along axis 1 (the longitudinal axis of the pipe), ε_1, and the second grid measures the principal strain along axis 2 (the circumferential axis of the pipe), ε_2, (Keil, 2017).

The monitoring system used in this research utilized eight strain gauges, which were attached at 0°, 90°, 180° and 270° relative to the pipe crown. At each position, two strain gauges were installed to measure the strains in the axial and circumferential directions. Figure 5.1 shows a schematic of the placement of the strain gauges inside the 10-m test section of the pipe.

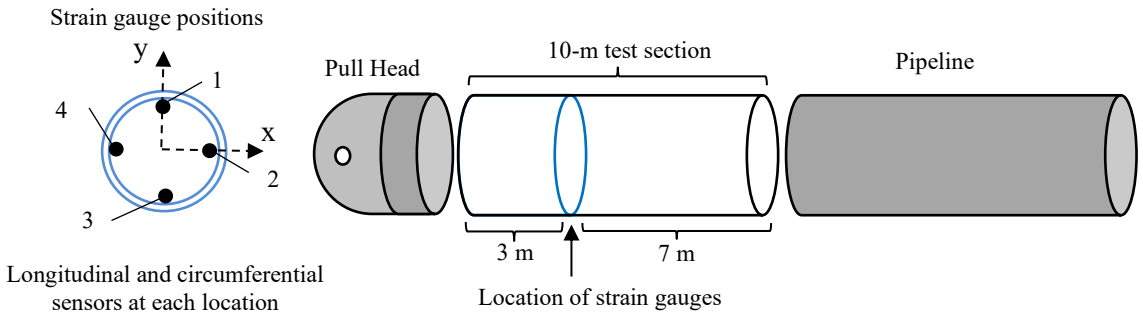

Figure 5.1. Strain gauge assembly

Due to the high likelihood of the strain gauges being damaged or destroyed during HDD operations if they were to be placed on the outside of the pipe, the strain gauges were installed inside the pipe. To eliminate any impact of the installation of sensors on the interior of the product pipe, the sensor assembly was installed inside a 10 m test section of the product pipe which was directly attached to the pullhead and welded in place to the front of the pipeline. The gauges were placed at a distance of approximately three meters from the beginning of the test section, as measured from where the test section was welded to the pullhead. This distance acts as a buffer to assist in minimizing any errors in the strain measurements due to the effect of the weld and the stiffness of the pullhead on the pipe section (a distance beyond of two to three times pipe diameter from the weld is considered an acceptable range to be outside of the heat affected zone and the stiffness effect).

The pipe section was cleaned and prepared and the gauges were welded onto the inside of the pipe. The recorder was fastened inside the pipe near the pull head end and the baffle assemblies were then installed to ensure gauges were protected. Once secured, this 10-m pipe section was taken to the site and welded on the front of the pull section. Twelve to twenty-four hours prior to the scheduled pullback, the recorder was inspected, turned on, and the pull head was installed on the pipe section. The recorder has a battery life and data storage capacity of 7 to 10 days depending on the ambient temperature. The recorder records data every two seconds for the entire duration of its battery life and memory capacity.

Figure 5.2 shows the gauges installed inside the test section of the product pipe.

Figure 5.2. Strain gauges installed inside the pipe

The recording instrumentation was fastened to the pipe wall in a watertight container designed to endure the hydrostatic pressures encountered during water fill for buoyancy control (Figure 5.3). Details about the calibration of the strain gauge system are provided in Appendix A.

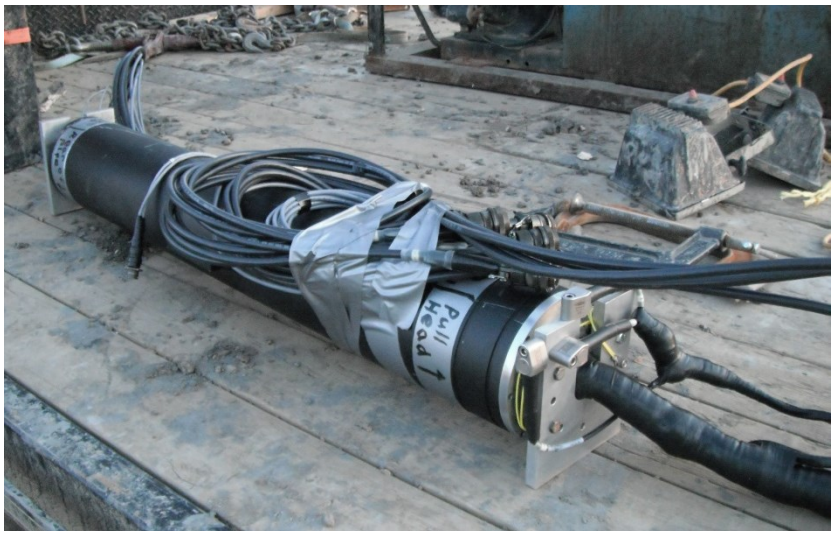

Figure 5.3. Watertight container hosting strain recording instrumentation

5.4 Strain-Stress Relationships

As discussed previously, the expected loading on the pipe during pullback at the location of strain gauges includes axial tensile stress from the pull force, axial bending stress distribution from bending in the horizontal and vertical planes, circumferential compressive stress from the external pressure on the pipe, circumferential tensile stress from internal water (if water is added to the pipe for buoyancy control), and the corresponding Poisson's effect on the axial and circumferential stresses on the pipe.

The assessment of the imposed strains and the separation of axial tensile and bending strain can be complicated, since the initial location of the strain gauges changes along the bore path due to the rotation of the pipe section. As the pipe is pulled into the borehole, some rotations transfer from the swivel and the reamer assembly to the pipe, causing the orientation of strain gauges to change constantly during the installation. However, stress components can be calculated from the strain measurements based on the biaxial stress condition and the fact that the strain gauges readings correspond to the principal stresses applied to the pipe, which are the longitudinal and circumferential stresses. As a thin-walled pipe, the pipeline will behave as a thin cylindrical shell and can be assumed to be subject to plane stress, a biaxial stress condition comprising the axial stress and hoop stress. The plane stress condition is based on the assumption that the pipeline is restrained in the axial direction, but that there is no restraint against radial deformation for the loading comprising the axial pull force, longitudinal bending from the imposed curvature, and the net external hoop pressure.

The effect of the restrained condition is that the combined axial stress comprises the pull force axial stress, curvature bending stress and Poisson's ratio of the net external hoop stress. The total combined stress in the hoop direction will, however, only include the net external hoop stress since due to the Poisson effect, the axial stress will only cause an unrestrained hoop strain due to the lack of radial restraint. When combining the axial stress components, it is necessary to include the direction of each component. Assigning a positive sign for tensile stress and a negative sign for compressive stress, the axial pull force stress is positive, while the bending stress is positive at the bottom of the pipe and negative at the top. Similarly, the hoop stress

due to the external pressure on the pipe is negative, and Poisson's ratio due to the applied hoop stress is positive.

The recorded strain data was analyzed to obtain the pipe stresses at the leading section of the pipeline. Based on the assumptions discussed above, the average values obtained from the stresses calculated based on each gauge measurement and the strain-stress relationship from Hooke's law were utilized to represent the overall stress condition applied to the pipe. The following equations summarize the strain-stress relationships at each gauge location (Figure 5.1):

$$E\varepsilon_{axial} = \sigma_{axial} = \sigma_{pull} \mp \sigma_{bending,x} + \vartheta\sigma_{hoop} \quad \text{at Gauges 1 \& 3} \quad (5\text{-}1)$$

$$E\varepsilon_{hoop} = \sigma_{hoop} - \vartheta(\sigma_{pull} \mp \sigma_{bending,x}) \quad \text{at Gauges 1 \& 3} \quad (5\text{-}2)$$

$$E\varepsilon_{axial} = \sigma_{axial} = \sigma_{pull} \mp \sigma_{bending,y} + \vartheta\sigma_{hoop} \quad \text{at Gauges 2 \& 4} \quad (5\text{-}3)$$

$$E\varepsilon_{hoop} = \sigma_{hoop} - \vartheta(\sigma_{pull} \mp \sigma_{bending,y}) \quad \text{at Gauges 2 \& 4} \quad (5\text{-}4)$$

where σ_{axial} is the total axial stress, σ_{pull} is the axial stress resulting from the pull force, σ_{hoop} is the circumferential stress, $\sigma_{bending,x}$ is the axial bending stress along the x-axis (which passes through gauges 2 and 4), $\sigma_{bending,y}$ is the axial bending stress along the y-axis (which passes through gauges 1 and 3), ε_{axial} is the measured axial strain, ε_{hoop} is the measured circumferential strain, E is the modulus of elasticity of the pipe, and ϑ is Poisson's ratio.

Using Equations 5-1 through 5-4, the strain-stress relationships can be written as in Equations 5-5 through 5-9:

$$\sigma_{pull} = \frac{E}{2\,(1+\vartheta^2)} \sum_{i=1}^{4} (\varepsilon_{axial,i} - \vartheta\varepsilon_{hoop,i}) \quad (5\text{-}5)$$

$$\sigma_{hoop} = \frac{E}{2\,(1+\vartheta^2)} \sum_{i=1}^{4} (\varepsilon_{hoop,i} + \vartheta\varepsilon_{axial,i}) \quad (5\text{-}6)$$

$$\sigma_{bending,x} = \frac{E}{2}(\varepsilon_{z,3} - \varepsilon_{z,1}) \quad (5\text{-}7)$$

$$\sigma_{bending,y} = \frac{E}{2}(\varepsilon_{z,4} - \varepsilon_{z,2}) \quad (5\text{-}8)$$

$$\sigma_{bending,total} = \sqrt{\sigma_x^2 + \sigma_y^2} \quad (5\text{-}9)$$

where $\varepsilon_{axial,i}$ is the axial strain measured at gauge i; $\varepsilon_{hoop,i}$ is the circumferential strain measured at gauge i; and $\sigma_{bending,total}$ is the resultant bending moment calculated from the bending moments acting along the x- and y-axis.

5.5 Field Measurements

The method outlined above for measuring strains on the pipe during installation was utilized in two major HDD crossings as part of a pipeline construction project in Alberta, Canada. The first installation (HDD-1) was of a 1,112 m river crossing with an elevation difference of over 100 m between the entry and exit sites. The second installation (HDD-2) was a 1,390-m installation across a waterbody in an 800-m-wide valley. Both crossings involved a steel pipeline (762 mm O.D., NPS 30) with a specified minimum yield strength of 483 MPa. For both HDD crossings, the strain imposed at the strain gauges was recorded every 2 seconds during the pullback phase. The pullback phase duration was 22 hours and 12 hours for HDD-1 and HDD-2, respectively. During pullback, water was added to the pipes during both crossings to reduce the required pull forces as a form of buoyancy control—however, the timing of the application of buoyancy control varied for the two HDD installations. The borehole profiles for the two HDD installations and the corresponding geotechnical conditions are included in Figure 5.4 and 5.5. The design parameters for both HDD installations are summarized in Table 5.1.

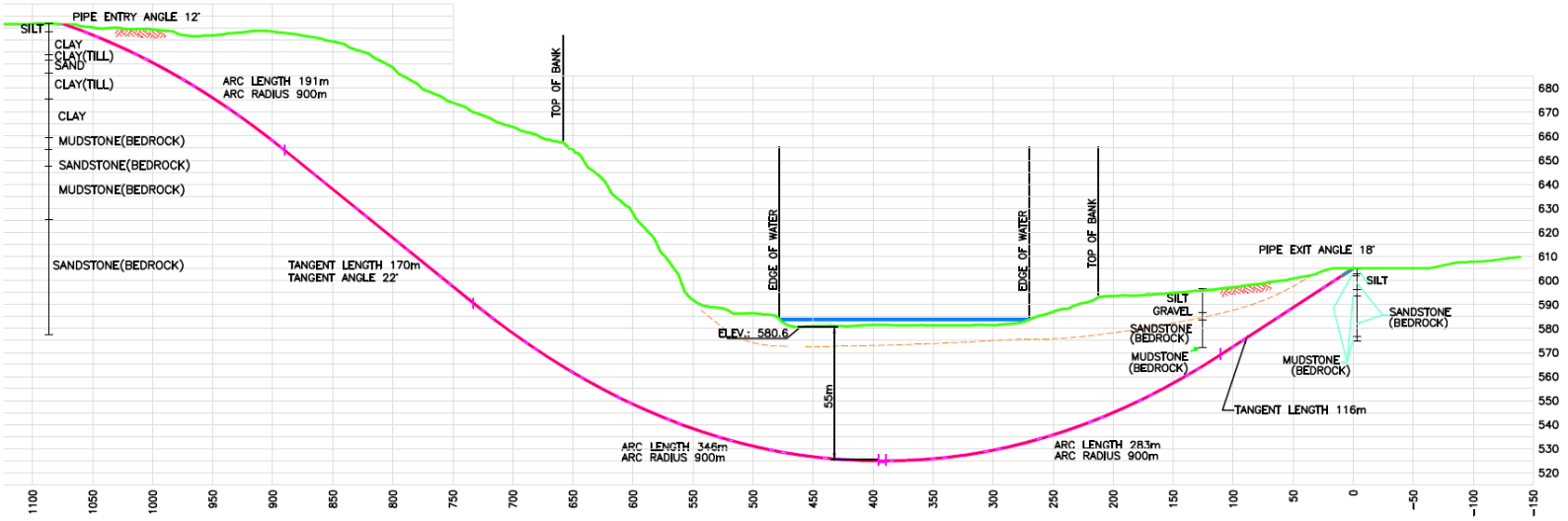

Figure 5.4. Drill path profile geometry for HDD-1

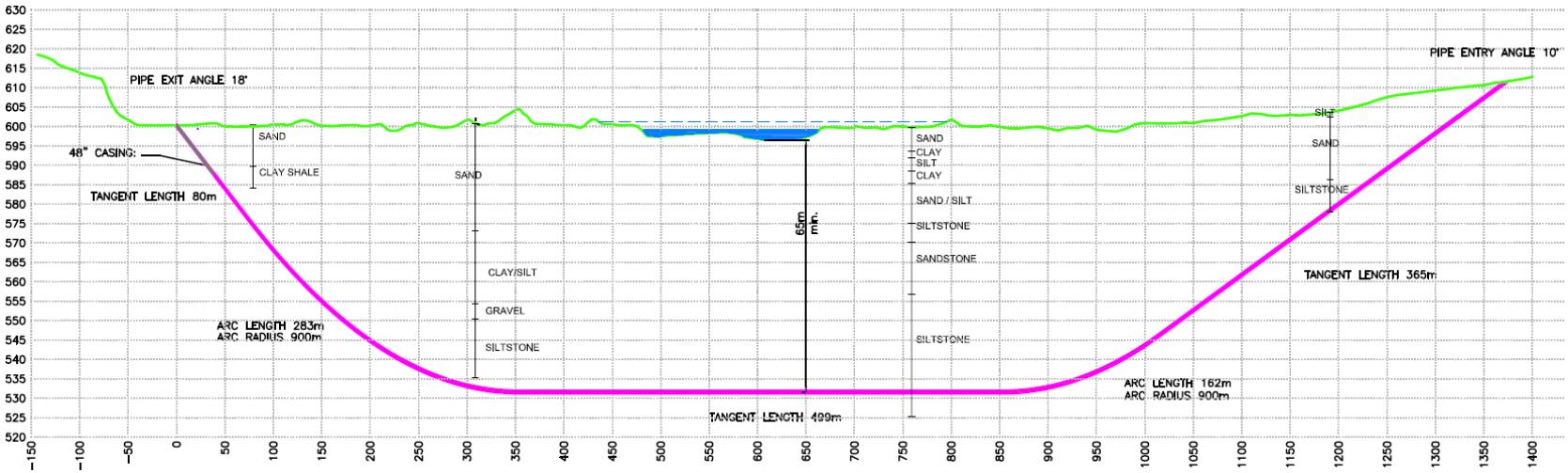

Figure 5.5. Drill path profile geometry for HDD-2

Table 5.1. Summary of design parameters for HDD installations with stress/strain gauges installed on product pipe test section

Design Parameters	HDD-1	HDD-2
Outside diameter of pipe (mm)	762	762
Wall thickness of pipe (mm)	15.8	15.8
Specified minimum yield strength of pipe (MPa)	483	483
Modulus of elasticity of pipe (MPa)	207,000	207,000
Radius of curvature (m)	900	900
HDD entry (pipe exit) angle	18°	18°
HDD exit (pipe entry) angle	12°	10°
Total crossing length (m)	1,112	1,389
Depth of cover of bore under waterbody (m)	55	65
Bottom depth of HDD bore from rig elevation (m)	68	80
Borehole diameter (mm)	1067	1067
Outside diameter of drill pipe (mm)	139.7	139.7
Wall thickness of drill pipe (mm)	10.54	10.54
Drilling fluid density (kg/m^3)[1]	1318	1378
Drilling rig size (kg-force)	200,000	300,000
Fluidic drag coefficient (Pa)	172	172
Friction coefficient between pipe and borehole	0.3	0.3
Friction coefficient between pipe and ground rollers	0.1	0.1

[1] Densities represent the maximum slurry density observed during the line pull

5.6 Strain Data

Figure 5.6 and 5.7 show the variation in the axial and circumferential strains recorded at each gauge for the duration of pullback for HDD-1 and HDD-2, respectively. The length of pipe installed along the bore path is also shown (secondary axis). The largest measured strains were significantly less than the strains corresponding to the elastic limit deformation for the pipe in stress-based design methods, i.e., 0.5% or 5000 microstrain, $\mu\varepsilon$ (PRCI, 2011); thus, these installations were governed by an elastic state.

Each spike in Figure 5.6 and 5.7 corresponds to the pull of the product pipe over the length of one joint of drill pipe (approximately 10 m). Figure 5.8 shows a typical variation of the axial and circumferential strain during pullback over the length of one joint. For each length of drill pipe (joint), the variation in axial strain

during pullback is characterized by an initial rapid increase in axial tensile strain, followed by a continuous variation in strain, then a rapid decrease and, finally, a longer period of essentially constant strain values before the beginning of pullback for the next joint. The initial rapid increase in tensile strain at the start corresponds to the application of the pull force required to exceed the initial static friction resistance and drilling mud drag and initiate the forward displacement of the pipeline segment. There is a rapid drop in the pull force at the end of the pullback of the drill pipe joint, corresponding to when one drill pipe segment is prepared for removal. During this time (i.e., removal of the drill pipe) that the pipeline remains stationary, constant axial strains are recorded at all gauges prior to the start of the next pullback cycle. The variation in circumferential strain during pullback of each drill pipe joint shows a recurring pattern, represented by a rapid increase in compressive strain due to the effect of Poisson's ratio and the axial strains, as seen in Figure 5.8.

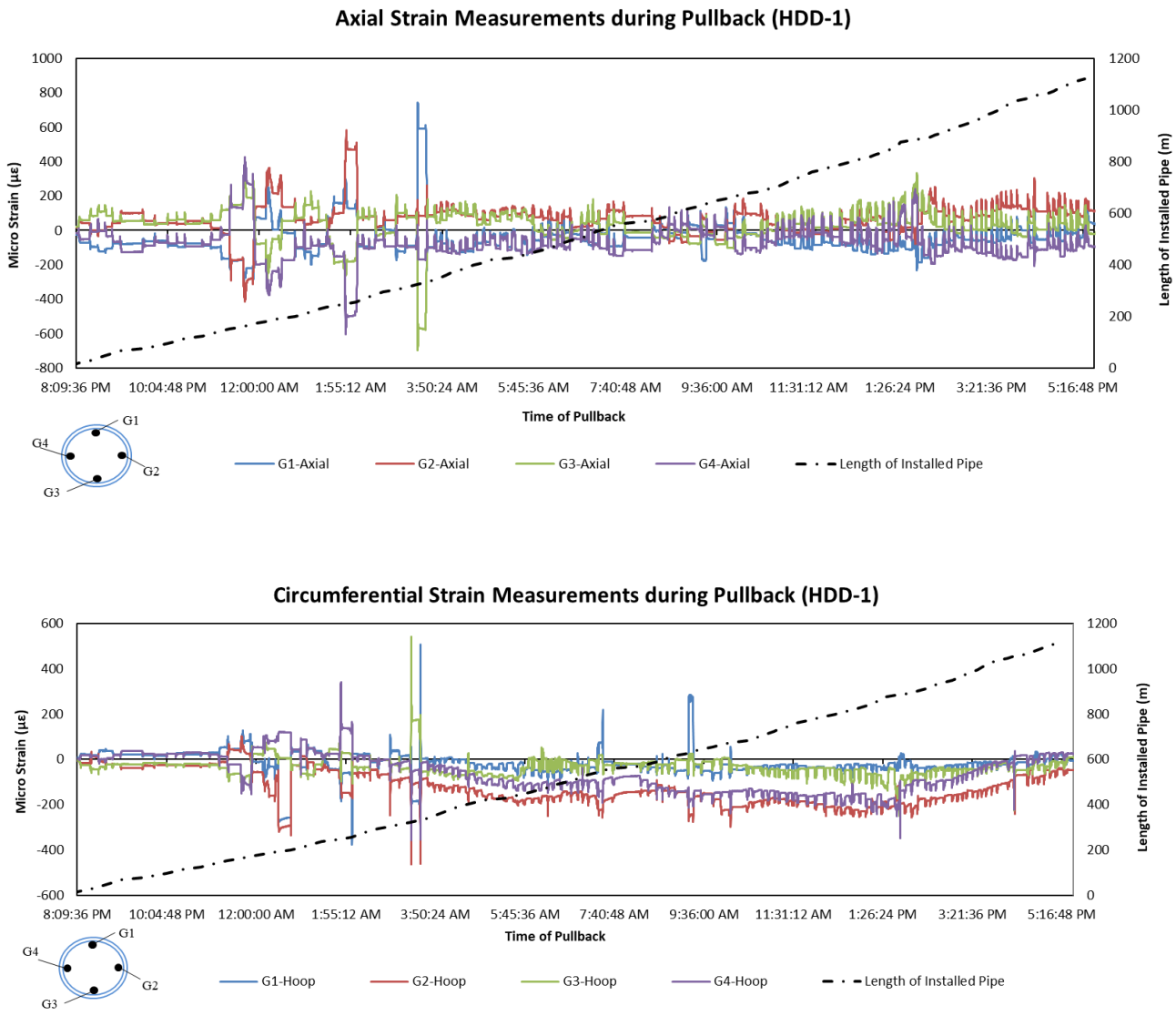

Figure 5.6. Raw data from strain gauges for HDD-1 (measured axial and circumferential strains during pullback)

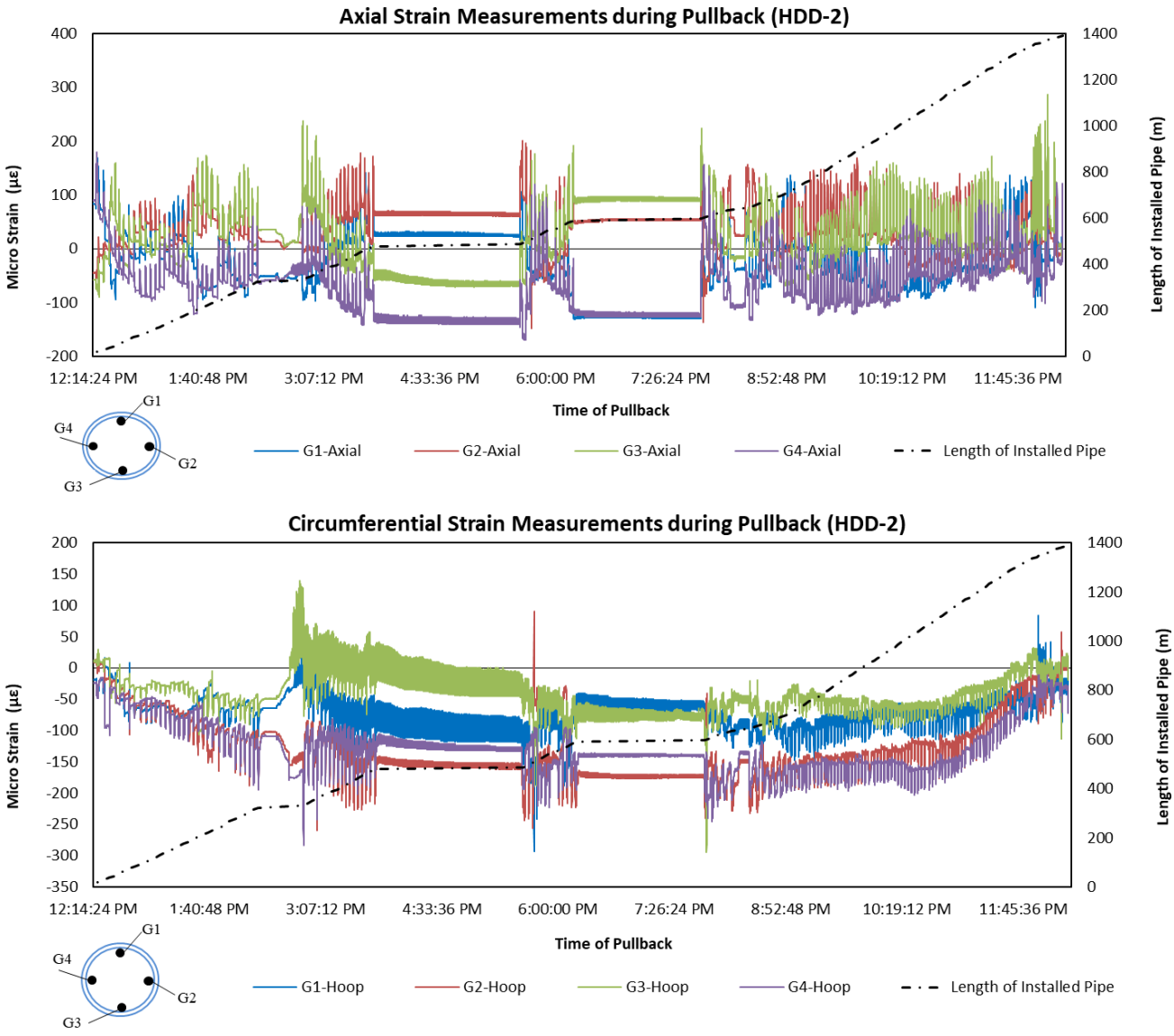

Figure 5.7. Raw data from strain gauges for HDD-2 (measured axial and circumferential strains during pullback)

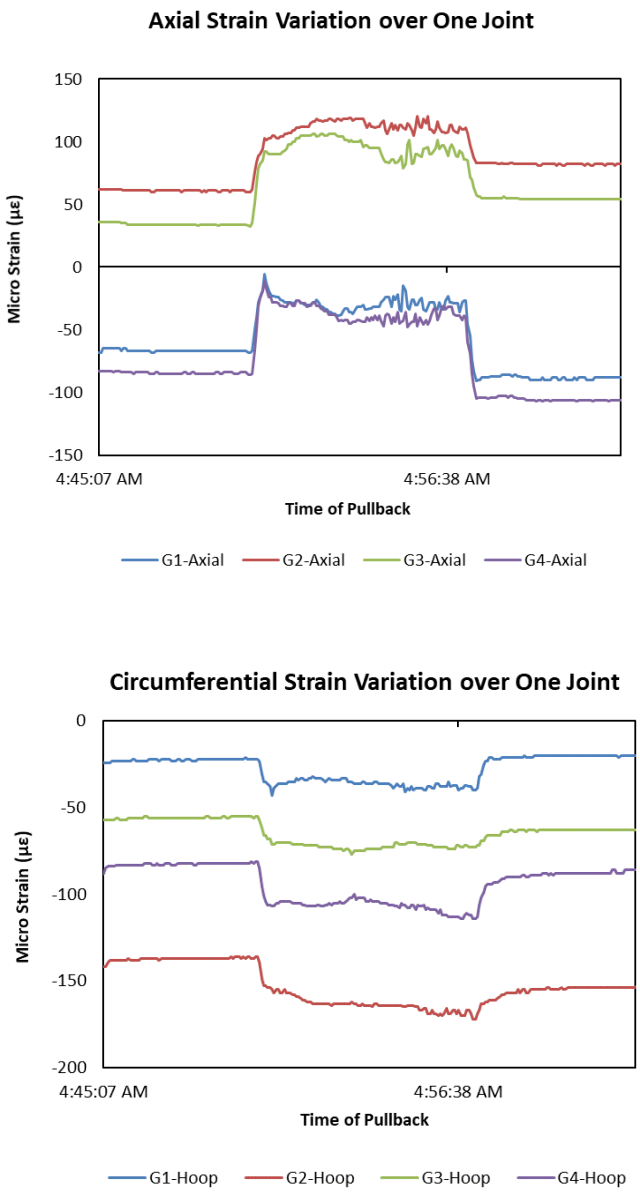

Figure 5.8. Typical variation in axial and circumferential strain over a single joint of drill pipe during pullback

5.7 Analysis

5.7.1 Theoretical Stress Predictions

An engineering assessment of the crossings was conducted using the PRCI method. The calculation accounts for the geometry of the crossings, pipe parameters, operating conditions, and typical

considerations such as drilling fluid properties, frictional forces, etc., as shown in Table 5.1. The maximum stresses resulting from the calculations are summarized in Table 5.2.

Table 5.2. Summary of design parameters for HDD installations

Design Parameters	HDD-1	HDD-2
Estimated Maximum Pull force - w/ buoyancy control[1] (kN)	513.4	784.1
Estimated Maximum Pull force - w/o buoyancy control (kN)	1375.3	2208.7
Allowable Tensile Stress (MPa)	434.7	434.7
Maximum Tensile Stress - w/ buoyancy control[1] (MPa)	13.9 (3.2% allowable)	21.4 (4.9% allowable)
Maximum Tensile Stress - w/o buoyancy control (MPa)	37.2 (8.6% allowable)	59.7 (13.7% allowable)
Allowable Bending Stress (MPa)	316.2	316.2
Bending Stress - based on design radius (MPa)	87.7 (27.7% allowable)	87.7 (27.7% allowable)
Maximum Bending Stress - based on minimum as-drilled radius[2]	210.9 (66.7% allowable)	134.6 (42.6% allowable)
Allowable Hoop Stress (MPa)	52.1	52.1
Maximum Hoop Stress (MPa)	32.2 (61.9% allowable)	25.4 (48.8% allowable)
Combined Stress Unity Check (Tension and Bending)	0.30	0.32
Combined Stress Unity Check (Tension, Bending, and Hoop)	0.51	0.37

[1] 100% of the pipe submerged in drilling fluid was assumed to be filled with water
[2] Tightest radius was based on the minimum as-drilled radius over a 30 m length while executing the pilot hole, which is 374 m for HDD-1 and 586 m for HDD-2

5.7.2 Stress Analysis from Strain Gauges

5.7.2.1 Tensile Stress

The strain gauge readings were used to calculate the average pulling stresses using Equation 5-5. The results are shown in Figure 5.9 and 5.10 for the two HDD crossings. The calculated values were compared with the theoretical predictions for cases with and without buoyancy control. The axial stress resulting from the average applied rig pull force was also calculated.

For both studies, the axial pulling stresses based on strain measurements were observed to have similar stress values due to the pull force applied by the drilling rig. This indicates that the system of strain gauges was able to measure the imposed forces under the applied load. Based on observations of the installations, the contractors added water into the pipes when the pull forces were increasing, and a partial buoyancy

control was utilized in both case studies. The predicted tensile stresses without buoyancy control were demonstrated to be the upper limit for the measured stresses, due to the partially filled pipeline during pullback. For the second installation (HDD-2), the contractor added more water into the pipe as the pullback progressed, and the tensile stress predicted using buoyancy control matched measured stresses throughout the last third of the installation.

For HDD-1, the maximum pulling stress measured during pullback (28.2 MPa) occurred when 855 m of the pipe was installed, within the exit tangent. (Figure 3.9). For HDD 2, the maximum pulling stress was captured at 590 m installed length (at 7:50:22 PM) with a stress value of 30.1 MPa. At this location, pullback operations resumed after a shutdown of approximately 90 minutes due to equipment repair. The maximum rig pull force was also observed at this location when pullback operations resumed, and pipe movement restarted. In both projects, the recorded axial strain levels are significantly lower than the axial strength capacity of the pipe (434.7 MPa).

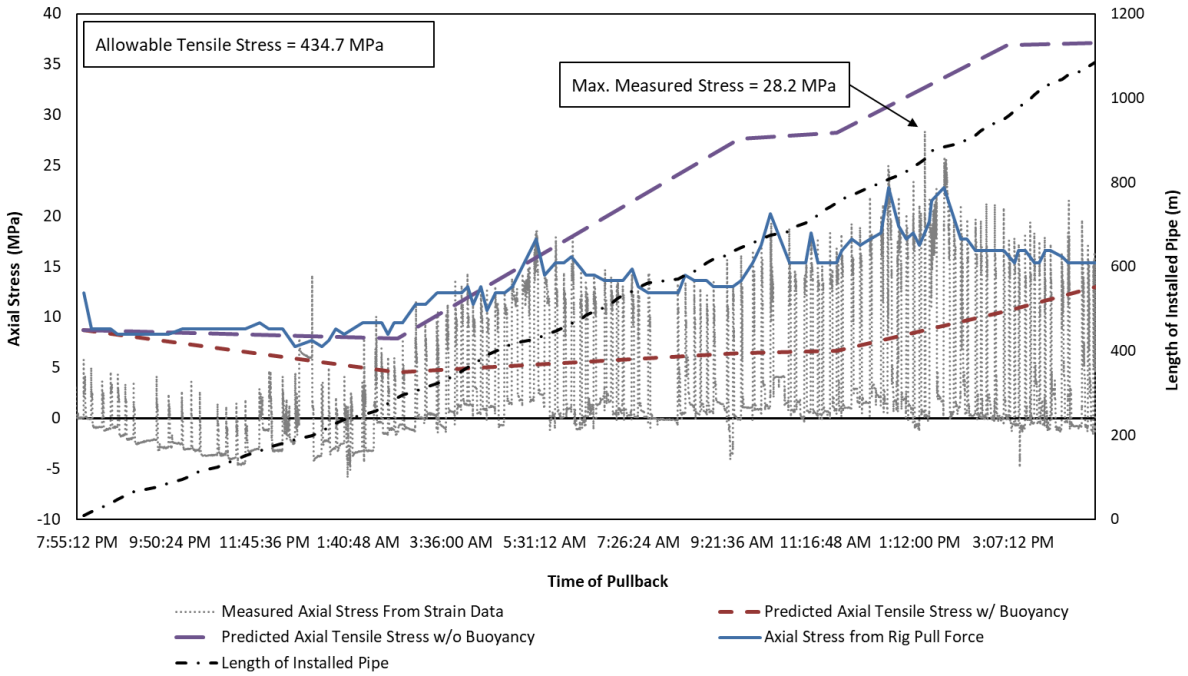

Figure 5.9. Comparison of axial stress based on measured strain data, predicted axial tensile stress and rig pull stress for HDD-1

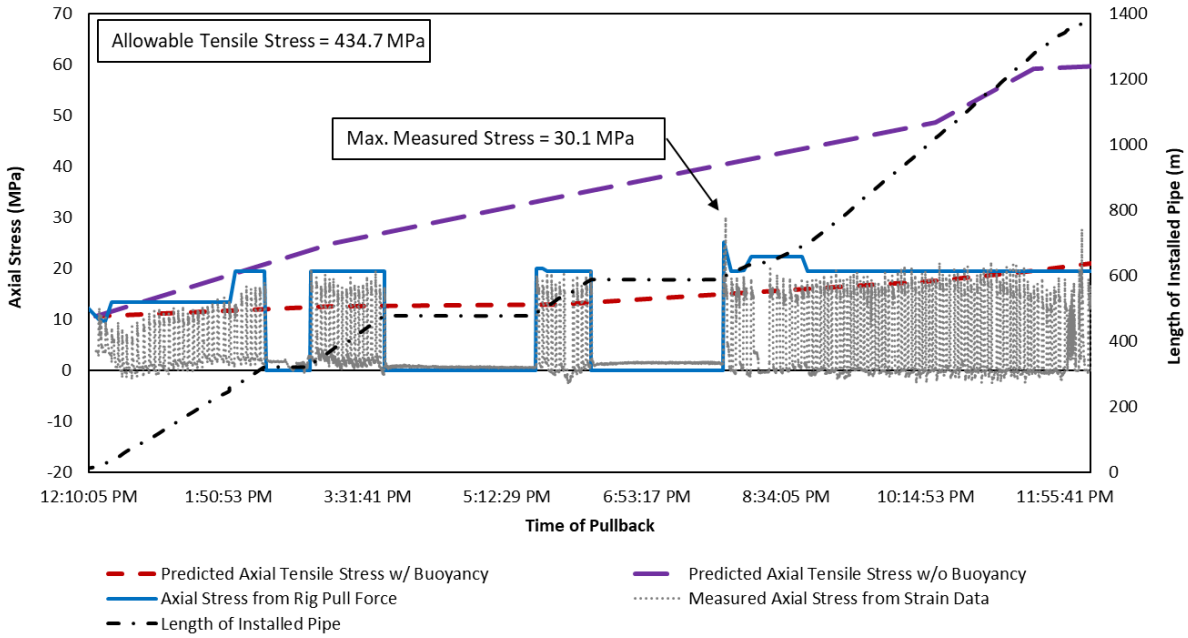

Figure 5.10. Comparison of axial stress based on measured strain data, predicted axial tensile stress and rig pull stress for HDD-2

5.7.2.2 Bending Stress

In addition to tensile stress, strain measurements were used to calculate the bending stress using Equation 5-7, 5-8 and 5-9. The maximum stress was calculated based on the outer diameter of the cross-section rather than the location of the strain gauges inside the pipe. As seen in Figure 5.11 and 5.12, the pipe cross-section was subject to bending moment components along the axes defined by each pair of gauges (Figure 5.1), with the resultant bending moment located along a different axis. The presence of a bending moment across each pair of gauges was observed at all locations along the borehole path, including the straight sections. This is due to the as-built condition of the drill path. The as-built HDD profile proceeds along a three-dimensional path, with incremental displacement in both the vertical and horizontal planes, resulting from the steering corrections that constantly take place while drilling to ensure that the actual hole conforms to the designed drill path.

As-built steering data obtained while drilling of the pilot hole was reviewed for each installation. The tightest as-built radius was identified for each borehole and used to estimate the maximum expected bending

stress, as in Table 5.2 and Figure 5.11 and 5.12. The bending stress—predicted based on the radius of curvature in the design—is also shown in these figures. On review of the bending stress calculated from strain data, the maximum bending stresses expected from the smallest as-built radii of the drill profiles were not observed in the strain gauge measurements, particularly for HDD-2.

Based on the strain data, the maximum bending stresses for HDD-1 and HDD-2 were 155.0 MPa and 39.4 MPa, respectively. The location of the maximum bending stresses observed for HDD-1 (Figure 3.11) does not correspond with any locations where the as-built radii (determined based on drilling survey data) is tight. Instead, the location of the maximum seems to be a result of locally imposed loading on the pipe inside the borehole. For HDD-2, the maximum observed bending stress was less than the predicted values and occurred at the location just before the pipe entered the surface casing, approximately 50 m away from the rig. While drilling the pilot hole at this location, the driller needed to steer tighter, adjusting the drill path trajectory to compensate for the deflection of the end of the casing from the designed path. This increased curvature seems to have caused a higher bending stress than the low bending expected within the straight section of the bore path.

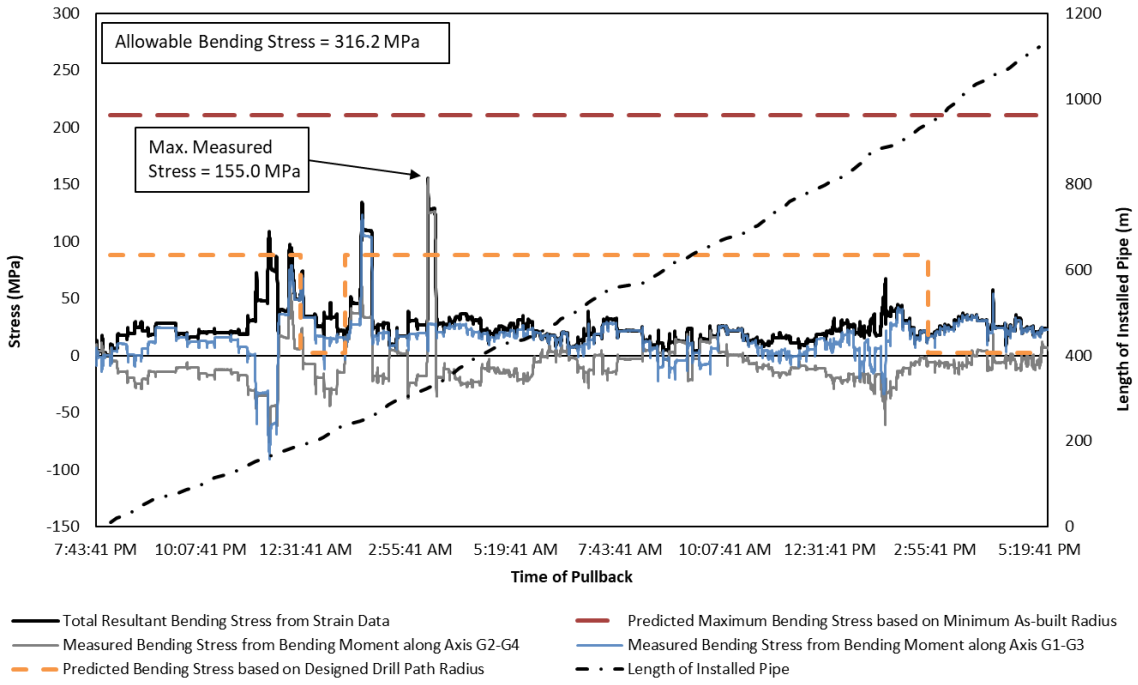

Figure 5.11. Axial bending stress on pipe calculated from measured strain data compared to maximum expected bending stresses for HDD-1

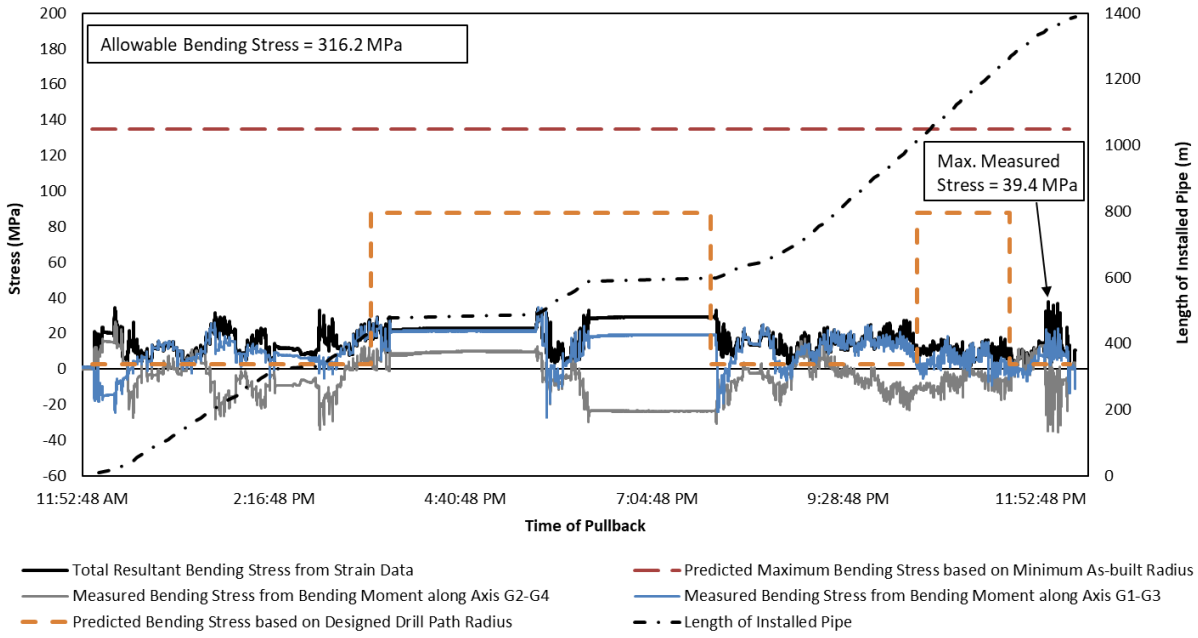

Figure 5.12. Axial bending stress on pipe calculated from measured strain data compared to maximum expected bending stresses for HDD-2

5.7.2.3 Circumferential Stress

Hoop stress was calculated from strain measurements using Equation 5-6 and compared with theoretical predictions for both HDD-1 and HDD-2, as shown in Figures 5.13 and 5.14, respectively. The predicted circumferential stress was calculated by following PRCI guidelines and determined based on the drilling fluid hydrostatic pressure and earth pressure, without accounting for the hoop tensile stress from the water inside the pipe used for buoyancy control. The heaviest drilling mud densities observed during pullback (given in Table 1) were used in the calculations for predicted hoop stress, giving conservative fluid pressure estimates.

For both installations, an increase in the measured compressive stress values is seen as the installation depth increases along the HDD profile (Figures 5.13 and 5.14). During pullback, positive increases in imposed tensile hoop stresses were observed due to the addition of water to the product pipe for buoyancy control. For both HDD-1 and HDD-2, multiple abrupt increases in circumferential stresses were observed. These unexpected high stress points may be due to locally imposed loading, ovaling of the pipe cross-section, or a surge effect caused by a rapid movement of the pipe section.

For the first installation (HDD-1), the hoop stress was expected to be zero for the first section, where the borehole was above the rig elevation and no drilling fluid was present. With the exceptions of a few anomalies in the stress (due to one of the effects explained previously), the circumferential stress calculated from the strain measurements showed a trend similar to the predicted values. The maximum circumferential stresses based on strain measurements are 35.2 MPa and 34.7 MPa for HDD-1 and HDD-2, respectively. While these stresses are greater than the predicted maximum circumferential stresses, they are still less than the maximum allowable hoop stress (52.1 MPa). For HDD-2, the time that the maximum hoop stress for HDD-2 occurred (at 7:50:22 PM) correlates with the maximum pulling stress applied to the pipe, as shown in Figure 5.10.

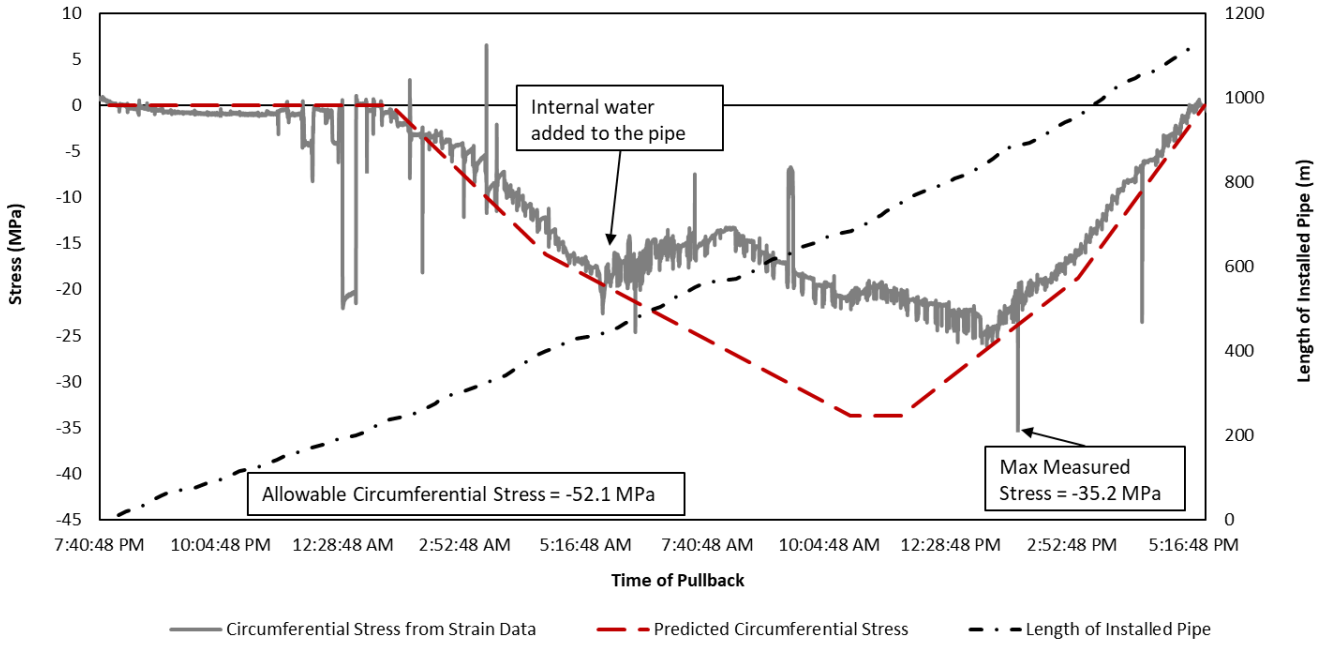

Figure 5.13. Circumferential stress calculated from strain measurements compared to predicted circumferential stress for HDD-1

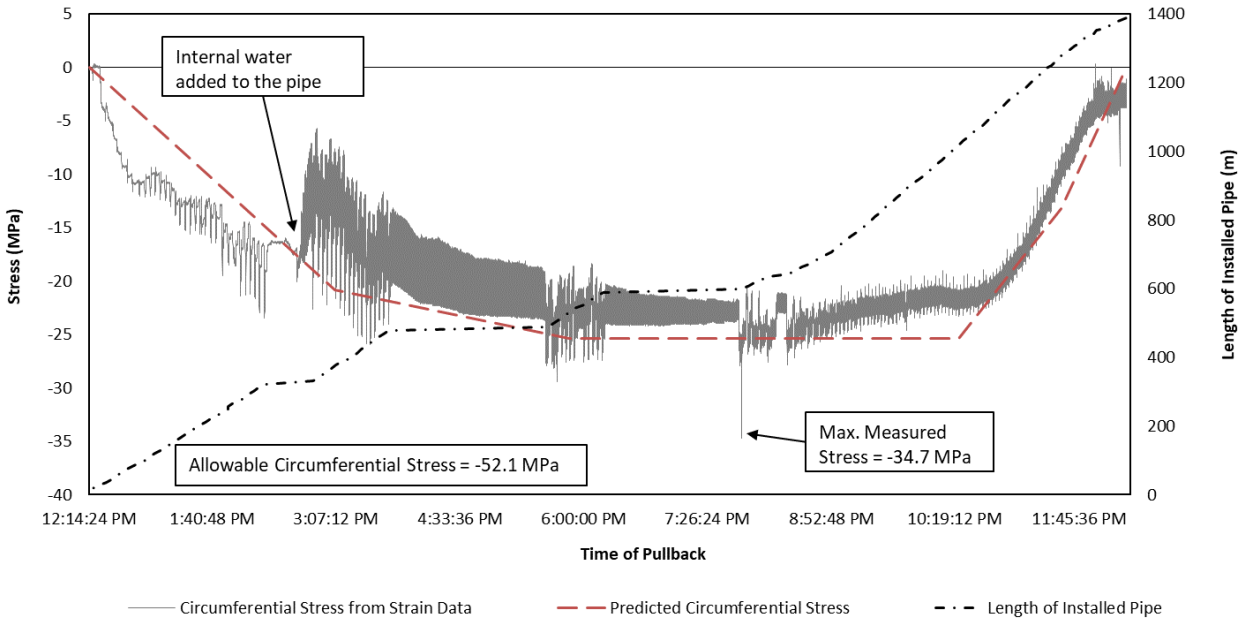

Figure 5.14. Circumferential stress calculated from strain measurements compared to predicted circumferential stress for HDD-2

5.7.2.4 Combined Stress

When the pipe is under longitudinal tension (due to tensile and bending stress) and compressive collapse pressure due to hoop stress, a full interaction load unity check must be satisfied. The pipe is under the worst-case stress condition when the most severe tensile, bending, and external hoop forces occur at the same time. In general, the most severe stress points are expected for locations with tight bend radii, high pull forces (closer to the rig side) and high hydrostatic drilling fluid pressure—i.e.,at the deepest point of the bore (Huey et al., 1996). For the theoretical stress prediction presented in Section 7.1, the location of the highest stress corresponds to beginning of the curve near the rig side at the deepest point of the drill path, with high pull forces near the rig.

The combined stress state is completed for two scenarios presented as unity checks: combined axial tension and bending; as well as combined axial tension, bending and compressive hoop stresses. These calculations are based on the established design for tubular members of offshore structures based on the American Petroleum Institute (API) guideline (API RP 2A-WSD, 2014) as referenced in PRCI (2015). The combined stresses were checked for HDD-1 and HDD-2 at critical locations along the borehole path, including the locations where the maximum stress values were obtained for each stress component. For HDD-1 (Table 5.3), the maximum combined stress under tension and bending is 0.51 and corresponded to the location of the maximum bending stress. The maximum stress value under combined tension, bending, and hoop stresses is 0.50 and occurred at the location of the maximum calculated hoop stress. The combined stress checks based on theoretical predictions were 0.30 of the allowable stress for the tension and bending stresses, and 0.51 of the allowable stress for the tension, bending, and hoop stresses, as presented in Table 5.2.

For HDD-2, the results of combined stress values are presented in Table 5.4. The maximum stress condition under all combined loads is 0.47 and occurs at the location where the maximum hoop stress and maximum axial pulling stress were calculated. The maximum combined stress under tension and bending was 0.15 and corresponds to the location of the maximum bending stress. The theoretical predictions resulted in a value of 0.37 for the combined tension, bending and hoop stresses, and 0.32 for combined tension and

bending stresses. Therefore, the maximum of all three combined stresses from strain measurements was higher than the theoretical calculated.

Table 5.3. Maximum combined stress checks for HDD-1

Location	Length of Installed pipe (m)	Time	Stresses – Calculated			Stress Check	
			Axial Pull Stress (MPa)	Bending Stress (MPa)	Circumferential Stress (MPa)	Combined T+B[1]	Combined T+B+C[2]
Max. Bending Stress	323	3:19:40 AM	6.3	155.0	-11.1	0.51	0.26
Max. Pulling Stress	855	1:18:32 PM	28.2	24.3	-25.1	0.14	0.27
Max. Hoop Stress	893	1:48:40 PM	20.7	34.5	-35.2	0.16	0.50
Theoretical High Combined Stress	717	11:06:48 AM	17.3	9.0	-20.2	0.07	0.16

[1] Combined stress check for axial tensile stress and axial bending stress
[2] Combined stress check for axial tensile stress, axial bending stress, and circumferential compressive stress

Table 5.4. Maximum combined stress checks for HDD-2

Location	Length of Installed pipe (m)	Time	Stresses – Calculated			Stress Check	
			Axial Pull Stress (MPa)	Bending Stress (MPa)	Circumferential Stress (MPa)	Combined T+B[1]	Combined T+B+C[2]
Max. Bending Stress	1352	11:58:50 PM	9.4	39.4	-3.3	0.15	0.02
Max. Pulling Stress	598	7:50:22 PM	30.1	12.1	-34.7	0.11	0.47
Max. Hoop Stress	598	7:50:22 PM	30.1	12.1	-34.7	0.11	0.47
Theoretical High Combined Stress	1026	10:22:12 PM	17.9	10.7	-21.4	0.08	0.18

[1] Combined stress check for axial tensile stress and axial bending stress
[2] Combined stress check for axial tensile stress, axial bending stress, and circumferential compressive stress

5.8 Discussion and Summary

Strain measurements acquired during two HDD steel pipe installations indicated that largest measured strains were significantly less than the strains corresponding to the elastic limit deformation of the pipe for stress-based design methods, indicating that an elastic state governed these installations. Abrupt increases

in axial tensile strain were recorded for all strain gauges at the start of the pullback due to the pull force required to overcome the resistance against pipe movement and advance the product pipe inside the borehole. The variation in circumferential strain during the pullback of each drill pipe joint shows a similar recurring pattern, represented by a rapid increase in compressive strain due to the effect of Poisson's ratio of the axial strains.

Aside from the portion of the pull force that causes axial straining of the drill pipes and the portion expended in overcoming resistances along the drill pipes and at the reamer and pullhead, most of the pull force is expected to be transmitted to the leading end of the product pipe. For both case studies, the axial pulling stresses arising from strain measurements showed that as pullback progressed, nearly the entire force applied by the rig was transferred to the product pipe at many locations along the process. It was also noted that although pull force estimations are based on the assumption that all sections of the pipe submerged within the drilling fluid are completely filled with water, in practice, during construction buoyancy water was added some time after pullback started; therefore, partial buoyancy control was utilized during pullback. Therefore, the pull force predictions completed with and without internal water effectively represent a lower and upper limit for the actual stresses imposed on the pipe. For HDD-2, the maximum pull force at the rig and maximum tension recorded by the strain gauges were recorded after a relatively long pause in pullback operations, when pipe movement resumed.

The presence of a bending moment across each pair of gauges was observed at all locations along the borehole path, including the straight sections, due to the effect of steering and corrections on the executed drill path. The maximum bending stresses expected—based on the smallest as-built radii of the design drill profile—were not identified in the bending stresses calculated based on strain gauges measurements. The maximum bending stresses (calculated based on strain data) showed a lower stress condition at the leading end of the pipe compared to the expected values, particularly for HDD-2. This could be a result of the placement of strain gauges at the front of the advancing pipeline, a location where the overall deformation of the pipe section may not be captured fully.

The circumferential stresses calculated from strain data were greater than predicted maximum hoop stresses, although the maximum observed drilling fluid densities (worst case scenario) were used to estimate the hoop stress along the borehole during pullback. During pullback, the reduction in compressive hoop stresses due to the addition of water to the pipe for buoyancy control was captured. For both HDD-1 and HDD-2, abrupt increases in circumferential stresses were observed in multiple instances, which was not expected. These high stress points may be due to locally imposed loading, ovaling of the pipe cross-section, or a surge effect caused by the rapid movement of the pipe section. For deep, large diameter HDD installations, circumferential stress can be the limiting factor. During pullback, the forces acting on the external surface of the pipe can be similar to those observed for deep-water offshore installations, where circumferential stress is a major consideration in the pipe design. The assumption of a high drilling mud density for hoop stress calculations during the design phase is highly recommended to ensure that a proper pipe grade and wall thickness are selected for the HDD installation.

Overall, the comparison of stress conditions based on strain data (as well as their combined interactions) with the theoretical engineering assessment indicates that the theoretical calculations provided estimates of stress conditions that are adequate for design purposes. However, the locations at which high strain/stress values were measured as well as the locations of the worst-case stress combinations were found to be different than the theoretical predictions. Since there is a high variability in the downhole conditions of the HDD borehole, this variability is reflected in stress or strain measurements. Unknown subsurface conditions, steering corrections while drilling the pilot hole, drilling fluid properties, imposed loadings from localized interactions between the pipe and borehole wall, hole condition prior to pullback, pipe ovality, the speed of installation, and any temporary shutdown during pullback all play a part in the stress/strain imparted onto the pipe section during installation by HDD.

5.9 Conclusion

A stress analysis of two steel pipes installed by HDD was conducted by analyzing strain measurements acquired during pullback. Installation stresses on the pipe were calculated based on data from strain

measurements during pullback, taken at four strain gauges installed at four quadrants inside the pipe wall. The stresses calculated based on strain measurements were compared with expected theoretical values based on the analysis method recommended by PRCI. Overall, the comparison of stress conditions based on strain data and the stresses from the theoretical engineering assessment indicated that engineering predictions provided estimates of stress conditions which are adequate for design purposes. However, the locations at which high strain/stress values were observed and their combined effect on the pipe section were found to be different than theoretical predictions. The high variability in the actual downhole conditions of the bore resulted in high variations in the strains and stresses measured inside the pipe during pullback. Of the different possible loading combinations, the circumferential stress can be the limiting stress factor for deep, large diameter installations. Strain measurements showed that predictions based on current design practice are not conservative enough to account for actual circumferential stresses. The strain monitoring and stress calculation discussed in this paper provide a strong basis for the expected behavior of steel pipes during HDD installations. It is recommended that strain monitoring be completed on additional HDD installations with different crossing geometries, pipe sizes and ground conditions to provide a comprehensive understanding of the behaviour of steel pipe during pullback.

6. Evaluation of Pull Force Imposed on HDD installed Steel Pipe using Strain Gauge Monitoring[1]

6.1 Introduction

Horizontal Directional Drilling (HDD) is one of the most practical trenchless methods for installing pipelines with minimal ground disruption (compared to open-cut construction). There are three essential stages in the HDD process: drilling the pilot hole, reaming, and pullback. The HDD process begins with drilling a small diameter borehole, referred to as a pilot hole, along a planned drill path. A bottom hole assembly (BHA) comprising a drill bit and steering tool is used to advance the pilot hole along sections of either straight or curved drill path. Once the pilot hole is completed and the drill bit emerges from the exit point, a reaming sequence is used to enlarge the borehole to a final size that is adequate for pipeline installation. Throughout each phase of the HDD construction, drilling fluid is utilized to assist with stabilizing the borehole while transporting the cuttings to the surface. The final step is pullback, when the product pipe is pulled into the borehole. The product pipe is connected to the drilling rig through a series of drill stem segments, a reamer, a swivel, and a pullhead. The rig pulls the drill stem, joint by joint, to install the product pipe.

To pull the product line inside the borehole, the applied load must overcome several resisting forces, including the net buoyant weight of the pipe, the friction between the borehole and the pipe sections, the fluidic drag resulting from the drilling fluid surrounding the pipe within the annulus, the friction between the pipe and the support equipment above ground, and the resistance due to length of drill strings in the hole and the BHA that follows the pull section. Pull force estimation is an essential part of the HDD design process, and provides a basis for selection of the proper equipment and adequate pipe strength. The loads developed during HDD installation are sometimes greater than the long-term operational loads, and can

[1] A version of this chapter has been published in International No-Dig 2019, 37th International Conference and Exhibition, Florence, Italy

govern the design requirements. The product pipe should be designed to have enough capacity to avoid damage during installation, while the HDD rig should be capable to successfully pull the pipeline into the bore (Baumert and Allouche, 2002).

6.2 Components of Pullback Load

The mechanics of pipe installation during an HDD crossing involve several factors due to interactions between the product pipe and the surrounding environment, including the ground surface, as well as slurry, soil, and bedrock within the borehole. The pullback operation begins with the entire length of the pipeline supported above ground using rollers and lifting equipment. During the initial stages of the pullback process, there is frictional resistance due to movement of the pipe against the surface of the rollers and lifting devices. Depending on the above-ground topography and the borehole profile, the weight of the pipe, can act as a resistance force or be along the pullback direction.

When the pipe is pulled inside a borehole filled with drilling fluid, there is a upward buoyant force that acts on the pipe. The amount of uplift force is a function of the outside diameter of the pipe; therefore, the submerged weight increases with pipe size. For pipe sizes equal or larger than NPS 24, the submerged upward mass of the pipe becomes significant and buoyancy control may be necessary. Buoyancy control is the practice of countering the upward buoyancy force acting on the pipe by increasing the weight of the pipeline by filling it with water. Alternatively, an inside liner within the pipe can be filled to achieve optimal buoyancy and minimize uplift forces, thus reducing the frictional forces between the pipeline and the bore. Inside the borehole, friction is the main resistance to pipe installation and is a function of the friction factor and contact force due to pipe-soil interactions. In addition to the pipe weight, the magnitude of the contact force at the soil-pipe interference depends on the bending stiffness of the pipe along the curved sections of the borehole, the radial displacement of soil at the pipe-soil contact points, and the stiffness of the soil.

In North America, the pull force method recommended by the Pipeline Research Council International (PRCI, 2015) is widely used for steel pipe installation using HDD technology. The designed drill path is

divided into a series of straight and curved sections within a vertical 2D plane, and the maximum pull force occurs at the end of the pullback process where the pipe exits the ground.

The axial tensile load required to pull the pipeline is calculated based on gravity, frictional drag, fluidic drag, as well as pipe deflection and stiffness calculations for the curves. If the designed profile includes bends in the horizontal plane, the calculations can be adapted to determine the normal force without including the component due to the section weight, since gravity does not act in the plane of the bend. The PRCI model does not consider the above-ground frictional component for the pipe, i.e., where the pipeline is laid out and supported on the ground—however, this component can simply be calculated and added to the model. The above-ground frictional component is typically at a maximum at the beginning of the operation and varies linearly with pipe length, ending at zero when the entire pipe length is installed in the borehole.

The calculated maximum pull force is used for installation stress analysis of the pipe. To estimate the total required rig load (which is used as a basis for rig size selection), the resistance due to pulling the drill rods can be added to the maximum pull force— this is calculated using the same equations with the drill rod properties instead of the product pipe. Finally, a safety factor is generally applied to provide an engineering contingency.

6.3 Strain Testing Methodology

A measurement system was implemented to capture the pipe strain during the entire pullback operation to evaluate the actual installation stresses. Due to the requirement of sensor information transmission and recording, and the high likelihood of the strain gauges being destroyed on the outer wall of the pipeline, the system was installed inside the pipe. To eliminate any impact on the interior of the product pipe due to the sensor installation, the strain gauge assembly was installed inside a 10 m test section of pipe located between the pullhead and the pipeline. The proposed monitoring system utilized eight strain gauges, which were attached to the interior of the pipe at positions 0°, 90°, 180° and 270° from the pipe crown. Two gauges were installed at each position to measure the strains in the axial and circumferential directions. The

monitoring system also captured and compensated for the influence of temperature changes on measuring strains. Figure 4 shows a schematic of the placement of the strain gauges inside the pipe.

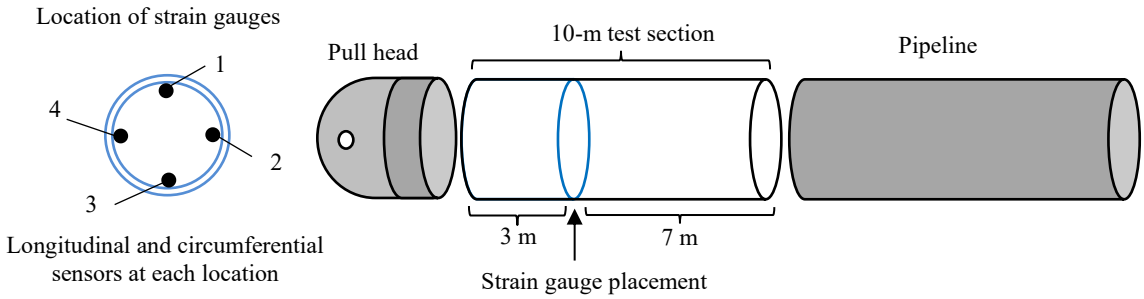

Figure 6.1. Strain gauge assembly

The gauges were placed at a distance approximately three meters from the edge of the test section (measured from where it was welded to the pullhead) to avoid measurement errors from the effect of the weld and the stiffness of the pullhead on the pipe section. The recording instrumentation was fastened to the pipe wall in a watertight container designed to endure the hydrostatic pressures encountered during water fill for buoyancy control.

6.4 Field Measurements

Field measurements for two major river crossings as part of a pipeline construction project in Alberta, Canada are discussed in this paper. HDD-1 involved a river crossing of 1,112 m with a significant elevation difference between the entry and exit sides. HDD-2 was a 1,390 m installation across a valley 800 m wide. Both crossings involved an NPS 30 steel pipeline. The HDD profiles and geotechnical conditions are included in Figure 6.2 and 6.3, and the design parameters used for the HDD installations are summarized in Table 6.1.

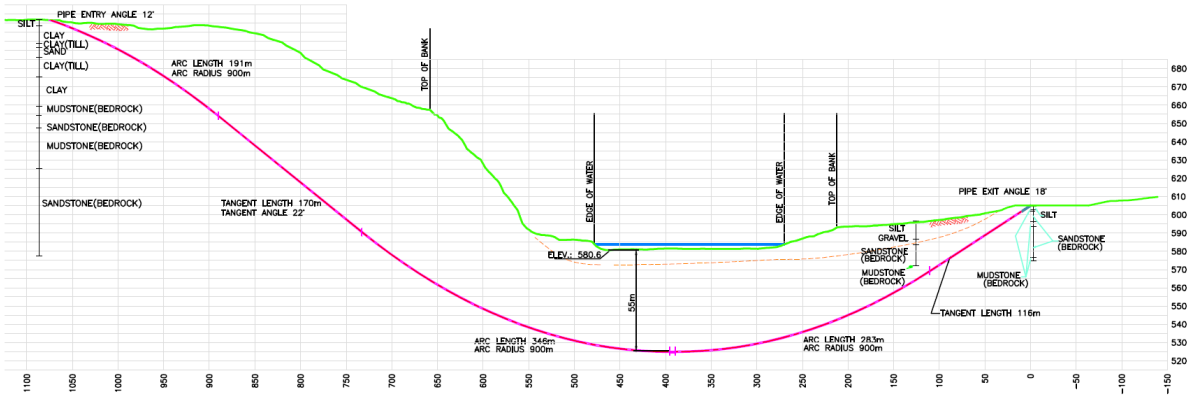

Figure 6.2. Profile geometry for HDD 1

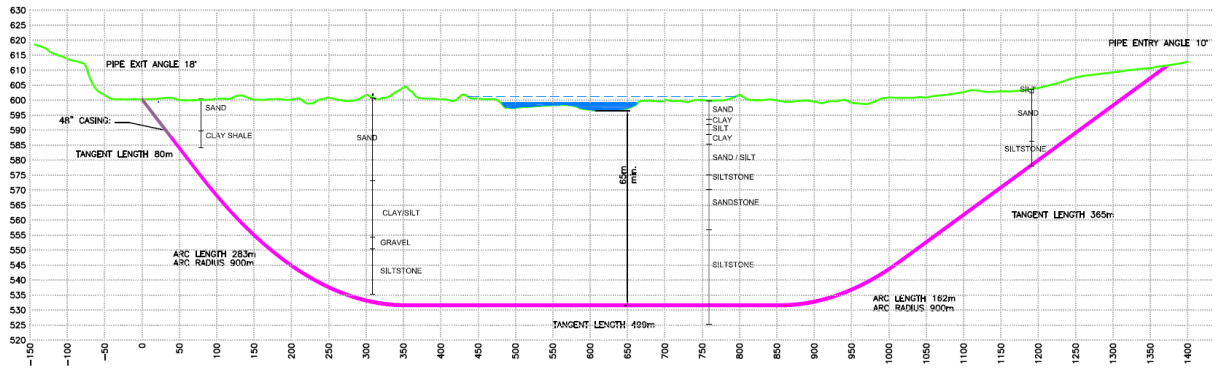

Figure 6.3. Profile geometry for HDD 2

Table 6.1. A summary of the design parameters used for HDD-1 and HDD-2

Design Parameters	**HDD 1**	**HDD 2**
Pipe outside diameter (mm)	762	762
Pipe wall thickness (mm)	15.8	15.8
Pipe grade (MPa)	483	483
Pipe modulus of elasticity (MPa)	207,000	207,000
Radius of curvature (m)	900	900
Total crossing length (m)	1,112	1,389
Borehole diameter (mm)	1067	1067
Drill pipe outside diameter (mm)	139.7	139.7
Drill pipe wall thickness (mm)	10.54	10.54
Drilling fluid density (kg/m^3)	1318	1378
Drilling rig size (lbs)	440,000	660,000
Fluidic drag coefficient (Pa)	172	172
Friction coefficient (pipe & borehole)	0.3	0.3
Friction coefficient (pipe & ground)	0.1	0.1

For each river crossing, the strains imposed at the strain gauges were recorded every two seconds during the entire pullback operation. The duration of the pullback operation was 22 hours and 12 hours for HDD 1 and HDD 2, respectively.

6.5 Strain Analysis

As the result of the external load during the pullback process, the loading imposed on the pipeline segment where the strain gauge assembly is located includes an axial tensile stress component from the axial pull force, an axial bending stress distribution from bending in the horizontal and vertical planes, the hoop compressive stress from the external hoop pressure (countered by internal buoyancy water), and the corresponding Poisson's ratio of the axial and circumferential stresses. A minor twisting moment due to the rotation of pipeline segment during the pullback process may also be present. Analysis of the recorded strain data is used to obtain the stresses imposed on the pipe in the leading section of the pipeline, where it experiences the maximum installation stress.

Figure 6.4 and 6.5 show the variation in axial strain recorded at each strain gauge for the duration of the pullback for HDD 1 and HDD 2, respectively. The maximum measured strains were significantly less than the strains corresponding to the elastic limit deformation of the pipe (0.5% or 5000 micro strain, με). Due to the long period of continuous recording and the resulting large data set, the recorded strains over the total pullback period are too compressed to allow a detailed assessment. To better see the strain variations, Figure 6.6 shows a typical strain variation over a shorter length of the drill path and represents three joints during the pullback process.

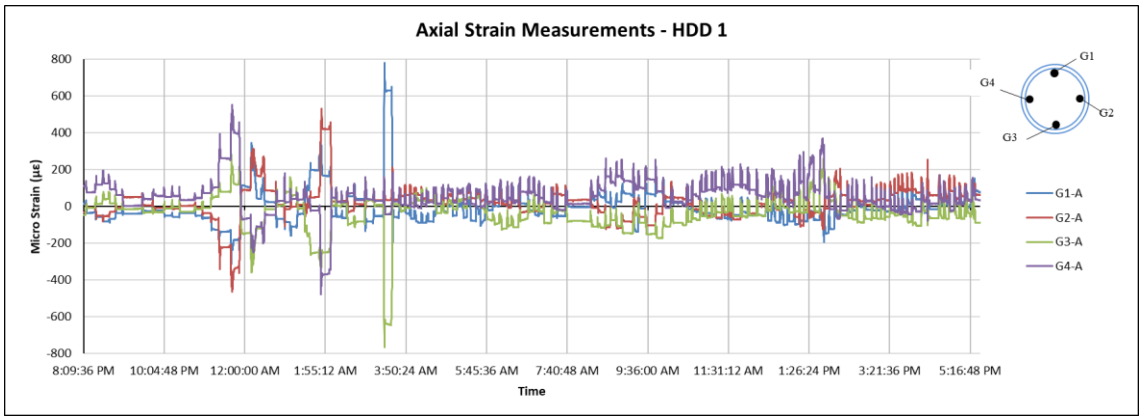

Figure 6.4. Raw data from strain gauges for HDD 1

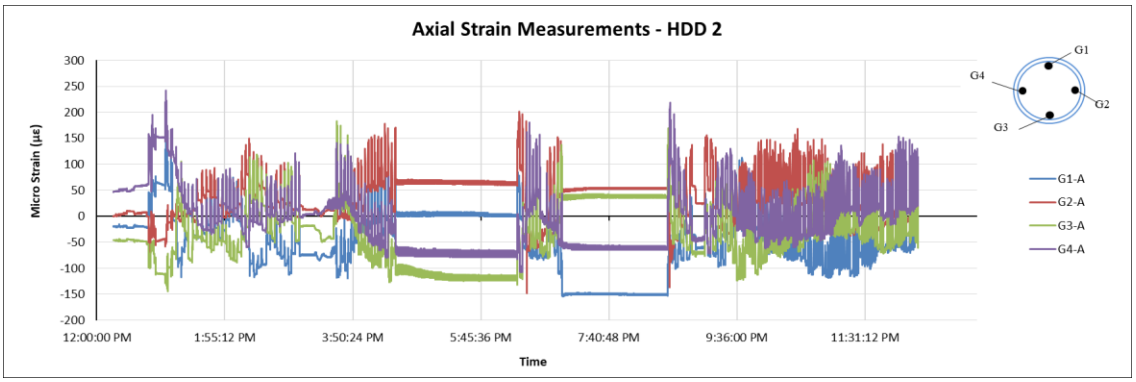

Figure 6.5. Raw data from strain gauges for HDD 2

As shown in Figure 6.6, the variation in axial strain during pullback for each length of a drill pipe joint involves an initial rapid increase in axial tensile strain, followed by a gradual strain variation, then a final

rapid decrease. Finally, a longer period of essentially constant strain is observed before the start of the pullback process for the next joint. This recurring pattern of axial strain variation closely represents the load applied to the front of the pipeline segment during pullback.

The initial rapid increase in tensile strain corresponds to the application of the pull force necessary to initiate forward displacement of the pipeline segment, and the applied pull force is required to exceed the initial resistance due to static friction. This is followed by a continued motion over the length of the joint due to the applied force, which can increase, constant or decrease gradually. Finally, there is a rapid drop in the pull force at the end of pullback of the drill pipe joint where the drilling rig stops. The time that the pipeline remained stationary during the removal of each drill pipe joint corresponded to constant axial strains recorded at all gauges until the start of the next pull-back cycle. The variation in hoop strain during the pullback of each joint of drill pipe shows a similarly recurring pattern: a rapid increase in compressive strain (largely due to Poisson's ratio of the corresponding axial strains) as seen in Figure 6.7.

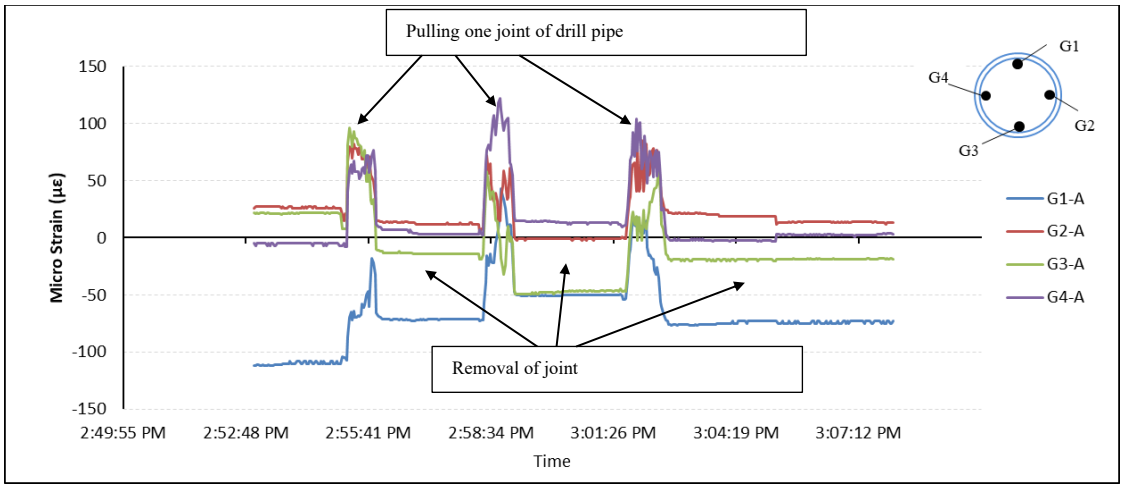

Figure 6.6. Axial strain during pullback over three joints of drill pipes

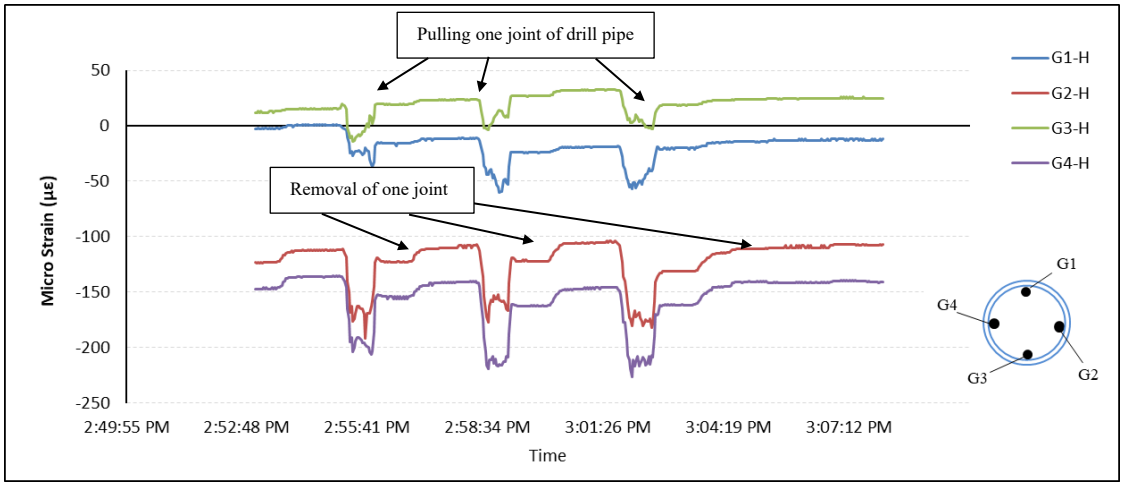

Figure 6.7. Circumferential strain measured while pulling three joints of drill pipes

At the start of pullback for each joint, the force necessary to pull the pipeline results in an abrupt increase in axial tensile strain. Therefore, the magnitude of the increase in the recorded axial strain when the pull force is applied for each joint can represent the strains due to the pull force applied to the pipe. Since each pair of strain gauge sensors (G1-G3 and G2-G4) were placed opposite sides of the pipe wall, the axial strain due to bending moments acting along the axis through each pair of gauges is expected to be equal but with opposite signs—i.e., the compressive bending strain measured on the one side and the tensile bending strain measured on the opposite side. Therefore, the average value of the increase in the axial strains recorded at the four locations can represent the deformation due to the axial force transferred to the pipe while pulling each drill string segment. The axial force applied to the product pipe at the location of strain gauge assembly can be calculated using Equation 6-1:

$$T_i = E\pi(R^2 - r^2)(\Delta\epsilon_1 + \Delta\epsilon_2 + \Delta\epsilon_3 + \Delta\epsilon_4)/4 \quad (6\text{-}1)$$

where T_i is the pull force exerted on the product pipe while pulling drill pipe joint "i", E is the modulus of elasticity of the product pipe, R is the outside radius of the pipe, r is the inside radius of the pipe, and $\Delta\epsilon_{1,2,3,4}$ is the increase in axial strain recorded at the strain gauges G1, G2, G3 and G4 at the beginning of pullback for drill pipe joint i.

Figures 6.8 and 6.9 show the axial force calculated from the measured strain data using Equation 6-1 for HDD 1 and HDD 2, respectively. Also shown are the recorded pull force at the rig and the theoretical force applied to the product pipe based on PRCI model with the addition of above ground friction. The timing of when buoyancy water was added during the pullback process is shown in both case studies; and after that point, theoretical calculations were completed using the pipe weight with and without internal water to define the lower and upper limit for the pullback forces, representing a zone for the application of buoyancy control using a partially filled pipe.

For both projects, the axial forces calculated from strain measurements and the rig load dropped at the beginning of the pullback as the product pipe started to move. The measured axial pipe forces contributed to approximately 60% of the recorded rig load at the initial lengths of installations. The difference between the axial load transferred to the pipe and the rig load decreased as pullback progressed. For many locations along the HDD profile, it was observed that the entire rig load was transferred to the pipe, as captured by the strain gauge measurements. The overall variation in pull forces transferred to the pipe (as captured by the strain measurements) matched the variation in the recorded rig loads. As pullback progressed, longer sections of the product pipe were installed, and a shorter length of drill stem remained in the borehole to be pulled. As pullback neared completion, the entire rig load was observed to be transferred to the product pipe, as expected. The locations of where the maximum axial force was measured during pullback were observed to match the maximum recorded rig load imposed on the pipeline for both case studies, which indicated that strain gauges worked well in capturing the imposed forces. The maximum forces were measured when approximately 800 m and 600 m of pipe was installed for HDD 1 and HDD 2, respectively. A maximum pull force of 807 kN was applied to the pipe during pullback for HDD 1, which is comparable to the rig force of 842 kN. In HDD 2, the maximum axial force applied to the pipe was 816 kN and the recorded rig force was 931 kN.

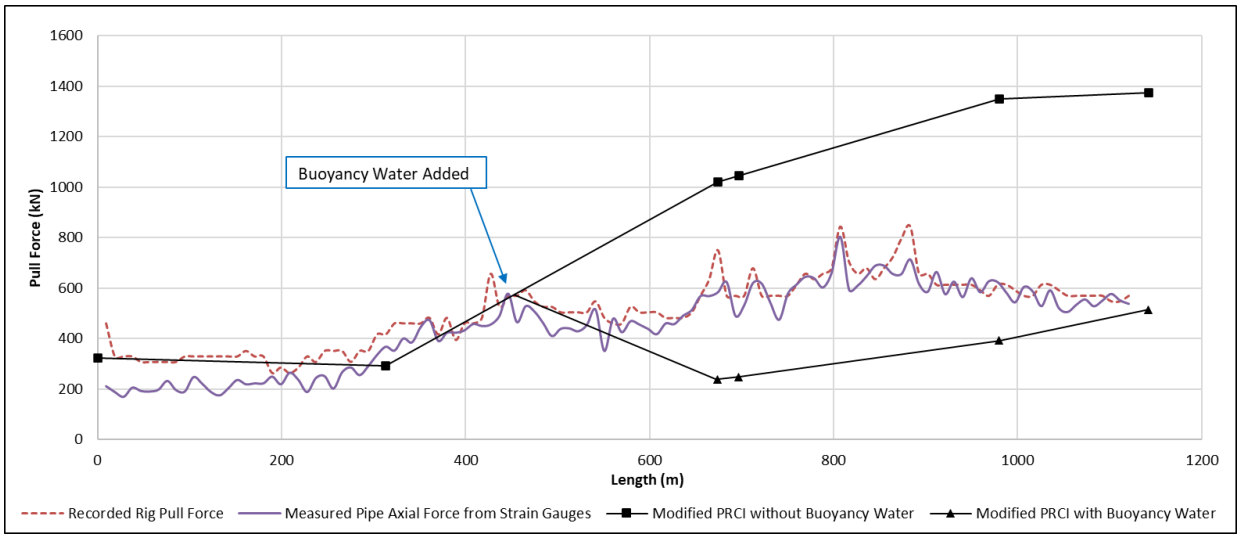

Figure 6.8. Calculated axial forces based on strain data, theoretical estimates and recorded rig pull force for HDD 1

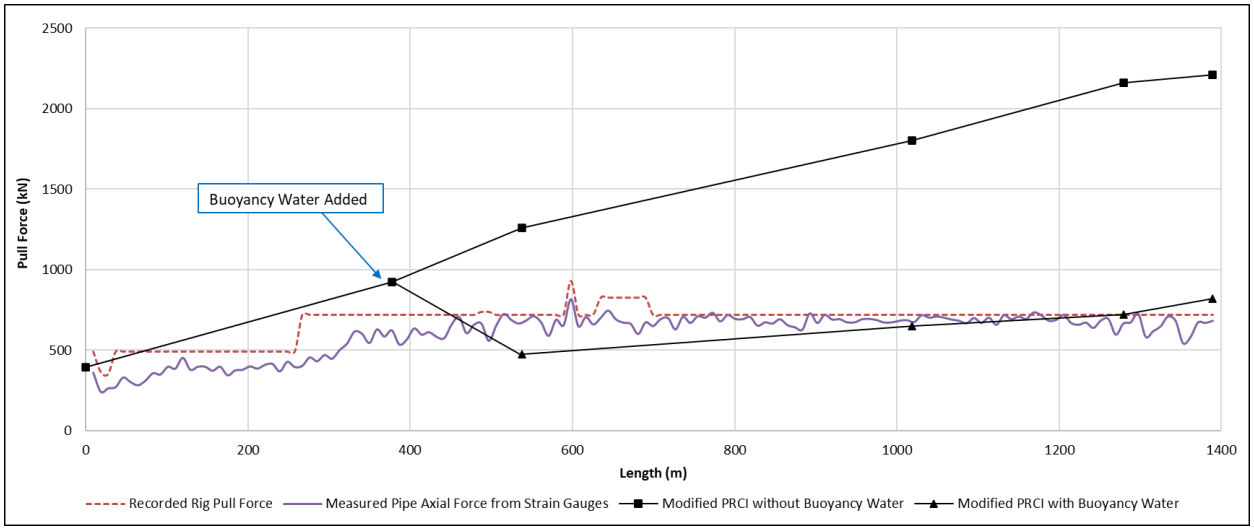

Figure 6.9. Calculated axial forces based on strain data, theoretical estimates and recorded rig pull force for HDD 2

Modified estimates of pull force based on the PRCI method for HDD 1 showed that the predicted pull forces were close prior to the addition of buoyancy water when about 460 m of pipe had been installed. After this, a decreasing trend in measured pull forces was seen. As previously discussed, water was not continuously added to the pipe, and the actual forces were greater than the PRCI model based on the full buoyancy weight of the pipe (i.e. a completely filled pipe for buoyancy control) while at the same time significantly smaller than for predictions without buoyancy control. For HDD 2, the predicted forces were greater than the axial

pipe forces calculated from strain measurements before internal water was added. Once the upward force on the pipe due to buoyancy control started to decrease, a relatively constant axial pipe forces calculated from strain measurements was observed afterward. The theoretical estimates using buoyancy showed a close correlation with the calculated forces from strain readings in HDD 2. For both projects, the theoretical estimations assuming that buoyancy control was used to fill the entire pipe were close to the measured forces at the end of the pullback using relatively high slurry densities (as outlined in Table 1). The densities considered were appropriate based on the slurry properties during pullback and the suspension of cuttings within the fluid.

6.6 Conclusions

The axial force transferred to the product pipe during installation of steel pipes using HDD was measured using a strain monitoring program implemented for two HDD crossings. It was observed that after an initial drop in force at the beginning of the pullback, the axial force transferred to the pipe contributed to about 60% of the recorded rig force. Furthermore, the difference between the axial load transferred to the pipe and the rig load decreased as the pullback progressed. It was noted that for many locations during pullback, the entire rig force was transferred to the product pipe. For both case studies, the locations of the maximum axial force imposed on the pipeline were observed to match the maximum recorded rig load.

Buoyancy control, which was utilized in both projects, caused a reduction in the pull forces, and this was captured in the forces calculated from the strain gauge measurements. Theoretical calculations completed with and without internal water represent a lower and upper limit for the actual forces, accounting for the partial application of buoyancy control (e.g., partially filled pipe) during construction. The PRCI model with the addition of above ground friction considering full buoyancy control, and relatively high slurry density, showed close predictions to the measured axial forces towards the end of pullback.

7. Chapter 7: Geometric Modeling of Pipes Installed by Horizontal Directional Drilling[1]

7.1 Introduction

Horizontal Directional Drilling (HDD) is a method used to install pipelines and utilities under waterbodies, roads, highways, shorelines, pipeline corridors, and other areas where open-cut construction is difficult to implement or infeasible. The HDD process includes drilling a borehole along a pre-determined alignment (pilot hole phase), enlarging the borehole by a reaming process, and installing the pipeline by pulling it inside the overcut borehole. The pilot hole phase consists of advancing a steerable drill bit along the design alignment from the drill rig entry to the exit location. The designed bore path includes a specified radius of curvature, which is dependent on the drilling equipment, product pipe, and operating conditions. Tracking is done using a magnetic or gyroscopic steering tool located within the drilling assembly, or alternately by a walkover system. The operator determines the location of the downhole steering tooling and postulates the location of the drill bit, inclination, and azimuth. This information is used to steer the drill along the pre-determined borehole path.

Once the pilot hole is complete, it can be enlarged by pulling or pushing hole openers or reamers through the existing hole to progressively enlarge the borehole until it is of sufficient diameter to allow the product pipe to be installed. During the final stage, pipe installation, curvature-induced bending stresses are imposed on the pipe cross-section as the pipeline is pulled through the curved sections of the drill path. The bending stress during installation forms part of the net longitudinal stress during pipeline operation. Therefore, the imposed bending stress affects both the installation and long-term performance of the pipeline (PRCI, 2015).

[1] A version of this chapter has been published in Proc., NASTT No-Dig North 2021 Conference, Vancouver, Canada.

7.2 Stress and Radius of Curvature

For HDD installations, the bending stress results from the curves within the drill profile, which bring the bore path to the elevation for the depth of cover required as part of the pipeline crossing. The bending stress is calculated as follows in Equation 7-1 (Timoshenko and Gere, 1972):

$$f_b = (ED)/(2R) \quad (7\text{-}1)$$

where f_b is the longitudinal stress resulting from bending; E is the modulus of elasticity; D is the outer diameter of the pipe, and R is the radius of curvature of the borehole.

Since the bending stress is affected by the radius of curvature, the allowable stress limits can be used to determine the minimum permissible radius for a drill path. The drill path cannot be constructed exactly as the designed profile. Inaccuracies in the downhole steering tooling, errors in surveying methods, variations in geotechnical conditions, unexpected soil reactions, and the skill of the driller are all contributing factors to the difference between the designed and as-built drill paths. It is important that both the design radius of curvature and the as-built radius of curvature are greater than the minimum permissible bend radius.

There should be a sufficient difference between the design radius and minimum bend radius to allow for constructability and steering corrections while drilling the pilot hole. As a rule of thumb, for steel pipelines, an acceptable radius of curvature in the design phase is generally equal to or greater than 1,200 times the nominal diameter of the product pipe. This guideline has been developed over the years based on experience related to constructability and typically results in a conservative radius of curvature.

HDD designers should account for the properties of the drilling rod and pipe when determining the minimum allowable bend radii. For small steel pipes or plastic pipes, the allowable bend radius of the drilling rods may be the critical limiting factor for the bend radius that can be achieved. For steel pipelines, pipe diameters are typically larger than drilling rod diameters; therefore, the minimum allowable bending radius of the pipe determines the drill path geometry. The maximum installation load and maximum in-service operating loads should be considered when calculating the minimum allowable bend radius. For instance, when the operational stress condition is more stringent than the installation load stress condition,

the minimum allowable bending radius is determined by calculating the radius associated with the bending stress, such that—combined with the maximum stresses under in-service operating conditions (including groundwater and earth pressure, line pressure, and thermal expansion)—the total longitudinal stress is equal to 90% of the specified minimum yield strength (SMYS) of the pipe material or the shear stress is equal to 45% of SMYS. This calculation is in accordance with Pipeline Research Council International design guidelines (PRCI, 2015), as suggested by the standards put forward by the Canadian Standards Association (CSA Z662) and American Society of Mechanical Engineers (ASME B31.4 and B31.8) for HDD applications.

7.3 Drilling Survey Calculation

For any directional drill employing non-gyroscopic, full-featured steering tools, three components are measured at any given point in the drill path to determine the drill bit position. The technique of measurement of these three components is termed a survey. The measured depth (along the drill path), inclination, and azimuth are measured, and these values are used to calculate the position at intervals while drilling (i.e., survey shot). At a minimum, these surveys are taken when drilling has progressed the length of a full joint of drill pipe, before adding the next joint. Contractors may conduct extra surveys at intermediate points—e.g., mid-joint—to increase the steering accuracy and make any necessary adjustments before drilling the remaining distance for the joint.

There are different survey calculation techniques based on angular measurements. The American Petroleum Institute (API Bulletin D20) provides an overview of directional drilling surveying methods. Of the different methods explained in this bulletin, the minimum curvature (MC) method is presented here. This technique (MC) is commonly used on HDD projects to calculate the distance from the entry point as well as horizontal offsets from the angular readings recorded during survey shots.

Figure 7.1 illustrates the parameters used in the MC method. This method involves the assumption that half the course length (i.e., the length between two downhole survey shots measured along the drilled path) is tangent to the previous inclination/azimuth projections, and the other half is tangent to the current

inclination/azimuth projections. Then, a ratio factor is used to fit a curve to the calculated tangents (PRCI, 2015):

$$DL = \cos^{-1}(\cos(I_2\text{-}I1) - \sin(I1)\sin(I2)(1 - \cos(A2\text{-}A1))) \quad (7\text{-}2)$$

$$RF = (2/DL)\tan(DL/2) \quad (7\text{-}3)$$

$$RF = 1 \text{ for small angles } (DL < 0.25°) \quad (7\text{-}4)$$

$$HD = (CL/2)(\sin(I1)\cos(A1) + \sin(I2)\cos(A2))\,RF \quad (7\text{-}5)$$

$$RT = (CL/2)(\sin(I1)\sin(A1) + \sin(I2)\sin(A2))\,RF \quad (7\text{-}6)$$

$$VT = (CL/2)(\cos(I1) + \cos(I2))\,RF \quad (7\text{-}7)$$

where *CL* is the drill course length; I_1 is the inclination angle of the previous survey point; I_2 is the inclination angle of the current survey point; A_1 is the deflection (azimuth) angle from the heading of the previous survey point; A_2 is the deflection angle from the heading of the current survey point; *HD* is the horizontal distance between the previous and current survey points; *RT* is the differential distance, to the right (positive values) or left (negative values) relative to the reference line between the previous and current survey points (Figure 7.1); and *VT* is the vertical distance between the previous and current survey points.

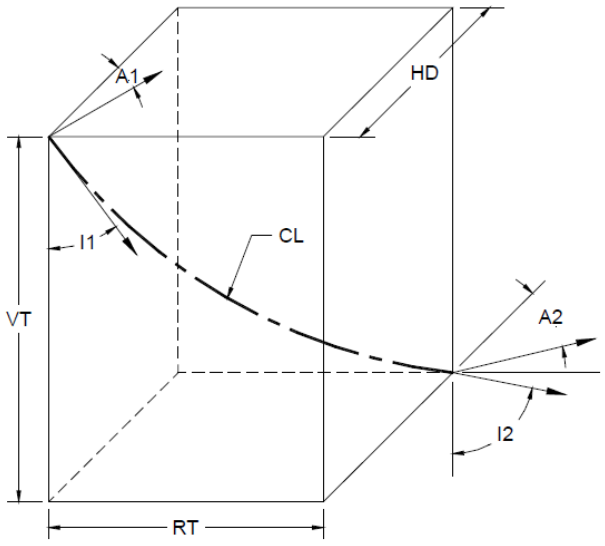

Figure 7.1. Downhole survey calculation definitions (PRCI, 2015)

The radius of curvature is calculated using the angular measurements at the survey points. When steering occurs entirely in either the horizontal or vertical planes, the radius of curvature can be calculated according to Equation 7-8 and 7-9:

$$R_V = (CL/|I2-I1|)\ (360 / 2\pi) \quad (7\text{-}8)$$

$$R_H = (CL/|A2-A1|)\ (360 / 2\pi) \quad (7\text{-}9)$$

where R_V is the average drilled radius over the course length in the vertical plane; R_H is the average drilled radius over the course length in the horizontal plane; and all angle measurements are in degrees.

The drill course length varies based on drill pipe length and is typically taken to be equivalent to a single joint of drill pipe (approximately 10 m or 30 ft). Along with drill course lengths equal to a single joint (1-jt) radius, longer drilled lengths over three joints (3-jt) or ten joints (10-jt) are also common in the industry. However, longer or shorter course lengths can also be used to calculate the radius of curvature of the drilled path.

HDD paths are sometimes designed with alignments that include horizontal and S-curves to avoid underground obstacles or meet construction footprint requirements and right of ways. In these cases, a combined curve is produced, with horizontal and vertical curves occurring simultaneously. The combined radius of curvature, R_C, can be calculated as in Equation 7-10:

$$R_C = SQRT((R_V^2\ R_H^2)) / (R_V^2 + R_H^2)) \quad (7\text{-}10)$$

In practice, while drilling a combined curve often arises from the actual drilling path, even when the designed drill path has a straight alignment from the entry point. The actual HDD profile proceeds along a three-dimensional path with incremental directional drilling occurring in both the vertical and horizontal planes, due to the continuous steering adjustments required to conform to the designed drill path; thus, the as-built drill profile is generally complex and includes combined curves.

7.4 Minimum Steering Tolerances

One of the critical design aspects of the radius of curvature is to account for steering tolerances during the drilling of the pilot hole. As discussed, the actual drill path cannot be constructed following the ideal curves

specified in the design drawings. Therefore, minimum allowable steering radii are prescribed to address the constructability of the designed directional drilling path, yet also ensure that the bending radii actually realized in practice with the pilot bore and imposed on the pipe within the final bore path meet the stress requirements (for both installation and operational stresses).

As the pilot hole progresses, steering radii are calculated based on survey data using the Equations 7-2 through 7-10 and compared with the minimum allowable limits. The as-built survey information is reviewed by the owner's representative and HDD designers to determine if any radius breaks occurred (i.e., curvatures under the minimum allowable radius) and if steering corrections are needed.

HDD designers may choose to use single joint, three joints or a longer course length of steering radius to be equal or greater than the minimum allowable bend radius of the product pipe. The goal is that the realized bending radii imposed on the pipe throughout the bore path is equal to or greater than the minimum allowable bending radius. A reasonable transition is needed between the minimum allowable values for a single-joint steering radius, three-joint steering radius, or steering radius over a greater length, so that the drill path follows the designed profile as closely as possible. For instance, a three-joint radius may be designed to be 10-20% greater than a single-joint radius, while being at least 25% smaller than the design radius, whereas a ten-joint radius may be designed as 90% of the design radius. For a given crossing, a wider gap between the minimum allowable steering radius and design radius (or higher steering tolerances) results in a more economical installation, since inefficiencies due to pilot hole re-drilling and steering corrections are minimized. However, a balance is necessary between constructability considerations—which give a preference to lower allowable minimum steering radii—and the increased stresses ultimately imposed on the installed pipe with decreasing radius of curvature.

There are several underlying assumptions behind pipe stress checks based on as-built surveys of the pilot hole. First, it is assumed that a full-sized borehole results from the drilling and reaming processes, with the centerline of the borehole corresponding to the centerline of the pilot hole. Second, it is assumed that, when installed, the pipeline is located at the center of the hole for the length of the entire alignment. It follows that the same bend radii indicated in the as-built survey are imposed on the product pipe. In reality,

regardless of the uncertainty related to the shape and condition of the final borehole, the pipeline is not at the center of the hole along the entire bore path. When installed, the path that describes the location of the centre of the pipeline has a different geometry, dictated by constraints at the top, bottom or side of the borehole at different locations along the bore path. Typically the borehole is 1.5 times or 12 in larger than the pipe diameter, and the overcut of the final borehole is another factor contributing to a different curvature for the pipe than dictated by the as drilled pilot hole. Other factors may also affect the position of the pipeline with the borehole, including soft ground conditions, unknown subsurface conditions, buoyancy forces and the application of internal water during installation (i.e., buoyancy control), among. Overall, it is expected that the installed pipeline potentially follows a different radius of curvature than the actual drilled pilot hole through various sections of the borehole.

7.5 New Method for As-Built Modeling

Bézier curves were applied to model possible scenarios of pipe position inside the hole using polynomial parametric functions and control points. Obtaining the best curve representation (curve fitting) to fit a series of measured data points has been an important topic in computer-aided geometric design, computer graphics and computer-aided design. Bézier curves are a powerful algorithm for geometric modeling, named after Pierre Bézier, who used them in the 1960s to design curves for the bodywork of Renault cars (Hazewinkel, 1997). They have many applications in engineering and technology—including railway routing, highway modeling, networks, animation, robotics, communications, eye-gaze-controlled interfaces, and many other fields—due to their computational simplicity (Maqsood et al., 2020). A brief introduction to the Bézier function is included in Equation 7-11 and 7-12 (Shene, 2011):

Given $n+1$ points, P_0, P_1, P_2, ... and P_n, in space, also termed the control points, for $0 \leq u \leq 1$, the Bézier curve, C, defined by these points is (Shene, 2011):

$$C(u) = \sum_{i=0}^{n} B_{n,i}(u) P_i \tag{7-11}$$

where the coefficients are defined as follows:

$$B_{n,i}(u) = n!/[i!\,(n-1)!]\; u^i (1-u)^{n-i} \tag{7-12}$$

The point that corresponds to u on the Bézier curve is the weighted average of all control points, where the weights are the coefficients of $B_{n,i}(u)$. The line segments P_0P_1, P_1P_2, ..., $P_{n-1}P_n$, joined in this order, form a control polyline. The functions $B_{n,i}(u)$, $0 \leq i \leq n$, are referred to as the Bézier basis functions or Bernstein polynomials. This parametric representation is useful to link the x and y coordinates of a curve to the variable u using polynomial functions. Therefore, changes in the value of u generate (x, y) coordinates in a curve, and the control points are the coordinate values that the desired curve should have. This means that for an n^{th}-order polynomial curve, w_0 and w_n are the start and end coordinates, respectively. Every coordinate in between is a controlling coordinate. A detailed description of Bézier curves can be found in Farin (2002).

Determining the path of the pipe inside the borehole can be done by defining a Bézier curve using the entry and exit points as the start and end coordinates, and all survey points recorded while drilling the bore as control points. As stated previously, the assumption for this approach is that the reamed borehole is enlarged uniformly around the center of the drilled pilot hole, i.e., enlarged hole has the same centerline as the pilot hole. When drilling in soft formations, the reamed borehole may not be enlarged uniformly around the pilot hole, because the reamer may sink and cut more at the lower part of the hole. If a survey of the reamed hole is available, this data is preferable for Bézier curve analysis rather than pilot hole data.

The degree of the polynomial curve is a function of the number of survey points. Consecutive curves can be utilized to model the geometry for the entire pipeline length. With this modeling, the calculated pipeline geometry comprises a series of curves that may have different radii with no discontinuity—i.e., there is no broken segment or deflection point, which corresponds to the expected objective of a successful pipeline installation. To accomplish this, the mathematical equations for the determination of Bézier curves were programmed in C++ as a CAD software extension library and utilized to do curve fitting to determine the pipeline path inside the reamed borehole based on case study data.

7.6 Case Study

An HDD crossing of the South Saskatchewan River in Alberta, Canada, was used as a case study for the proposed method to determine the as-built pipe path. The crossing involved installation of a steel NPS 30 (762 mm O.D.) pipeline in a 1145 m long borehole with a final diameter of 42 in (1066.8 mm) and a 900 m design radius. The geotechnical formation included overburden silt and clay till, underlain by sandstone and mudstone bedrock, with most of the crossing drilled through bedrock. The minimum allowable bend radius of the pipe was determined to be 490 m, and this limitation was due to operational stresses. The minimum design steering tolerances specified were a 385 m radius (over one joint) and a 555 m radius (over three joints). This crossing was selected as a case study for further analysis due to challenges encountered during its construction.

The as-built profile of the pilot hole based on the survey points during drilling is shown in Figure 7.2. One-joint and three-joint steering radii were calculated based on Equation 7-8 through 7-10, according to accepted industry practice. Based on the survey points, the calculated steering radii indicated several locations where the steering radius was under the minimum recommended tolerances. At the time of construction, discussions were held between project stakeholders regarding the steering breaks. The pilot hole was approved when further analysis indicated that the pipeline met the stress limits due to a lower operating pressure and temperature than in the initial design. The application of the Bezier algorithm for modelling the fit of the pipe inside the borehole based on the survey points is discussed below.

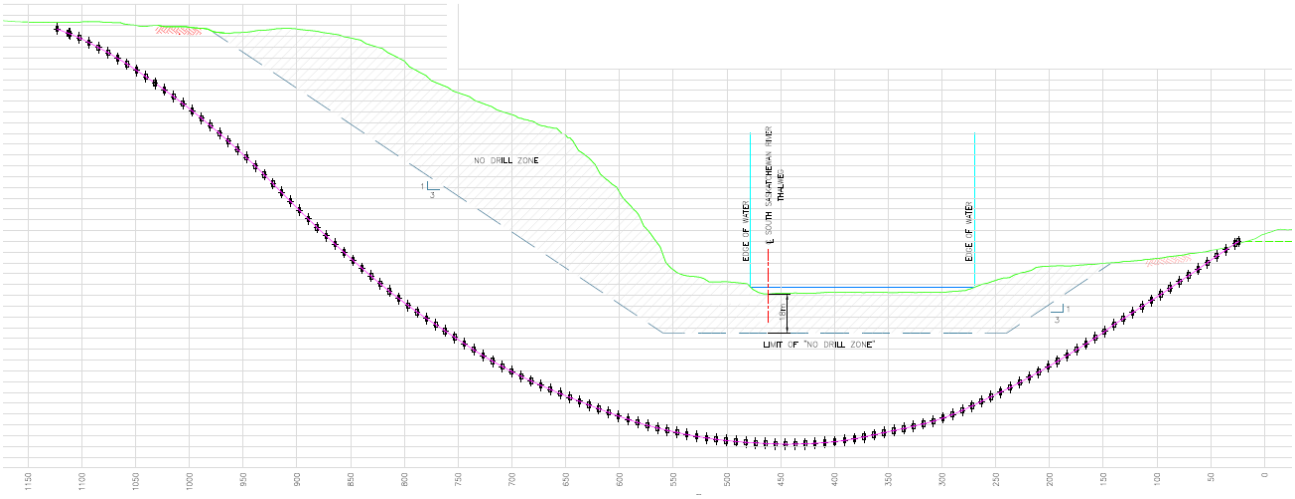

Figure 7.2. Drill path as-built profile showing survey points for every joint

The drilling survey points of the pilot hole were used as the control points for the Bézier curves, representing the centerline of the 42-in borehole for calculations based on the new method. Vertical and horizontal steering data were also utilized to ensure that the pipeline modeling included the combined curve geometries and the resulting tighter radii.

To better compare the potential pipe curvatures, 3D modeling was done using Civil 3D software to evaluate the best pipe-curve fitting scenario. Figure 7.3 shows the modeled pipeline and the measured radii inside the final hole, assuming that the final borehole was enlarged uniformly around the center of the pilot hole. The inserts in Figure 7.3a and 7.3b indicate the pipe position inside the hole at different locations and illustrate how the pipe conforms to the borehole geometry. This scenario can be treated as the ideal realized bending radii imposed on the pipe; i.e., the largest possible radius of curvature based on the survey points.

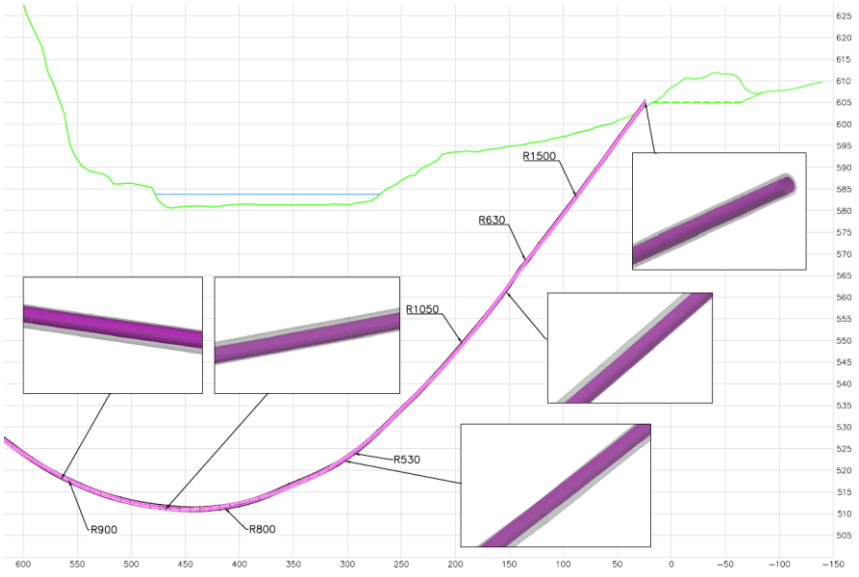

a. HDD entry side

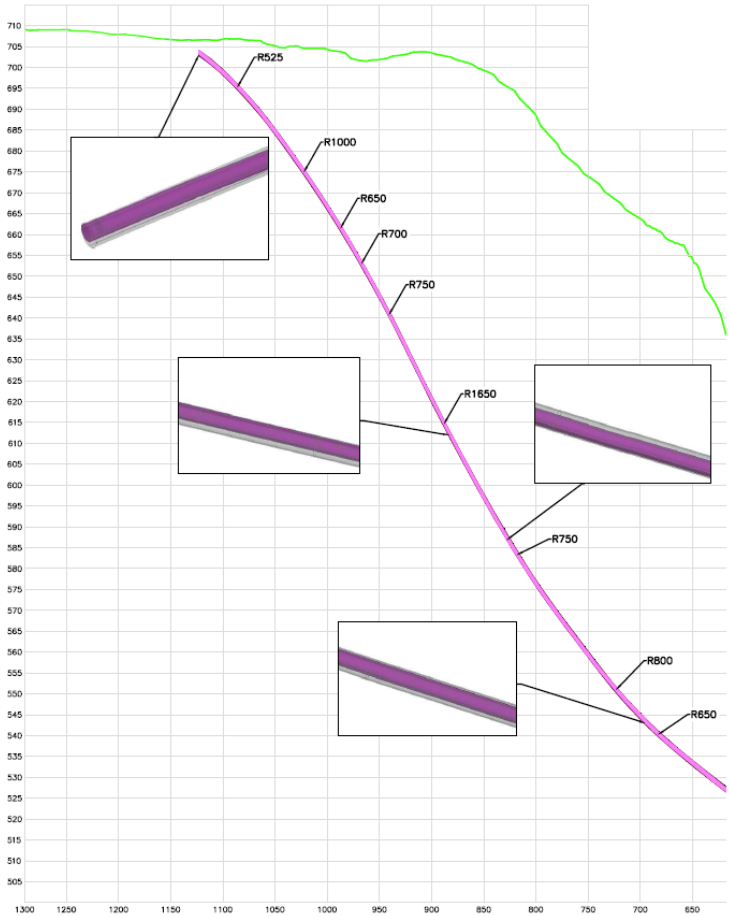

b. HDD exit side

Figure 7.3. 3D model of pipeline inside the borehole (best curve fit)

Figure 7.4 includes a graph of the as-built radius of curvature determined based on survey points using different methods: a conventional radius calculation over one and three joints based on Equation 7-8 through 7-10; the radius based on Bézier curves determined over one joint and three joints, and the drafted best curve fit. Radii larger than the design radius (900 m) were limited to 900 m in the vertical axes to ensure the clarity of the illustration (Figure 7.4).

The conventional one-joint radius shows the highest degree of variation along the drill path, with the tightest radii due to the calculation of the radius over the smallest course length. The conventional three-joint steering radius shows a relatively smoother curvature since it assumes uniform curvature over three consecutive joints.

A series of curvatures representing the pipe inside the hole were generated by the Bézier algorithm. The radii over one and three joints determined using the Bezier function (with the survey data as control points) resulted in a smoother drill path compared to the radius calculated using the conventional method. Based on the radii calculation resulted using the Bézier function, one would expect that the pipe actually may have a smoother curvature through some of the doglegs along the as-built alignment —i.e., the points where the radius of curvature is low.

The portions of the alignment with the tightest bend radii occurred approximately 300 m from the entry point, as well as in the last few meters of the borehole (near the exit). Near the entry and exit points, the pipe position may change due to tie-in requirements within the end sections, so the exit point geometry was not analyzed. However, further attention was given to the radii calculated using the various methods for the section located approximately 300 m from entry, as summarized in Table 7.1.

A comparison of the steering radii based on survey data (over one joint and three joints) and the physical pipe-curve fitting analysis—such as Bézier curves and 3D drafting best fit—indicates that it is possible that the pipeline could follow different curvatures along the bore path. When comparing the minimum allowable bend radius with the steering radii, care must be taken, since these radii of curvature are different in nature. Although an as-built analysis based on a conventional steering radius calculation is a practical, simple tool

to evaluate pipe stress in the absence of knowledge of the actual as-built borehole geometry, additional attention must be given to the possible physical curvature of the pipe inside the hole.

It is important to note that the shape of final reamed borehole is highly dependent on the geotechnical condition along the alignment. In harder formations such as bedrock (e.g., the case study discussed above), the assumption that the reaming process results in a borehole that is enlarged uniformly around the center of the pilot hole is reasonable. However, it is possible that in soft formations the reamer may sometimes sink while enlarging the borehole, creating localized sections along the bore path with a tighter bend radius than indicated by the survey points taken along the drilled pilot bore. More attention must be given to the determination of the pipe bend radius under these conditions (e.g., soft formations) because the product pipe may have a tighter bend radius than indicated by the as-drilled radius of the pilot hole.

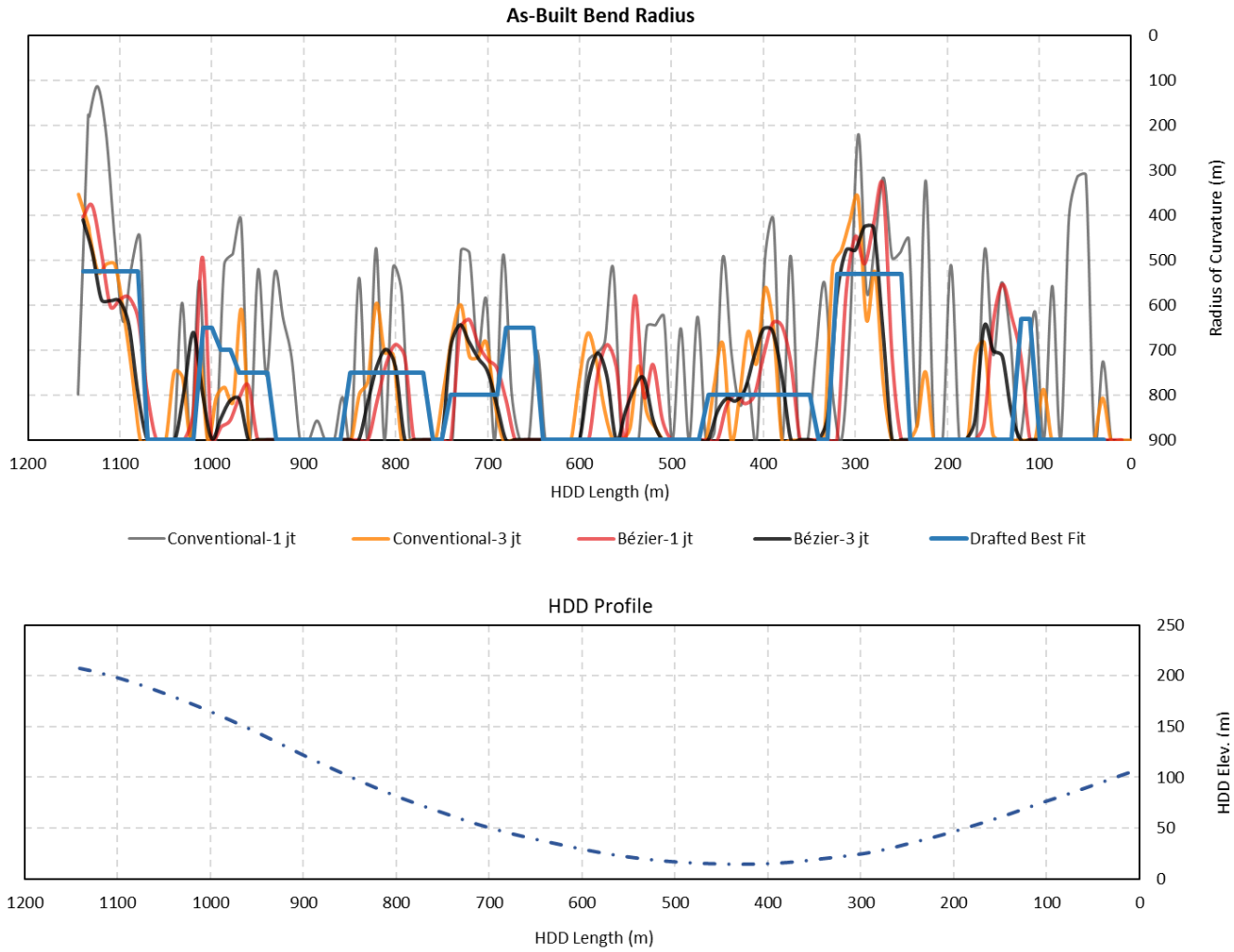

Figure 7.4. Graph indicating the radius of curvature based on conventional calculations, Bezier curve fitting and drafted best fit along the HDD alignment

Table 7.1. Tightest bend radius within the drill profile (approximately 300 m from entry)

Radius drill length	Conventional radius calculation during pilot hole	Measured radius based on Bézier curves	Measured radius based on drafted best fit curve*
One joint radius (~10 m)	220	334	530
Three joint radius (~30 m)	362	425	530

* The curve modeled at this location is an arc with a radius of 530 m and a length of 71 m.

7.7 Conclusion

A review of bend radius calculations based on downhole survey measurements was presented in this paper. The underlying assumption behind the as-built pipe stress check based on current industry practice is to assume that the pipe is in the center of the hole along the entire bore path, with a bend radius similar to the pilot hole. However, the installed pipeline may actually have a different geometry, dictated by constraint points at different locations within the borehole. The bending radius of the pipe within the enlarged borehole is not necessarily similar to the steering radii for the pilot hole.

Application of geometric modeling of the pipe inside the borehole based on Bézier curves were explained and applied for a case study involving a steel NPS 30 pipe installed using HDD in a 1145 m river crossing. The bend radii calculated using the Bézier method give a theoretical representation of the realized bending radii of the pipe along the bore path. The proposed as-built modeling method using Bézier curves allows for an engineering assessment of the surveyed drill path to check the limiting pipe stress conditions based on likely pipe curvature scenarios.

The radius calculation is highly dependent on the chosen course length. The choice of a one-joint radius rather than a three-joint radius can give results that are significantly different from the radii calculated based on conventional method or pipe curvature modeling methods such as the Bézier algorithm or 3D drafting best fit.

In the absence of knowledge of the actual reamed borehole geometry, a key assumption in all the methods for the calculation of bending radii discussed in this paper is that the reamed borehole is enlarged uniformly around the center of the drilled pilot hole. However, it is possible that the reamer may sink in soft formations, creating localized sections within the bore path with a tighter bend radius than the drilled pilot bore. More attention must be given to bores drilled in these conditions, since the product pipe may actually have a tighter bend radius inside the bore than indicated by the as-drilled pilot hole radius. More detailed investigations are required to evaluate the final pipe bend radius for different geotechnical conditions and how this compares to the survey data acquired while drilling the pilot hole.

8. Chapter 8: Verification of Product Pipe Bend Radius in Large-Diameter HDD Application in Dense Soil[1]

8.1 Introduction

Horizontal directional drilling (HDD) is the trenchless method where the pipeline is installed underground by being pulled inside an overcut borehole. With advancement of the HDD technology, the application of large diameter pipelines in HDD installations is increasing (Podbevsek et al. 2009). An important design parameter of HDD crossings is the radius of curvature or bend radius of the bore geometry, which defines the bending stress imposed on the pipe. Excessive bending can overstress the product pipe and increase the risk of damage to the coating and the pipe. The bending radius has become a critical consideration for large diameter pipes, since serious problems have arisen from HDD crossings designed with relatively small bending radii (Silva et. al. 2009).

On the other hand, the drill path cannot be constructed exactly according to the designed profile. Potential directional control issues can be resulted from rapidly changing variations in geotechnical conditions, intersecting bedrock structure at low angles, drilling in soft formations or encountering difficult ground condition such as cavities, fractures, faults, boulders, and cobbles (CAPP, 2004; Steve et. al. 2009; Royal et. al. 2010). In addition, steering problems can occur due to faulty tracking systems, and improper selection of downhole tools for the subsurface conditions (Rig worker, 2022). Therefore, verification of the bend radius of the product pipe based on the as-built drill path is a critical step for pipeline owners to accept the as-drilled bore before allowing the contractor to install the product pipe.

The as-built analysis is generally completed using the bend radii calculated from the drilled pilot hole survey data to determine if minimum allowable radius limits are met. There are some underlying assumptions made when assessing product pipe curvature based on pilot hole radius. First assumption is that the centers of the

[1] A version of this chapter has been submitted to the ASCE Journal of Pipeline Systems Engineering and Practice.

final reamed hole and the pilot hole are the same. This is a reasonable assumption in dense soil and hard formation while in soft and loose formations, it is possible that the reamer may sink and the actual reaming pass my deviate from the pilot bore path. Second assumption is that the installed pipeline is located at the center of the hole along the entire alignment, following the same bend radii as the as-drilled pilot hole. This is not a reasonable assumption because the pipeline follows a different geometry dictated by constraints present at the top, bottom or sides of the hole at different locations along the bore path; thus, the bend radius of an installed pipeline will differ from the pilot hole radius. Calculation of bending radius based on as-drilled pilot hole geometry may lead to unacceptable bend radius, while the product pipe may have different radius in places due to the overcut of the final borehole. To overcome the pitfalls of using pilot hole bend radius and better predict potential bend radius of the pipe inside the borehole, the concept of geometric modeling is proposed in this chapter and applied in a case study. An HDD crossing through dense soil consisting of dense sand and hard clay till is discussed in this chapter, where the geometry of the installed pipe was surveyed using an in-line inspection (ILI) tool. A comparison between bend radius of the installed pipe and as-drilled pilot hole radius is presented. The application of the proposed geometric modeling method is tested using the case study project.

8.2 Background

8.2.1 Radius of Curvature

The curvature is defined as the rate of change of the direction of a curve with respect to distance along the curve (Britannica 2013). At any point on a circle, curvature is the inverse of the radius of curvature. The radius of curvature or bend radius can be defined as the distance from the center of the circular path, in a plane, to the perimeter (Slavin 2011). The smaller the bend radius, the tighter the curvature of the drill path, which causes greater bending stresses on the pipe. In HDD, the bending stress imposed on the pipe during installation is a natural result of the curves in the bore path. The bending stress is calculated based on Equation 8-1 (Timoshenko and Gere, 1972):

$$f_b = \frac{ED}{2R} \tag{8-1}$$

where f_b is the longitudinal stress resulting from bending; E is the modulus of elasticity; D is the outer diameter of the pipe; and R is the radius of curvature of the element.

The bending stress during installation also contributes to the net longitudinal stress during pipeline operations. Therefore, the imposed bending stress affects both the installation and long-term performance of the pipeline. Established practices for the design of HDD projects outline the formulas used to calculate bending and combined stresses during installation and operation (PRCI 2015, DCA 2015, and Bennett and Ariaratnam 2017). The allowable limits for bending and combined stresses are defined in pipeline design codes such as API (2014), ASME B31.8 (2018), ASME B31.4 (2019), CSA Z662 (2019), and NEN (2020) and can be used to determine the minimum permissible radius for a drill path. The allowable bend radius is defined as the acceptable degree of curvature that can be imposed on the product pipe without risk of significant damage to the pipe (Trenchlesspedia 2021). When determining the minimum allowable bend radius, two factors must be considered. First, the maximum load on the pipe must be considered, whether it occurs during installation or operation. Furthermore, when calculating the minimum allowable bend radius, individual or combined stresses must be taken into account at all points along the drill path. As previously stated, the drilled path cannot be constructed exactly according to the designed bore path. To allow for constructability and steering corrections while drilling the pilot hole, the designed radius of curvature must be greater than the minimum permissible bend radius. A rule of thumb in the HDD industry is that the design radius of curvature for large diameter steel pipes is generally equal to or greater than 1,200 times the nominal diameter of the product pipe (Ariaratnam and Allouche 2000). This has arisen based on experience with constructability over years of HDD, rather than being based on any theoretical analysis. The Drilling Contractors Association Technical Guidelines (DCA 2015) recommends the following equation for determining the bending radius based on HDD geometry:

$$R_{design} = C\sqrt{Dt} \tag{8-2}$$

where R_{design} is the designed radius of curvature; C is a soil-dependent constant known as the soil characteristics constant (with values given in Table 8.1 for different soil types); and t is the pipe wall thickness. While there is currently no consensus in HDD practice on how the design radius for large diameter steel pipes should be determined, in general, the design radius ranges from 1,000 to 2,000 times the nominal diameter of the product pipe for these projects (Silva et. al., 2009).

Table 8.1. Soil characteristics constant, C (DCA, 2015)

Soil Condition	Cone Penetration Test, CPT (MPa)	Standard Penetration Test, SPT (blows/30 cm)	Elastic modulus (MPa)	C
Sand, very dense	>20	>50	100-200	8,500
Sand, medium density	10-20	25-50	50-100	9,400
Sand, low density	5-10	10-25	20-50	10,200
Clay, dense	>2	>8	10-25	10,500
Clay, medium density	1-2	2-8	5-10	11,500
Soft clay, silt	<1	<2	0-5	12,500

8.2.2 Bend Radius Calculation from Drilling Survey

For any directional drill conducted using magnetic or gyro steering tools, three components are measured at any given point in the drill path to determine the drill bit position. The measured depth (i.e., the distance away from the rig along the drill path), inclination or pitch, and azimuth are measured, and these values are used to calculate the position of the bottom hole assembly at intervals while drilling. The inclination (I) describes the pipe tilt with respect to the horizontal plane, and the azimuth (A) specifies the angle between the pipe direction and the local magnetic field of the earth. The technique for the measurement of these three components (depth, inclination and azimuth) is termed a survey, and a single measurement while drilling is termed a survey shot. At a minimum, a survey shot is taken when drilling has progressed a full drill pipe joint, before adding the next joint.

The as-drilled HDD profile proceeds along a three-dimensional path, with incremental drilling occurring in both the vertical and horizontal planes, due to the continuous steering required to conform to the designed drill path. The horizontal component of the bend radius (R_H) is a function of changes in azimuth, while the

vertical component of the radius of curvature (R_V) depends on changes in inclination over the measured distance. The following equations are used to calculate the total combined radius of curvature:

$$R_H = \frac{L}{(\Delta A)} \frac{360}{2\pi} \tag{8-3}$$

$$R_V = \frac{L}{(\Delta I)} \frac{360}{2\pi} \tag{8-4}$$

$$R_C = \sqrt{\frac{\mathrm{R}_V^2 \times \mathrm{R}_H^2}{\mathrm{R}_V^2 + \mathrm{R}_H^2}} \tag{8-5}$$

where L is the distance measured along the bore path; ΔA is the change in the azimuth angle over the distance between the two survey points; ΔI is the change in the inclination angle over the distance between the two survey points; R_C is the total combined radius of curvature; and all angle measurements are in degrees.

The as-drilled bend radii are calculated based on drilling survey information (using Equation 8-3, 8-4, and 8-5) and compared with the minimum allowable bend radius. The data are reviewed by the owner's representative and HDD designers to determine if any radius breaks—i.e., any points at which the bend radius was below the minimum allowable bend radius—occurred. The goal is that the realized bending radii imposed on the pipe is equal to or greater than the minimum allowable bending radius throughout the bore path. In the directional drilling industry, it is common practice to take the average over a 30-m (100-ft) length to determine the radius of curvature of the drill path at any location (API, 1985).

8.3 Geometric Modeling of Pipe inside the Borehole based on as-drilled Survey Data

Obtaining the best representation of the curve that fits a series of measured data points (curve fitting) has been an important topic in both computer graphics and computer-aided geometric design. Among the various computational methods that exist for geometric modeling, Bézier curves are a powerful method, initially developed in the 1960s and 1970s by Paul de Casteljau and Pierre Bézier to design curves for the automotive industry (Farin, 1988); however, they have been utilized in other problems involving curvature. Bézier curves have many applications in engineering and technology—including railway routing, highway

modeling, networks, animation, robotics, communications, eye-gaze controlled interfaces, and many other fields—due to their computational simplicity (Maqsood et al., 2020). A brief introduction to the Bézier function is included below.

Given $n+1$ points $P_0, P_1, P_2, \ldots$ and P_n in space as the control points, for $0 \leq u \leq 1$, the Bézier curve C, of degree n, defined by these points is (Shene, 2011):

$$C(u) = \sum_{i=0}^{n} B_{n,i}(u) P_i \tag{8-6}$$

$$B_{n,i}(u) = \frac{n!}{i!\,(n-1)!}\, u^i (1-u)^{n-i} \tag{8-7}$$

The polygon formed by connecting the sequence of control points $P_0P_1, P_1P_2, \ldots, P_{n-1}P_n$ is known as the control polygon. The shape of a Bézier curve largely reflects the shape of its control polygon, making it is a popular choice for designing geometry (Floater, 2015). This parametric representation is useful for linking the coordinates of a curve in space to the variable u using polynomial functions. For instance, for a curve in the coordinate plane of x and y, changes in the value of u generate an (x, y) coordinate of a curve. The control points are the coordinate values that the desired curve should follow. This means that for an n^{th} order polynomial curve, P_0 and P_n are the start and end coordinates of the curve, respectively; and every coordinate in between is a controlling coordinate. For example, for a curve that starts at coordinate (5, 20), is controlled by coordinate (15, 10), and ends at coordinate (25, 14), a quadratic Bézier curve ($n = 2$) can be defined, as shown in Figure 8.1.

$$x = (1-u)^2 \times 5 + 2(1-u)u \times 15 + u^2 \times 25$$

$$y = (1-u)^2 \times 20 + 2(1-u)u \times 10 + u^2 \times 14$$

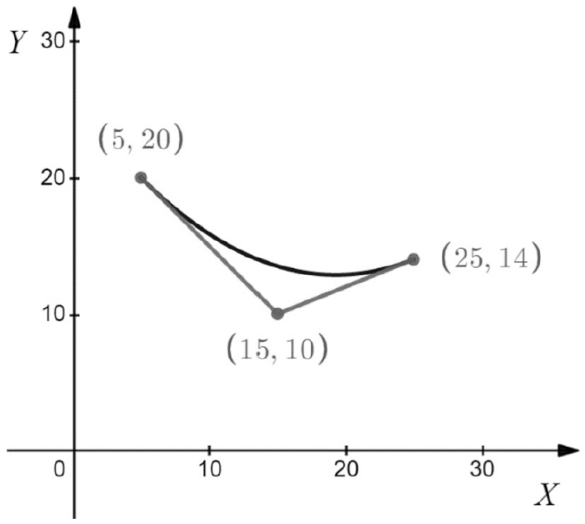

Figure 8.1. A quadratic Bézier curve

The fitting of the curve of a pipe inside a borehole can be done in a similar way, by using the centre of the bore at the entry and exit points as the start and end coordinates, with all the survey points measured in between as control points. The as-drilled path acts as the control polygon. Spheres with centers at the as-drilled survey points and diameters equal to the diameter of the final reamed hole can be used to define the boundary conditions for the modeled pipe path. Based on this method, the modeled pipe geometry constitutes a series of curves that are joined smoothly, with no discontinuities. The mathematical functions to apply the Bézier algorithm were programmed in C++ as a CAD software extension library and can be easily applied to any as-drilled survey points within a 3D CAD program.

In the absence of knowledge of the actual reamed borehole geometry, a key assumption in the geometric modeling of the pipe path using this method is that the reamed borehole is enlarged uniformly around the center of the drilled pilot hole, i.e., the final hole has the same centerline as the drilled pilot hole. However, while enlarging the borehole, the reamer may have actually cut more from the crown or bottom of the hole at some sections along the bore path, resulting in a final reamed hole which does not have the same centerline as the pilot hole. In worst-case scenarios, such as drilling in soft formations, it is possible that

the reamer may sink, which creates localized sections within the bore path that have a tighter bend radius than the drilled pilot bore. If a survey of the reamed hole path is available, this data can be used for Bézier curve analysis rather than pilot hole data.

The next section describes a large-diameter HDD project (selected as a case study) where the actual geometry and curvature of the installed pipe were measured using a ILI tool. Then, the Bézier curves generated based on the data collected along the pipe path were applied to model the pipe curvature inside the hole. The resulting path was compared with the path predicted based on survey data of the as-drilled pilot bore.

8.4 Case Study Description

An HDD crossing involving a 914 mm outside diameter (NPS 36) steel pipe with a wall thickness of 20.4 mm installed underneath two highways and several railway tracks near Edmonton, Canada was selected to study the curvature of the installed pipeline and compared it with drilling survey data. The topography in the area was generally flat, with a slight elevation gain towards the exit side. The crossing was approximately 990 m long, with a maximum depth of cover of 44 m. The drill profile geometry included a drilling entry angle of 14 degrees, an exit angle of 12 degrees and a designed bend radius of 1000 m. The minimum allowable bend radius was determined to be 570 m based on the installation and operational conditions of the product pipe.

The subsurface stratigraphy at the crossing location consisted of alternating layers of clay till, and sand. The clay till was described as silty, having medium to high plasticity, and having a stiff to hard consistency. The sand was described as fine to medium grained and compact to dense. The primary unit that HDD passed through included dense subsoil conditions below 7 m from ground surface; the Standard Penetration Test (SPT) N values ranged from 39 and 63 (blows per 30 cm of penetration) in clay till, and 33 to 50 (blows per 30 cm of penetration) in sand, indicating hard and dense soils.

A 15 m section of 1524 mm (60 in) surface casing was installed at entry point to mitigate any sloughing during reaming. The pilot hole was completed using 168.3 mm (6-5/8 in) drill pipes, a 203 mm (8 in) mud

motor, and a 311 mm (12-1/4 in) drill bit. A wireline magnetic guidance system (ParaTrack 2) was utilized to steer the bit while drilling the pilot hole. The pilot hole was surveyed each time a new joint of drill pipe was added to the drill string, approximately every 10 m. The drilling survey data was utilized to map the as-drilled location of the bore path. The final reamed borehole was enlarged to a diameter of 1219.2 mm (48 in) using an XTR rock reamer to accommodate the installation of the product pipe.

After completion of the pipeline project, an ILI tool was utilized to map the installed pipeline centerline. The ILI system includes an inertial measurement unit that employs gyroscopes and accelerometers, which measure the pipeline location during the tool run. Inertial data was collected at the rate of 100 samples per second, corresponding to one sample every 2 cm, with an average tool travel speed of 2 m/s. The mapping data provides accurate 3D coordinates (northing, easting, and elevation) for the pipeline centerline.

Figure 8.2 shows the location of the center of the pipeline compared to the centerline of the as-drilled pilot hole. The horizontal axis shows the distance along the borehole from the entry point, where the drill rig was set up, to the exit location (970 m away), and the vertical axis shows the bore path depth.

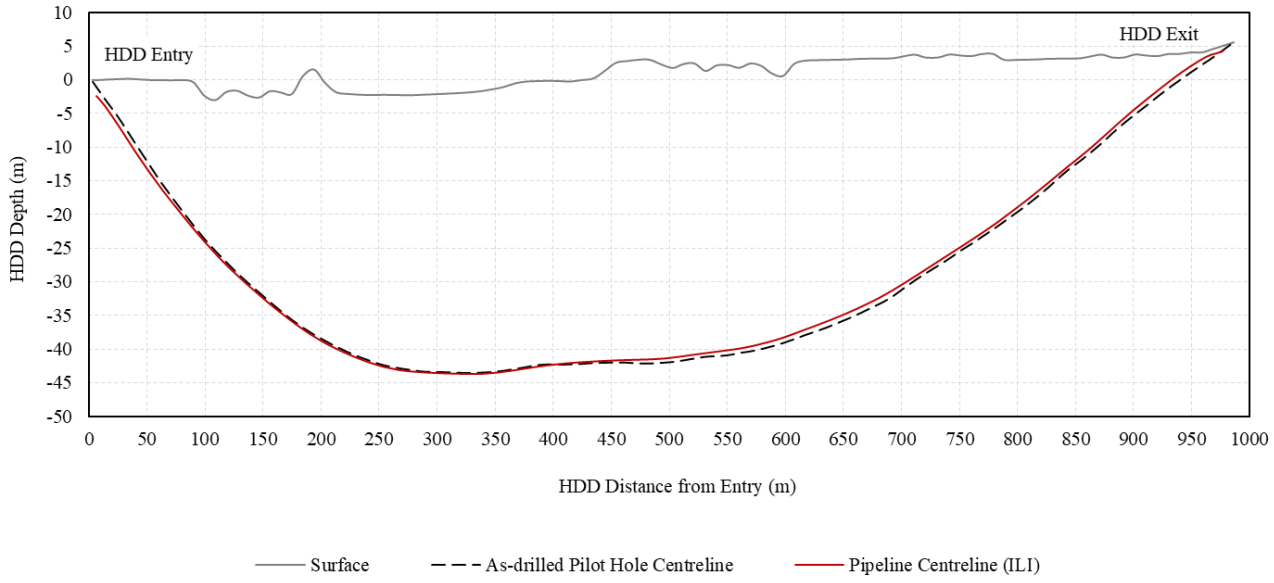

Figure 8.2. Borehole geometry showing a comparison between the as-drilled pilot hole and actual path of the installed pipeline

The ILI mapping data suggests that the actual pipeline location was approximately 0.8 m below the as-drilled survey data near the entry point. The two alignments came progressively closer to each other throughout the entry curve until a point approximately 300 m downhole. Between 300 m and 400 m, a steering correction was observed within the as-drilled pilot hole. This was due to some navigation challenges caused by poor wireline connections when crossing the highway. These issues caused the drill path to be lower than the planned alignment at 300 m, and a steering correction was made to return to the planned elevation. It appears that throughout this portion of the bore (300 m to 400 m) the installed pipeline maintained a straighter alignment than the planned pilot hole geometry, and the pipe continued slightly above the as-drilled pilot hole towards the exit point. A maximum difference in elevation of 1 m—between the centerlines of the as-drilled survey data (determined using ParaTrack 2) and the pathway of the installed pipe (surveyed using ILI)—was observed at approximately 650 m from the entry point. This difference between the location of the centerline of the installed pipeline and the surveyed path of the as-drilled pilot hole indicates the possible discrepancies that can arise when relying only on survey data from the pilot hole. Regardless of any systematic or random errors involved with the surveying methods employed in this project, the variations in the centerline of the pipeline path compared to the pilot hole survey indicates that there are differences between the curvature of the actual installed pipeline and the drilled path.

8.5 Comparison of Calculated Pipeline Curvature based on As-Drilled and ILI Surveys

The coordinates of the pipeline centerline measured using ILI were used to calculate the pipeline curvature, using Equation 8-3 through 8-5. The bend radii calculated using this method were compared with the radii of curvature calculated from the survey data acquired while drilling the pilot hole. The bend radii were calculated every 10 m and averaged over each consecutive 30 m. For both the as-drilled pilot hole and ILI survey, bend radii were determined for a total of 94 points along the length of the HDD borehole. Figure 8.3 shows a histogram of all radius ranges obtained from the as-drilled pilot hole survey and ILI survey of the pipeline path. While the bend radii calculated based on the survey of the as-drilled pilot hole include five values in the range between 450 m and 650 m, the bend radii calculated on the basis of the survey of

the actual pipeline path does not include any bend radii within these ranges. Instead, for the installed pipeline, higher frequencies of calculated bend radii were seen within the ranges of 750 m to 800 m and 800 m to 850 m. Moreover, the histogram (Figure 8.3) also indicates a higher frequency of bend radii values over 1200 m for the survey of the installed pipeline path than based on survey data for the as-drilled pilot hole. Overall, the histogram indicates that the path of the installed pipeline generally has larger radii of curvature than the radii based on the survey data collected while drilling the pilot hole.

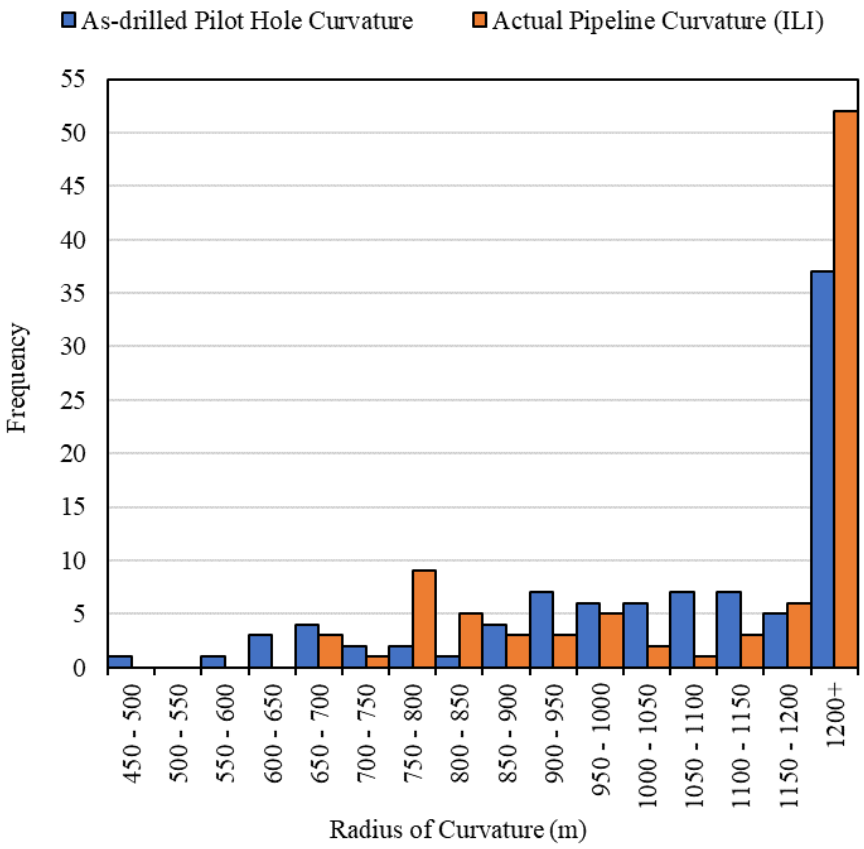

Figure 8.3. Frequency of bend radius values based on survey data for the pilot hole and the as-built path of the installed pipeline

Figure 8.4 shows the radii of curvature along the HDD profile based on the survey measurements taken while drilling the pilot hole and the survey of the path of the installed pipeline. It is particularly important to focus on the locations with high curvatures and thus locations that correspond to high bending stress on the pipeline. To give a clearer illustration, any radii larger than 1200 m were not included in Figure 8.4,

since these represent straighter sections where the imposed bending stress is well below the allowable limits. The minimum allowable bend radius (570 m) is shown as a horizontal line for reference. The as-drilled pilot hole and actual pipeline location are also shown, so that the bend radii can be related to the distance along the HDD profile.

There are two locations where the radii of curvature calculated based on pilot hole survey data were smaller than the minimum allowable radius: a bend radius of 552 m at distance of 110 m, and a bend radius of 482 m at a distance of 700 m. However, based on the ILI survey data for the installed pipeline, the bend radii of the installed pipeline were greater than the allowable limit at all locations. The bend radius of the installed pipeline at 700 m (which represents the location of tightest curvature according to the pilot hole survey data) was 758 m.

The smallest bend radius based on survey data of the installed pipe is 665 m at a distance of 70 m from the entry. At the same location, a bend radius of 612 m was calculated based on the survey data acquired while drilling the pilot hole. While the smallest radii of curvature for the path of the actual installed pipe are still greater than smallest radii calculated based on the pilot hole survey data, there are two locations where the bend radius determined based on the ILI survey is less than the bend radius based on the pilot hole survey data (from 590 m to 610 m and from 790 m to 800 m). However, at most locations throughout the HDD alignment, the installed pipeline followed a path with larger bend radii and larger bend radii compared to the radii calculated based on the pilot hole survey.

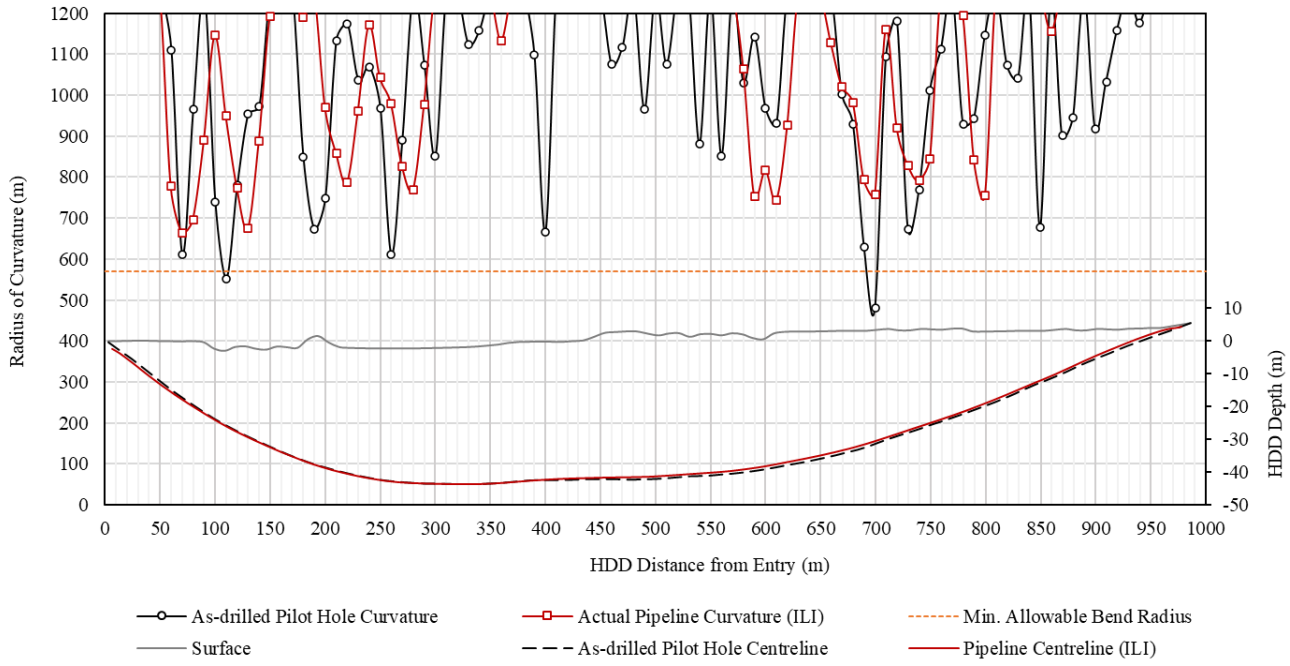

Figure 8.4. Comparison between the radius of curvature based on survey of the pilot bore and survey of the pipeline location

8.6 Application of Geometric Modeling to Determine Minimum Pipe Radius along the As-Drilled Hole

To verify the conformance of the as-drilled hole with the allowable bending radius imposed on the product pipe, geometric modeling of the pipe inside the borehole was conducted. Once the geometry of the path of the pipe inside the borehole was modeled, the radius of curvature was calculated using the method applied to determine the bend radii based on the pilot hole survey data and survey data of the installed pipe (as described in Section 8.3.2). Figure 8.5 shows the position of the pipe inside the reamed borehole according to the geometric model developed using Bézier curves. This illustrates the theoretical position of the pipe within the overcut borehole and how this path can follow different curvatures than the path defined by the center of the as-drilled pilot hole.

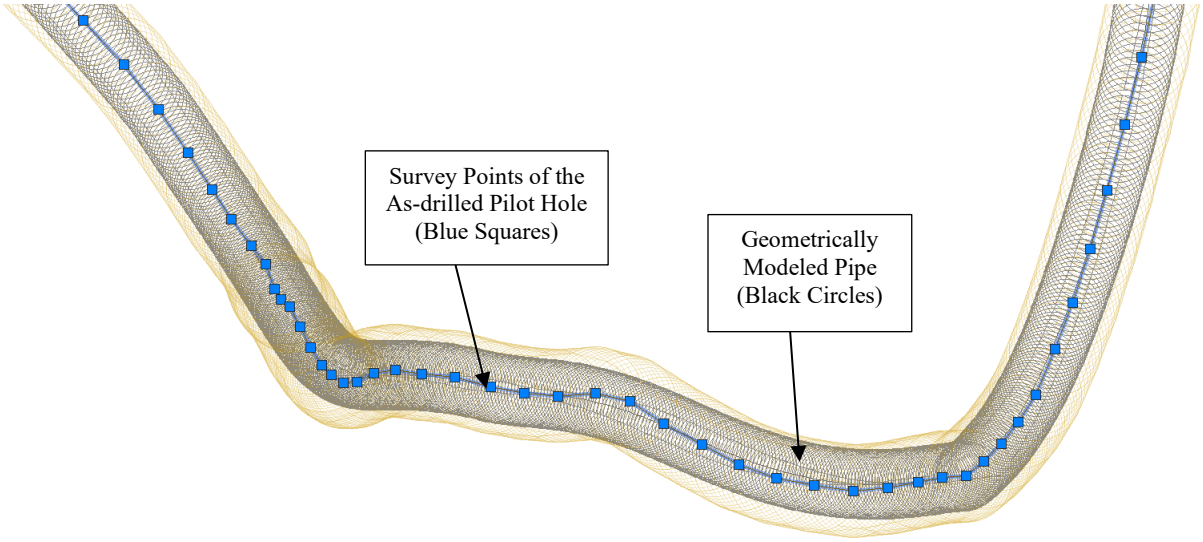

Figure 8.5. Path determined by geometric modeling of the pipe inside the borehole compared with the path defined by the survey data from the as-drilled pilot hole

Table 8.2 summarizes the smallest bend radii of the pipe determined based on geometric modeling (determined from pilot hole survey data) at different sections of the HDD path. The minimum bend radii calculated from pilot hole survey data and the survey of the actual pipeline path are also included (Table 8.2). The smallest radius calculated based on the geometrical model of the pipe path was 596 m, at a distance of 110 m to 130 m from the entry, corresponding to a bend radius of 552 m calculated based on the survey data for the pilot hole at the same location. In this section of the drill path, the smallest radius calculated based on survey data of the actual pipeline path was found to be 665 m. The other critical location is 700 m from the entry, where the smallest radius (482 m) was calculated based on pilot hole survey data. Geometric modeling indicated a bend radius of 750 m at this location, while the bend radius of the pipeline was 758 m (based on calculations from the survey of the pipeline path). This indicates a close representation of the pipe path based on the geometric modeling for this point.

Table 8.2. Comparison of bend radii based on geometric modeling, bend radii calculated based on survey data while drilling the pilot hole, and ILI survey data

Location of Smallest Bend Radii based on Geometric Modeling	Min. Bend Radius based on Geometric Modeling (m)	Min. Bend Radius based on Survey of Pilot Hole (m)	Min. Bend Radius based on Survey of Installed Pipeline (m)
110-130 m	596	552	665
260-270 m	769	611	770
690-700 m	750	482	758
720-730 m	684	673	791

It is interesting to look at two specific locations (110 m and 700 m from the entry). Based on geometric modeling, theoretically, at these locations, the product pipe was expected to have bend radii larger than the minimum allowable bend radius (570 m). However, the bend radii of the pilot hole based on the pilot hole survey data were smaller than the minimum allowable bend radius. Furthermore, based on the survey of the installed pipeline, the bending radii at these locations were also determined to be higher than the minimum allowable bend radius.

8.7 Conclusions

The actual position and geometry of a 914-mm steel pipe within an HDD bore along the alignment was assessed using two sets of survey data. Comparisons were made between the position of the centerline of the pipeline based on ILI survey data and the data acquired from survey of the pilot hole while drilling. Differences were observed between the final location of the installed pipe and the as-built path of the pipe defined by the centerline of the pilot bore. Bend radii of the actual pipeline path were calculated and compared with those calculated based on pilot hole survey data for the length of the borehole. Particular attention was paid to the locations along the borehole with the smallest bend radii, since tight bends at these locations indicate a higher bending stress and thus a higher risk of overstressing the product pipe. In all locations where the pilot hole survey data included radii smaller than the minimum allowable bend radius, the actual pipeline curvatures were larger than the allowable limit. Furthermore, throughout the HDD alignment, the actual installed pipeline had larger bend radii at most locations compared to the path defined

based on pilot hole survey data. While there were two locations identified along the bore path where the bend radius determined on basis of ILI survey data of the installed pipeline is less than the bend radius based on the pilot hole survey data, at both points the bend radii based on the survey of the installed pipe path were well above the minimum allowable bend radius.

To check the curvature imposed on the product pipe based on the geometry of the as-drilled pilot bore, the Bézier curve method was utilized for geometric modeling of the pipe inside the reamed borehole (with the assumption that the final reamed borehole was enlarged uniformly around the centre of the pilot bore). The smallest bending radii indicated by geometric modeling of the bore path of the product pipe in the reamed hole (based on pilot hole survey data) gave a better representation of the curvature of the actual pipeline along the bore, as opposed to using bend radii based on survey data from the as-drilled pilot hole as a metric to assess the actual bend radii imposed on the installed pipe.

Although data from more than 90 survey points along the 970-m drill path were analyzed, this study was limited to a single HDD project. Similar investigations—using ILI survey data of pipelines installed in different geotechnical conditions and borehole diameters—should be conducted to evaluate the bend radii of the installed pipe and compare it with bend radii calculated based on data from surveys conducted while drilling the pilot hole and geometric modeling of the product pipe within the enlarged bore. This will allow the applicability of the proposed geometric modeling method to be assessed based on data from additional projects.

9. Chapter 9: Conclusions and Recommendations

9.1 Introduction

This chapter presents the summary and the contributions of this research. This chapter also discusses the limitations of this research and provides recommendations for future works.

9.2 Research Summary

In this thesis, several issues related to the design and engineering of steel pipelines by HDD were investigated in depth, including accuracy of pull force estimation, pull force estimation for bundled pipes, stress-strain analysis of steel pipes during pullback, and investigation of the actual curvature imposed on the product pipe based on its path within the enlarged bore. The key findings of this work are summarized below.

9.2.1 Accuracy of Pull Force Analysis

To assess the accuracy of pull force estimation of steel pipes in HDD crossings based on current design practice guidelines, a comparison of predicted and actual drill rig pull forces was completed using data from 200 HDD crossings. In most cases, for small pipes (i.e., those with diameters between 64 mm and 324 mm) the data indicated that pull forces were underestimated (with a mean prediction error of -0.130 kN/m). As pipe diameters increase, the observed trend indicated a shift towards higher predicted pull forces compared to pull forces measured in the field during installation of the product pipe (mean prediction error of 0.010 kN/m and 0.195 kN/m for medium and large pipes, respectively) . Trends from the comparison of calculated and measured pull force indicate that the predictions generally tend towards underestimation for short crossings less than 300 m (with mean prediction error of -0.117 kN/m) to overestimation for crossings longer than 700 m (with mean prediction error of 0.124 kN/m). Analysis of the 200 case studies suggests that underestimation of actual pull forces is more common for soft formations (with mean prediction error of -0.128 kN/m) than for crossings completed in hard formations (with mean prediction error of

0.082 kN/m). A comparison of predicted and measured pull forces for different HDD equipment indicates more underestimation of pull forces for projects involving mini HDD rigs (with mean prediction error of -0.128 kN/m) than maxi HDD (with mean prediction error of 0.056 kN/m).

A review of the same 200 case studies showed significant underestimations in some cases, especially for crossings with predicted pull force predictions of less than 250 kN, despite the conservative assumptions used in the calculation of pull force. Among the projects studied, pull forces were underpredicted for most crossings with the possibility of poor bore conditions—including HDD projects with small pipe diameters, shorter length, bores in soft formation, and installations with mini HDD rigs.

To account for actual borehole (non-ideal) conditions, the negative mean prediction error obtained from the pull force analysis can be taken as a measure of the amount of additional resistance that needs to be overcome by the estimated pull force in crossings of a similar scope. Moreover, pull force estimations should allow for contingencies based on the project scope, geotechnical conditions, and the expected execution plan. More conservative values for borehole friction coefficient, mud density and assumption of buoyancy control when designing smaller scope HDD projects with non-ideal bore conditions can be used, resulting in larger pull force estimates. Similarly, lower values of the borehole friction coefficient, fluidic drag coefficient, and mud density can be considered for the design of larger HDD projects, where the bore condition may be closer to ideal before pullback. Finally, inclusion of safety factors during the planning phases is critical to allow for sufficient HDD designs and constructability. Appropriate safety factors could range from a lower limit of 1.25 to 1.5 for large projects (with a high level of construction effort) to an upper limit value of 2.5 to 3 for small projects where poor bore conditions are more likely.

9.2.2 Pull Force Estimation for Bundled Steel Pipes

The concept of a single equivalent pipe was investigated in this thesis as a means to calculate the pull force required for bundled steel pipe installations by HDD. The equivalent pipe is defined such that it has properties—e.g., dry weight, submerged weight, and stiffness—equivalent to those of all the individual pipes in the bundle. A review of five case studies involving bundled HDD installations of two to six pipes

(including steel pipes from NPS 3 to NPS 16) was conducted and pull force predictions were compared to pull forces measured during installation. The results indicated that the accuracy of pull force predictions improved significantly when calculations were based on the PRCI method using the proposed equivalent pipe parameters. The average accuracy of the pull force estimations based on the proposed equivalent pipe parameters utilized in PRCI resulted in +26%. Comparisons showed that the prediction accuracies were +227% and +97% for predicted pull forces using the NEN 3650 and the sum of individual pull forces determined by PRCI, respectively. The study suggested that the simple equivalent pipe method can be used to extend the PRCI method to include pull force estimation for bundled steel pipes in medium to large HDD crossings.

9.2.3 Strain Monitoring Program and Stress Calculation

A strain monitoring program was implemented in two major HDD installations, including 762 mm O.D. steel pipe in crossings over a kilometer. The strain measurements were presented in the form of pipe strains along the drill path over time for installation. Stress-strain relationships for pipe installation were developed and installation stresses were calculated using the strain measurements. The installation stresses on the pipe were calculated based on data from strain gauges installed at four quadrants inside the pipe wall, just behind the pullhead. The stresses calculated from the strain measurements were compared with the expected theoretical values determined using the analysis method recommended by PRCI.

The locations within the bore path at which high strain/stress values were recorded and their combined effect on the pipe section were found to be different than provided by theoretical considerations. The high variability in the downhole condition of the bore along the alignment resulted in high variation in the measured strains on the pipe during pullback. For both case studies, the axial pulling stresses arising from strain measurements showed that as the pullback was progressed, almost entire rig force was transferred to the product pipe at many locations along the process. The presence of bending moment across each pair of gauges was observed at all locations along the borehole path, including the straight sections due to the as-

built condition of the drill path. The maximum bending stresses expected based on the smallest as-built radii of the drill profiles were not identified in the bending stresses based on the strain gauges recordings. For both installations, multiple abrupt increases in circumferential stresses were observed beyond the expected pattern. These high stress points may be due to locally imposed loading, pipe cross-section ovaling, or a surge effect caused by the rapid movement of the pipe section. The circumferential stresses calculated from strain data were greater than predicted maximum hoop stresses, although heaviest drilling fluid densities observed during pullbacks (worst case) were applied to entire pullback operation to estimate the hoop stress along the borehole. The strain measurements during installation showed that the stress predictions based on current design practice are not conservative enough to account for the actual circumferential stresses on the pipe. Among the different loadings on the pipe, the circumferential stress imposed on the pipe can be the limiting factor for deep, larger-diameter installations.

9.2.4 Pipe Curvature Analysis

A new method to calculate the pipe bend radii based on as-drilled survey data and the borehole overcut size using the concept of geometric modeling and Bézier curves was developed. In the absence of knowledge of the actual reamed borehole geometry, a key assumption within the proposed method is that the reamed borehole is uniformly enlarged around the center of the drilled pilot hole. Application of the geometric modeling of the pipe inside the borehole based on Bézier curves was applied for a case study. A 3D model of the pipe curvature inside the reamed borehole was also developed to evaluate what the best pipe-curve fitting scenario would look like. A series of curvatures representing the pipe inside the hole were generated by the Bézier algorithm. The Bézier function resulted in larger radii over one and three joints at most locations along the drill path compared to the conventional calculated radius over the same course length while radii calculated based on Bézier curves were still smaller than the best fit curve scenario determined by 3D modeling. Geometric modeling analysis—such as Bézier curves and 3D model—showed that the installed pipe can have different radii of curvature along the bore path than the radii determined from pilot hole drilling survey data.

The application of the Bézier curves was further tested in a case study project with a 914 mm outside diameter (NPS 36) steel pipe HDD project through dense soil where the actual location of the installed pipe was assessed using the surveys from an ILI tool. Comparisons were made between the centerline position of the pipeline based on the ILI survey and the survey of the pilot hole while drilling. Variations were seen between the final location of the installed pipe and the as-built path defined by the centerline of the pilot bore. The bend radius of the actual pipeline was calculated and compared with the pilot hole radius for the length of the borehole. Particular attention was paid to the locations along the borehole with the smallest bend radii, since the tight bends at these locations indicate larger bending stress and a higher risk of overstressing the product pipe. In all areas where the pilot hole survey data included radii smaller than the minimum allowable bend radius, the actual pipeline curvatures were larger than the allowable limit. Throughout the HDD alignment, the actual installed pipeline followed a smoother curvature with larger bend radii at most locations compared with the as-drilled pilot hole survey. While there were two locations along the bore path where the bend radius determined on basis of the ILI survey of the installed pipeline is less than the bend radius of the as-built pilot hole, at both points the values based on the survey of the installed pipe was well above the minimum allowable bend radius.

To check the curvature imposed on the product pipe based on the as-drilled pilot bore and the borehole overcut, the Bézier curve method was utilized for geometric modeling of the pipe inside the reamed borehole. The smallest bending radii suggested by geometric modeling along the bore path gave a better representation of the tight curvatures of the actual pipe as opposed to using as-drilled pilot hole radii as a metric for the bending radii imposed on the pipe.

9.3 Research Contributions

The main contributions of this research are as follows:

1- Assessment of the commonly used engineering assumptions in pull force estimation and evaluation of the prediction's accuracy based on the scope of the HDD crossings. Because it is an accepted engineering practice to use input parameters that will result in larger pull forces to account for worst

case scenarios, predicted pullback forces were calculated using the higher range of industry accepted values for pullback parameters (friction factors, fluidic drags, and mud properties) to evaluate the accuracy of the pull force estimations. It was concluded that higher values of design inputs that results in larger pull forces (including borehole friction coefficient, mud density and buoyancy assumption resulting in heavier pipe weight) should be considered for smaller HDD projects with less ideal bore conditions. Similarly, lower values of borehole friction coefficient, fluidic drag coefficient, mud density and buoyancy assumption resulting in lighter pipe weight and frictions can be considered for larger projects with more ideal construction conditions.

2- Identification of the appropriate safety factors for pull force calculation during design phases of the HDD projects. The observed deviations between predicted and observed pull forces suggest that safety factors may range to an upper value of 2.5 to 3 for smaller projects with poor bore conditions and 1.25 to 1.5 for large projects involving proper conditioning of the borehole and effective cuttings removal that assists with reducing excessive mechanical work during pullback.

3- Expand applicability of PRCI pull force prediction method to bundle pipe installations based on the concept of an equivalent single pipe. The accuracy of pull force predictions improved significantly compared to actual recorded pull forces when calculations were based on the modified PRCI method using the proposed equivalent pipe parameters. The simple equivalent pipe method can be used to extend the PRCI method for pull force estimation of steel bundled pipes in medium to large HDD crossings.

4- Assess the expected strain and stress behavior of steel pipes during HDD installations and evaluate different installation loads imposed on the pipe using strain gauges during different stages of the pullback operation. The strain monitoring and stress calculation described in this thesis provided new information on the expected behavior of steel pipes during HDD installations that can be referenced by the industry. In addition, the strain monitoring methodology used in this work can be implemented in other projects.

5- Development and incorporation of a geometric modeling technique to predict pipe position within the reamed borehole which can be used for as-built stress analysis and identifying any sections within the drilled path that may require steering corrections or re-drill. Verification of the bend radius of the product pipe based on the as-built drill path is a critical step in pipeline owners accepting the as-drilled bore and allowing the contractor to install the product pipe. The proposed geometric modeling method can be used by HDD designers and the owner's representatives during completion of the pilot hole to ensure that pipe bend radius will fall within the acceptable ranges.

9.4 Research Limitations and Suggestion for Future Works

Research limitations and the recommendations for future research are presented as follow to further advance the work presented in this thesis.

- As part of the collection of 200 case studies, detailed soil characteristics of many of the case studies were not available and the geotechnical classification in this research was limited to soft vs. hard formations based on the executed drilling methodologies (jetting vs mud motor drilling). For similar future research, the case study database can be expanded in multiple directions for different soil types within each soft and hard formation category. This can include data samples of pull forces in highly competent rock versus highly fractured rock. The comparison of predicted and measured pull forces can be also expanded for different bore geometries since the geometry of an HDD alignment has a large influence on pull forces. Expanding the data base for pull force prediction accuracy would provide valuable information and insight to the industry as to the types of factors that could be used in the prediction mode to better match the actual load.
- Evaluation of the concept of single equivalent pipe was investigated in five case studies as part of this thesis. More bundled pipe installation projects can be studied to further evaluate the application of this concept. The mechanics of pipe installation during a bundled HDD is more complicated than installation of a single pipe, due to the interactions of the product pipes with each other and the surrounding environment, including the drilling fluid inside the borehole and the borehole walls.

Future research can be focused on a detailed analysis of the bundled pipe installation to more accurately predict the borehole and fluid frictions applied to bundled pipes downhole.

- The strain measurements obtained from strain gauges used in this thesis are the strains from the local loading imposed at the leading edge of the pipe section. The global pipe deformation on pipe sections more remote from the leading end might not be captured by the applied strain gauge arrangement. For future research, it is recommended to install an additional strain gauge assembly at a distance further away from the present assembly for future strain monitoring works to allow for a comparison between strain readings at two different sections along the pipe. A suitable distance could be around 10 times pipe diameters.
- The strain measurements gathered in this thesis were limited to two crossings. It is recommended that more HDD installations be conducted with strain monitoring for different crossing geometries, pipe sizes and ground conditions to provide a comprehensive understanding of the stresses on steel pipe during pullback. With measurement of strains during installation for multiple HDD crossings of varying pipe diameter, pipe grade, wall thicknesses, and for different geotechnical conditions and crossing geometries, revisions to current calculation method could be evaluated to better match the actual loads.
- Advancements in fibre optic sensors for strain measurements could be an opportunity to supplement the initial strain monitoring work discussed in this thesis. Fibre optic sensors provide a reliable method for monitoring the response of buried pipelines, not only during the installation, but the during long-term operations. Installation of longitudinally arranged fibre Bragg grating sensors for the entire length of the HDD pipe section could facilitate continuous monitoring of axial strains along the full length of the pipeline, from the initial lifting of the pipeline before pullback to the final position of the installed pipe.
- In this thesis, verification of the installed pipeline geometry using in line inspection tool was limited to a single project. Similar investigations using in line inspection tools should be conducted for

bores in different geotechnical conditions and of various diameters to evaluate the pipe bend radius and allow further comparisons of the actual curvature of the pipe with bend radii based on survey data from the pilot hole or geometric modeling. This will allow the applicability of the proposed geometric modeling method to be verified on additional projects.

References

Allouche, E. N., Ariaratnam, S. T., and Lueke, J. S. 2000. "Horizontal directional drilling: profile of an emerging industry." Journal of Construction Engineering and Management, 126(1), 68-76.

Allouche, E. N., Ariaratnam, S. T., and MacLeod, C. W. 2003. "Software for planning and cost control in directional drilling projects." Journal of construction engineering and management, 129(4), 446-453.

API (American Petroleum Institute). 2014. *Recommended Practice for Planning, Designing and Constructing Fixed Offshore Platforms - Working Stress Design*. ANSI/API RP 2A-WSD-14. Twenty-second Edition, Washington, US.

API (American Petroleum Institute). 1985. *Directional Drilling Survey Calculation Methods and Terminology*. API Bulletin D20, Washington, DC.

Ariaratnam, S.T. and Allouche, E.N., 2000. "Suggested practices for installations using horizontal directional drilling." *Practice Periodical on Structural Design and Construction*, 5(4), pp.142-149. https://doi.org/10.1061/(ASCE)1084-0680(2000)5:4(142)

ASCE (American Society of Civil Engineers). 2014. *Pipeline design for installation by horizontal directional drilling: ASCE manual of practice.* American Society of Civil Engineers, Reston, VA.

ASME (American Society of Mechanical Engineers). 2018. *Gas Transmission and Distribution Piping Systems*. ASME B31.8. New York, NY: ASME.

ASME (American Society of Mechanical Engineers). 2019. *Pipeline Transportation Systems for Liquid Hydrocarbons.* ASME B31.4. New York, NY: ASME.

ASTM (American Society for Testing and Materials). 2020. *Standard guide for use of maxi-horizontal directional drilling for placement of polyethylene pipe or conduit under obstacles, including river crossings*. ASTM F 1962-20, West Conshohocken, PA: ASTM.

ASTM (American Society for Testing and Materials). 2018. *Standard Test Method for Standard Penetration Test (SPT) and Split-Barrel Sampling of Soils*. ASTM D1586 / D1586M – 18, West Conshohocken, PA: ASTM.

Atalah, A., Kariuki, J., and Najafi, M. 2009. "Cost Comparison between horizontal directional drilling and open-cut construction methods in Nairobi, Kenya." Journal of construction engineering and management, 361(41073), 144.

Baroid Fluids Handbook. 1998. Baroid Drilling Fluids, Inc. Houston, TX.

Barton, Steve, Card, Kirk, and Garrett Pierce. 2009. "Delivering Steering Success in Problematic Soft-Formation Directional Wells." *SPE Drill & Compl* 24 (2009): 537–544. doi: https://doi-org.login.ezproxy.library.ualberta.ca/10.2118/115138-PA

Baumert, M. E., and E. N. Allouche. 2002. "Methods for estimating pipe pullback loads for horizontal directional drilling (HDD) crossings." *J. Infrastruct. Syst.*, 8(1): 12-19. https://doi.org/10.1061/(asce)1076-0342(2002)8:1(12).

Baumert, M. E., Allouche, E. N., and Moore, I. D. 2004. "Experimental investigation of pull loads and borehole pressures during horizontal directional drilling installations." *Canadian Geotechnical Journal*. 41(4): 672-685. https://doi.org/10.1139/t03-090

Baumert, M. E., Allouche, E. N., and Moore, I. D. 2005. "Drilling fluid considerations in design of engineered horizontal directional drilling installations." *Int. J. Geomech*., 5(4): 339–349. https://doi.org/10.1061/(ASCE)1532-3641(2005)5:4(339)

Bennett, D., and Ariaratnam, S. T. 2017. *NASTT's Horizontal Directional Drilling (HDD): Good Practices Guidelines*. North American Society for Trenchless Technology.

Biswas, P. and Langdon, P. 2015. "Multimodal intelligent eye-gaze tracking system." *International Journal of Human-Computer Interaction*, 31(4), 277-294.

Britannica, the Editors of Encyclopaedia. 2013. "Curvature". *Encyclopedia Britannica*. Accessed October 10, 2021. https://www.britannica.com/science/curvature.

Bruce, W. A., Amend, W. E., Wang, Y. Y., and Zhou, H. 2012. “Guidelines to Address Pipeline Construction Quality Issues.” Final report to Pipeline Research Council International, Inc. for PRCI MATH-5-1.

Bueno, S. M. 2021. “Celebrating HDD at 50.” Trenchless Technology (magazine). Accessed August 25, 2021. https://trenchlesstechnology.com/celebrating-hdd-at-50/

Cai, L., G. Xu, M. A. Polak, and M. Knight. 2017. “Horizontal directional drilling pulling forces prediction methods – a critical review.” *Tunn. Undergr. Space Technol.,* 69: 85–93. https://doi.org/10.1016/j.tust.2017.05.026

Cai, L., and M. A. Polak. 2019. “A theoretical solution to predict pulling forces in horizontal directional drilling installations.” *Tunnelling Underground Space Technol*. 83 (Sep): 313–323. https://doi.org/10 .1016/j.tust.2018.09.014.

Canadian Infrastructure Report Card. http://canadianinfrastructure.ca/en/strom-water.html.

CAPP (The Canadian Association of Petroleum Producers). 2004, “Planning Horizontal Directional Drilling for Pipeline Construction”. CAPP 2004-0022, Calgary, AB.

Chehab, A. G., and Moore, I. D. 2007. “One-Dimensional Calculations for Axial Pullback Force Distributions in Pipes During Directional Drilling Installations.” In 2007 International Geo Conference, Ottawa.

Chehab, A.G. 2008. “Time dependent response of pulled-in-place HDPE pipes.” Ph.D. thesis, Queen′s University, Kingston, Canada.

Cheng, E., and M. A. Polak. 2007. “Theoretical model for calculating pulling loads for pipes in horizontal directional drilling.” *Tunn. Undergr. Space Technol.*, 22(5-6): 633-643. https://doi.org/10.1016/j.tust.2007.05.009.

Cholewa, J.A., R.W.I. Brachman, and I.D. Moore. 2010. “Stress–strain measurements for HDPE pipe during and after simulated installation by horizontal directional drilling.” *Tunnelling Underground Space Technol*. 25 (6): 773-781. https://doi.org/10.1016/j.tust.2009.09.002.

Code of Federal Regulations (CFR), Title 49, Part 192 Transportation of Natural and Other Gas by Pipeline: Minimum Federal Safety Standards

Code of Federal Regulations (CFR), Title 49, Part 195 Transportation of Hazardous Liquids by Pipeline

Conroy, P. J., Latorre, C. A., and Wakeley L. D. (2002). "Installation of Fiber Optic Cables under Flood-Protection Structures Using Horizontal Directional Drilling Techniques." Geotechnical and Structures Laboratory, US Army Corps of Engineers, ERDC/GSL TR-02-8.

CSA (Canadian Standards Association). 2019. *Oil and gas pipeline systems.* CSA Z662-19. Toronto, ON: CSA Group.

DCA (Drilling Contractors Association). 2015. *Horizontal Directional Drilling – Technical Guidelines*. DCA-Europe.

Duan, D. M., Jurca, T., and Zhou, C. 2014. "A stress check procedure for pipe lowering-in process during pipeline construction." In 2014 10th International Pipeline Conference (pp. V001T03A006-V001T03A006). American Society of Mechanical Engineers.

Duyvestyn, G. 2009. "Comparison of predicted and observed HDD installation loads for various calculation methods." Proc., NASTT's No-Dig Show, Toronto, Canada.

El Chazli, G., S. Hinchberger, M. Baumert, and E. N. Allouche. 2005. "Experimental investigation of borehole and surface friction coefficients during HDD installations." In Proc., *North American Society for Trenchless Technology No-Dig Conference and Show*. Cleveland, OH: North American Society for Trenchless Technology.

Faghih, A., Yi, Y., Bayat, A. and Osbak, M. 2015. "Fluidic drag estimation in horizontal directional drilling based on flow equations." *Journal of Pipeline Systems Engineering and Practice*, *6*(4), p.04015006. https://doi-org.login.ezproxy.library.ualberta.ca/10.1061/(ASCE)PS.1949-1204.0000200

Farin, G. 1988. "Geometry in design: the Bezier method." In *Mathematical Aspects of Scientific Software*, 89-99. Springer, New York, NY. https://doi.org/10.1007/978-1-4684-7074-1_4

Farin, G. 2002. *Curves and surfaces for CAGD: A Practical Guide*. Fifth edition, Morgan Kaufmann.

Floater, M. S. 2015. “Bezier curves and surfaces”. An entry for the Encyclopedia of Applied and Computational Mathematics, Springer, Berlin, Heidelberg.

Fowler, J. R. and Langner, C. G. 1991. "Performance Limits for Deepwater Pipelines", OTC 6757, 23rd Annual Offshore Technology Conference, Houston, Texas, May 6-9.

Gawedzki, W., and Tarnowski, J. 2015. “Design and testing of the strain transducer for measuring deformations of pipelines operating in the mining-deformable ground environment.” Measurement Science Review, 15(5), 256-262.

Gelinas, M., M.A. Polak, and R. McKim. 2000. “Field tests on high density polyethylene pipes installed using horizontal directional drilling.” *J. Infrastruct. Syst.*, 6(4): 130–137. https://doi.org/10.1061/(asce)1076-0342(2000)6:4(130)

Goerz, B., J. Taylor, and M. Martens. 2014. “Longitudinal and Circumferential Pipe Stress in Horizontal Directional Drills.” In Proc, *North American Society for Trenchless Technology 2014 No-Dig Show.* Orlando, FL: North American Society for Trenchless Technology.

Gokhale S., Hamm R., and Sterling R. 1999. “A comprehensive survey on the state of horizontal directional drilling in North America provides an inside look at this increasingly growing industry.” Direct Drilling, Vol. 7, p. 20-23.

Haciislamoglu, M., and Langlinais, J. 1990. “Non-Newtonian flow in eccentric annuli.” *J. Energy Resour. Technol.*, 112(3): 163-169. https://doi.org/10.1115/1.2905753

Hassan, M. K., S. Alam, C. Bartlett, and E. N. Allouche. 2014. “Experimental Investigation of Soil-Pipe Friction Coefficients for Thermoplastic Pipes Installed in Selected Geological Materials.” In Proc, *North American Society for Trenchless Technology 2014 No-Dig Show.* Cleveland, OH: North American Society for Trenchless Technology.

Hazewinkel, M. 1997. “Encyclopaedia of Mathematics: Supplement. 1.” Springer Science and Business Media.

Huey, D. P., J. D. Hair, and K. B. McLeod. 1996. “Installation loading and stress analysis involved with pipelines installed in horizontal directional drilling.” In *Proc., North American Society for*

Trenchless Technology 1996 No-Dig Show, Cleveland, OH: North American Society for Trenchless Technology.

Khan S., Bennett D., McCrary S., and Iseley T. 1994. "Mini-Horizontal Directional Drilling: State-of-the-Art Review." Trenchless Technology Center at Louisiana Tech University, Ruston, Louisiana.

Keil, S. 2017. "Technology and practical use of strain gages: with particular consideration of stress analysis using strain gages." John Wiley and Sons.

Kirby M. J., and Kramer S. R. 1996. "Design guidelines and procedures for guided horizontal drilling, Part II." No-Dig Engineering, p. 13-15.

Kruse, H. M. G., and H. J. A. M. Hergarden. 2010. "Soil loads on Pipelines, the Dutch approach." In *Proc., 5th Pipeline Technology Conference*, Hannover, Germany.

Latorre C. A., Wakeley L. D., and Conroy P. J. 2002. "Guidelines for Installation of Utilities Beneath Corps of Engineers Levees Using Horizontal Directional Drilling." Geotechnical and Structures Laboratory, US Army Corps of Engineers.

Liu, M., Wang, Y. Y., and Rogers, G. 2008. "Stress analysis of pipe lowering-in process during construction." In 2008 7th International Pipeline Conference (pp. 223-228). American Society of Mechanical Engineers.

Loh, J. T. 1990. "A Unified Design Procedure for Tubular Members", OTC 6310, 22nd Annual Offshore Technology Conference, Houston, Texas, May 7-10.

Lubrecht, M. D. 2012. "Horizontal Directional Drilling: A Green and Sustainable Technology for Site Remediation." ACS Publications 2484-2489.

Maidla, E. E. 1987. "Borehole Friction Assessment and Application to Oilfield Casing Design in Directional Wells." Doctoral dissertation Louisiana State University, Department of Petroleum Engineering, Baton Rouge, LA.

Maidla, E. E., and A. K. Wojtanowicz. 1990. "Laboratory study of borehole friction factor with a dynamic-filtration apparatus." *SPE Drill. Eng.*, *5*(03): 247-255. https://doi.org/10.2118/18558-PA.

Maqsood, S., Abbas, M., Miura, K. T., Majeed, A., and Iqbal, A. 2020. “Geometric modeling and applications of generalized blended trigonometric Bézier curves with shape parameters.” *Advances in Difference Equations*, 550 (2020). https://doi.org/10.1186/s13662-020-03001-4

Najafi, M. 2010. *Trenchless Technology Piping: Installation and Inspection*. McGraw-Hill, New York.

Najafi, M. 2014. *Trenchless Technology: Pipeline and Utility Design, Construction, and Renewal.* McGraw-Hill, New York.

NASTT’s Horizontal Directional Drilling (HDD) Good Practices Guidelines. 2017. Cleveland, OH: HDD Consortium.

NEN (Royal Netherlands Standardization Institute). 2020. *Requirements for Pipeline Systems*. NEN 3650:2020, Delft, Netherlands: Netherlands Standardization Institute.

Petroff, L.J. 1997. “Design Guidelines for Directional Drilled PE Pipe”, American Society of Civil Engineers Congress on Trenchless Technology.

PRCI (Pipeline Research Council International). 2015. *Installation of Pipeline by Horizontal Directional Drilling – an Engineering Guide.* PR-277-144507-R01. Chantilly, VA: Pipeline Research Council International Inc.

PRCI (Pipeline Research Council International). 2011. *Second Generation Models for Strain-Based Design*. Catalog No. L5XXXX. Houston, TX: Pipeline Research Council International Inc.

Piping Design and Analysis Software, AutoPIPE. Bentley Systems Incorporated.

Podbevsek, F., H. J. Brink, and J. Spiekhout. 2009. "Horizontal directional drilling: the influence of uplift and downlift during the pull-back operation." *Journal of Pipeline Engineering,* 8(4), 283-287.

PHMSA (Pipeline and Hazardous Materials Safety Administration). 2015 "Operator annual report". Accessed October 30, 2021. https://primis.phmsa.dot.gov/comm/FactSheets/FSPipelineMaterials.htm

Polak, M. A., and A. Lasheen. 2001. “Mechanical modelling for pipes in horizontal directional drilling.” *Tunn. Undergr. Space Technol.*, 16(1), 47-55. https://doi.org/10.1016/s0886-7798(02)00020-2

Polak, M. A., Duyvestyn, G. and Knight, M. 2004. “Experimental strain analysis for polyethylene pipes installed by horizontal directional drilling.” *Tunnelling Underground Space Technol.* 19 (Mar): 205-216. https://doi.org/10.1016/j.tust.2003.11.003.

Puckett, J. S. 2003. Analysis of theoretical versus actual HDD pulling loads. In *Proc, Pipelines 2003 - Pipeline Engineering and Construction International Conference 2003*, Reston, VA: American Society of Civil Engineers. https://doi.org/10.1061/40690(2003)146

Rabiei, M., Yi, Y., Bayat, A., Cheng, R. and Osbak, M., 2017. “Estimation of hydrokinetic pressure and fluidic drag changes during pipe installations via HDD based on identifying slurry-flow pattern change within a borehole.” *Journal of Pipeline Systems Engineering and Practice*, 8(4), p.04017020. https://doi.org/10.1061/(ASCE)PS.1949-1204.0000285

Rig worker, 2005. “HDD Risk Identification.” Accessed May 07, 2022. https://www.rigworker.com/horizontal-directional/hdd-risk-identification.html

Royal, A.C.D., Riggall, T.J. and Chapman, D.N., 2010. “Analysis of steering in horizontal directional drilling installations using down-hole motors.” *Tunnelling and Underground Space Technology*, 25(6), pp.754-765. https://doi.org/10.1016/j.tust.2010.06.004.

Scott, C., Etheridge, B., and Vieth, P. 2008. “An Analysis of the Stresses Incurred in Pipe During Laying Operations.” In 2008 7th International Pipeline Conference (pp. 197-204). American Society of Mechanical Engineers.

Sen, M., and Zhou, J. 2008. “Evaluation of Pipeline Stresses During Line Lowering.” In 2008 7th International Pipeline Conference (pp. 213-221). American Society of Mechanical Engineers.

Sheiner, L. B., and Beal, S. L. 1981. Some suggestions for measuring predictive performance. *Journal of pharmacokinetics and biopharmaceutics*, 9(4), 503-512. https://doi.org/10.1007/BF01060893

Shene, C. K. 2011. “CS3621 Introduction to Computing with Geometry Notes.” Department of Computer Science, Michigan Technological University, https://pages.mtu.edu/~shene/COURSES/cs3621/NOTES/ (accessed Dec. 4, 2020)

Stein, D., Mollers, K., and Bielecki, R. 1989. “Microtunnelling”, Ernst and Sohn, Berlin, Germany.

Silva, D.M.L.D., Rodrigues, M.V., Venaas, A. and Medeiros, A.R.D. 2009. “Methodology for definition of bending radius and pullback force in HDD operations.” In *Proc., Presented at the Rio Pipeline Conference and Exposition 2009*, Rio de Janeiro, Brazil: Brazilian Petroleum, Gas and Biofuels Institute.

Slavin, L.M., 2011. “Guidelines for use of mini-horizontal directional drilling for placement of high density polyethylene pipe.” *In Pipelines 2011: A Sound Conduit for Sharing Solutions*. pp. 882-89. https://doi.org/10.1061/41187(420)81

The Plastic Pipe Institute® (PPI). 2009. *Handbook of Polyethylene Pipe*. Second Edition; PPI, Wash., DC.

Timoshenko, S. P. and Gere, J. M. 1972. “Mechanics of Materials”. New York: Van Nostrand Reinhold Company, p. 9.

Trenchlesspedia, 2021. "Allowable Bend Radius". Accessed October 17, 2021. https://www.trenchlesspedia.com/definition/2224/allowable-bend-radius

Trenchlesspedia, 2021. "Why the Oil and Gas Pipeline Industries are Eyeing Horizontal Directional Drilling". Accessed November 06, 2021. https://www.trenchlesspedia.com/why-the-oil-and-gas-pipeline-industries-are-eyeing-hdd/2/3247

Trenchless Technology. (2011). “Horizontal Directional Drilling Guide.” Trenchless Technology Supplements. Retrieved from www.trenchlessonline.com.

Yan, X., S. T. Ariaratnam, S. Dong, and C. Zeng. 2018. “Horizontal directional drilling: State-of-the-art review of theory and applications.” *Tunnelling Underground Space Technol.* 72: 162–173.

Zhang, F., Liu, M., Wang, Y. Y., and Bruce, W. A. 2014. “Stress Analysis of Lifting and Lowering-in Process.” In 2014 10th International Pipeline Conference (pp. V001T03A012-V001T03A012). American Society of Mechanical Engineers.

Appendix A: 200 Case Studies Summary

Table A.1 presents predicted and actual loads for all case studies. The following classifications were used for the different project categories in this paper and listed in Table 9 for each case study.

- Pipe outside diameters: 60-324 mm (small pipes), 355-559 mm (medium pipes), diameters 610-914 mm with no buoyancy control (large pipes w/o BC), and 610-1067 mm filled with buoyancy control (large pipes w/ BC).
- Crossing lengths: shorter than 300 m, 300-700 m, and longer than 700 m.
- Formation: soft formation (soft or loose soils with SPT N-Values less than 30) vs. hard formation (hard or dense soils with SPT N-Values greater than 30 and rock).
- Equipment size: mini HDD (17-50 tonnes rigs), midi HDD (63-181 tonnes rigs) and maxi HDD (200-500 tonnes rigs).

Table A.1. Summary of 200 case studies

Project #	Pipe OD (mm)	HDD Length (m)	Equipment Size	Formation	Buoyancy Control (Yes/No)	Predicted Pull Force[1] (kN)	Observed Pull Force (kN)	Predicted Force / Length (kN/m)	Observed Force / Length (kN/m)
1	60	432	Mini HDD	Hard	No	14.8	26.7	0.034	0.062
2	114	776	Midi HDD	Soft	No	71.2	324.7	0.092	0.418
3	114	78	Mini HDD	Soft	No	5.9	10.2	0.076	0.131
4	114	66	Mini HDD	Soft	No	5.9	4.4	0.090	0.067
5	168	189	Mini HDD	Soft	No	32.6	146.8	0.173	0.777
6	168	640	Midi HDD	Hard	No	100.8	280.2	0.158	0.438
7	219	820	Maxi HDD	Hard	No	115.7	324.7	0.141	0.396
8	219	362	Mini HDD	Soft	No	65.2	133.4	0.180	0.369
9	219	426	Mini HDD	Hard	No	80.1	200.2	0.188	0.470
10	219	829	Midi HDD	Hard	No	169.0	242.0	0.204	0.292
11	219	498	Midi HDD	Hard	No	109.7	189.0	0.220	0.380
12	219	523	Midi HDD	Hard	No	91.9	142.3	0.176	0.272
13	219	548	Midi HDD	Soft	No	103.8	155.7	0.189	0.284
14	219	534	Midi HDD	Soft	No	109.7	209.1	0.205	0.392
15	219	392	Mini HDD	Hard	No	83.0	127.2	0.212	0.325
16	219	314	Mini HDD	Hard	No	68.2	117.4	0.217	0.374
17	219	447	Midi HDD	Hard	No	68.2	62.3	0.153	0.139
18	219	489	Midi HDD	Soft	No	105.3	164.6	0.215	0.337

19	219	222	Mini HDD	Hard	No	50.4	111.2	0.227	0.501
20	273	239	Mini HDD	Soft	No	68.2	244.7	0.285	1.024
21	273	255	Midi HDD	Hard	No	163.1	133.4	0.640	0.523
22	273	208	Midi HDD	Soft	No	151.2	120.1	0.727	0.577
23	273	221	Mini HDD	Hard	No	83.0	115.7	0.376	0.523
24	324	2011	Maxi HDD	Soft	No	65.2	464.9	0.032	0.231
25	324	1979	Maxi HDD	Hard	No	747.3	462.6	0.378	0.234
26	324	1994	Maxi HDD	Hard	No	774.0	462.6	0.388	0.232
27	324	415	Midi HDD	Hard	No	118.6	89.0	0.286	0.214
28	324	953	Maxi HDD	Hard	No	160.1	75.6	0.168	0.079
29	324	807	Maxi HDD	Hard	No	154.2	554.8	0.191	0.688
30	324	820	Maxi HDD	Hard	No	151.2	391.4	0.184	0.477
31	324	503	Midi HDD	Hard	No	210.5	142.3	0.419	0.283
32	324	527	Midi HDD	Soft	No	222.4	329.2	0.422	0.625
33	324	431	Midi HDD	Soft	No	180.9	84.5	0.420	0.196
34	324	423	Midi HDD	Soft	No	169.0	75.6	0.400	0.179
35	324	362	Mini HDD	Soft	No	127.5	169.0	0.352	0.467
36	324	362	Mini HDD	Soft	No	127.5	160.1	0.352	0.442
37	324	425	Mini HDD	Hard	No	154.2	360.3	0.363	0.848
38	324	847	Maxi HDD	Hard	No	329.2	298.0	0.389	0.352
39	324	430	Mini HDD	Hard	No	109.7	320.3	0.255	0.745
40	324	1470	Maxi HDD	Hard	No	542.7	533.8	0.369	0.363
41	324	2011	Midi HDD	Soft	No	717.6	464.9	0.357	0.231
42	406	323	Midi HDD	Hard	No	189.8	106.8	0.588	0.331
43	406	1000	Maxi HDD	Hard	No	590.1	787.8	0.590	0.788
44	406	838	Maxi HDD	Hard	No	486.3	373.7	0.580	0.446
45	406	382	Midi HDD	Hard	No	234.3	349.3	0.613	0.914
46	406	972	Maxi HDD	Hard	No	563.4	195.7	0.580	0.201
47	406	1042	Maxi HDD	Hard	No	554.5	489.3	0.532	0.470
48	406	1,462	Maxi HDD	Hard	No	714.7	568.6	0.489	0.389
49	406	606	Midi HDD	Hard	No	323.2	186.8	0.533	0.308
50	406	549	Midi HDD	Hard	No	305.4	339.8	0.556	0.619
51	406	861	Maxi HDD	Hard	No	510.1	226.9	0.592	0.263
52	406	265	Midi HDD	Hard	No	192.8	129.0	0.727	0.487
53	406	246	Midi HDD	Soft	No	139.4	177.9	0.567	0.723
54	406	183	Midi HDD	Soft	No	145.3	97.9	0.794	0.535
55	406	345	Midi HDD	Hard	No	216.5	173.5	0.627	0.503
56	406	505	Maxi HDD	Soft	No	311.4	244.7	0.617	0.484
57	406	228	Midi HDD	Soft	No	148.3	422.6	0.650	1.853
58	406	411	Midi HDD	Hard	No	249.1	400.3	0.606	0.974
59	406	361	Midi HDD	Hard	No	222.4	382.5	0.616	1.060
60	406	608	Maxi HDD	Hard	No	364.8	222.4	0.600	0.366
61	406	360	Maxi HDD	Hard	No	222.4	258.0	0.618	0.717
62	406	661	Maxi HDD	Hard	No	406.3	622.8	0.615	0.942

63	406	275	Midi HDD	Hard	No	148.3	133.4	0.539	0.485
64	406	194	Midi HDD	Soft	No	127.5	266.9	0.657	1.376
65	406	402	Mini HDD	Soft	No	246.1	484.9	0.612	1.206
66	406	415	Midi HDD	Hard	No	249.1	186.8	0.600	0.450
67	406	690	Maxi HDD	Hard	No	382.5	395.9	0.554	0.574
68	406	313	Midi HDD	Hard	No	177.9	155.7	0.568	0.497
69	406	223	Midi HDD	Soft	No	166.1	249.1	0.745	1.117
70	406	259	Midi HDD	Soft	No	198.7	235.8	0.767	0.910
71	406	354	Midi HDD	Hard	No	207.6	160.1	0.586	0.452
72	406	240	Midi HDD	Hard	No	177.9	84.5	0.741	0.352
73	406	296	Midi HDD	Soft	No	225.4	89.0	0.761	0.301
74	406	274	Midi HDD	Soft	No	204.6	266.9	0.747	0.974
75	406	216	Midi HDD	Hard	No	172.0	64.5	0.796	0.299
76	406	1048	Midi HDD	Hard	No	569.4	207.4	0.543	0.198
77	508	974	Maxi HDD	Hard	No	691.0	542.7	0.709	0.557
78	508	459	Maxi HDD	Hard	No	427.0	547.1	0.930	1.192
79	508	424	Midi HDD	Hard	No	335.1	195.7	0.790	0.462
80	508	952	Maxi HDD	Hard	No	726.5	1125.4	0.763	1.182
81	508	639	Midi HDD	Hard	No	593.1	271.3	0.928	0.425
82	508	460	Midi HDD	Hard	No	441.9	209.1	0.961	0.454
83	508	582	Midi HDD	Hard	No	536.8	613.9	0.922	1.055
84	508	352	Maxi HDD	Hard	No	281.7	231.3	0.800	0.657
85	508	273	Midi HDD	Soft	No	266.9	222.4	0.978	0.815
86	508	213	Midi HDD	Soft	No	180.9	266.9	0.849	1.253
87	508	358	Midi HDD	Hard	No	355.9	293.6	0.994	0.820
88	508	398	Midi HDD	Hard	No	370.7	253.5	0.931	0.637
89	508	703	Midi HDD	Hard	No	590.1	342.5	0.839	0.487
90	508	310	Midi HDD	Soft	No	296.5	195.7	0.957	0.631
91	508	276	Mini HDD	Soft	No	284.7	195.7	1.031	0.709
92	508	382	Midi HDD	Soft	No	326.2	275.8	0.854	0.722
93	508	252	Mini HDD	Soft	No	249.1	151.2	0.988	0.600
94	508	239	Mini HDD	Soft	No	243.2	231.3	1.017	0.968
95	508	189	Midi HDD	Hard	No	183.9	240.2	0.973	1.271
96	508	225	Mini HDD	Soft	No	207.6	231.3	0.923	1.028
97	508	374	Midi HDD	Soft	No	355.9	311.4	0.951	0.833
98	508	451	Midi HDD	Hard	No	430.0	231.3	0.953	0.513
99	508	198	Mini HDD	Soft	No	166.1	231.3	0.839	1.168
100	508	609	Maxi HDD	Hard	No	575.3	467.1	0.945	0.767
101	508	1328	Maxi HDD	Hard	no	1067.6	978.6	0.804	0.737
102	508	489	Midi HDD	Soft	no	415.2	289.1	0.849	0.591
103	508	646.2	Midi HDD	Hard	No	222.4	324.7	0.344	0.503
104	508	806.1	Maxi HDD	Hard	No	355.9	355.9	0.441	0.441
105	508	332	Midi HDD	Soft	No	184.2	182.4	0.555	0.549
106	508	341	Midi HDD	Soft	No	281.7	400.3	0.826	1.174

107	508	796	Maxi HDD	Hard	No	386.1	676.1	0.485	0.849
108	508	529	Midi HDD	Hard	No	474.5	316.4	0.897	0.598
109	508	312	Maxi HDD	Hard	No	246.1	246.2	0.789	0.789
110	508	878	Maxi HDD	Hard	No	477.7	196.5	0.544	0.224
111	508	577	Maxi HDD	Hard	No	459.6	422.6	0.797	0.732
112	508	987.6	Maxi HDD	Hard	No	768.1	662.8	0.778	0.671
113	508	556	Midi HDD	Hard	No	533.8	266.9	0.960	0.480
114	508	925	Midi HDD	Hard	No	688.0	355.9	0.744	0.385
115	508	211	Mini HDD	Soft	No	186.8	166.8	0.885	0.791
116	508	459	Midi HDD	Soft	No	236.3	293.6	0.515	0.640
117	508	356	Midi HDD	Soft	No	281.7	333.6	0.791	0.937
118	508	707	Maxi HDD	Hard	No	340.1	471.5	0.481	0.667
119	508	297	Maxi HDD	Hard	No	162.8	253.5	0.548	0.854
120	508	559	Midi HDD	Hard	No	278.8	204.6	0.499	0.366
121	508	329	Midi HDD	Hard	No	246.1	400.3	0.748	1.217
122	508	239	Mini HDD	Soft	No	195.7	240.9	0.819	1.008
123	508	249	Midi HDD	Soft	No	133.2	364.8	0.535	1.465
124	508	429	Midi HDD	Hard	No	311.4	306.9	0.726	0.715
125	508	529	Midi HDD	Soft	No	278.5	257.3	0.526	0.486
126	508	173	Mini HDD	Soft	No	151.2	166.8	0.874	0.964
127	508	426	Midi HDD	Hard	No	308.4	275.8	0.724	0.647
128	508	126	Mini HDD	Soft	No	130.5	111.2	1.036	0.882
129	508	358	Midi HDD	Soft	No	275.8	246.7	0.770	0.689
130	508	313	Midi HDD	Soft	No	252.1	200.0	0.805	0.639
131	508	373	Midi HDD	Soft	No	293.6	355.9	0.787	0.954
132	508	195	Midi HDD	Soft	No	169.0	133.4	0.867	0.684
133	508	326	Midi HDD	Soft	No	258.0	333.6	0.791	1.023
134	508	1041	Maxi HDD	Hard	No	597.0	984.8	0.573	0.946
135	508	310	Midi HDD	Soft	No	243.2	222.4	0.784	0.717
136	508	340	Midi HDD	Soft	No	258.0	218.0	0.759	0.641
137	610	309	Midi HDD	Hard	No	424.1	222.4	1.372	0.720
138	610	878	Maxi HDD	Hard	No	1052.7	800.7	1.199	0.912
139	610	434	Midi HDD	Hard	No	557.5	232.5	1.285	0.536
140	610	1032	Maxi HDD	Hard	No	1248.5	460.8	1.210	0.447
141	610	976	Maxi HDD	Hard	No	1029.0	635.2	1.054	0.651
142	610	1,552	Maxi HDD	Hard	No	1589.5	511.5	1.024	0.330
143	610	621	Midi HDD	Hard	No	332.1	489.3	0.535	0.788
144	610	581	Midi HDD	Hard	No	667.2	427.0	1.148	0.735
145	610	880	Maxi HDD	Hard	No	1088.3	507.1	1.237	0.576
146	610	291	Midi HDD	Soft	No	453.7	213.5	1.559	0.734
147	610	232	Midi HDD	Soft	No	335.1	302.5	1.444	1.304
148	610	208	Midi HDD	Soft	No	344.0	146.8	1.654	0.706
149	610	376	Midi HDD	Hard	No	498.2	249.1	1.325	0.663
150	610	515	Maxi HDD	Soft	No	646.5	489.3	1.255	0.950

151	610	271	Midi HDD	Soft	No	367.7	489.3	1.357	1.806
152	610	422	Midi HDD	Hard	No	536.8	376.3	1.272	0.892
153	610	430	Midi HDD	Hard	No	542.7	711.7	1.262	1.655
154	610	606	Maxi HDD	Hard	No	753.2	504.9	1.243	0.833
155	610	441	Maxi HDD	Hard	No	560.5	582.9	1.271	1.322
156	610	713	Maxi HDD	Hard	No	910.4	582.7	1.277	0.817
157	610	304	Midi HDD	Hard	No	412.2	387.0	1.356	1.273
158	610	266	Midi HDD	Soft	No	358.8	400.3	1.349	1.505
159	610	422	Midi HDD	Soft	No	533.8	734.0	1.265	1.739
160	610	435	Midi HDD	Hard	No	533.8	800.7	1.227	1.841
161	610	677	Maxi HDD	Hard	No	771.0	533.8	1.139	0.788
162	610	393	Midi HDD	Hard	No	498.2	266.9	1.268	0.679
163	610	233	Midi HDD	Soft	No	385.5	333.6	1.655	1.432
164	610	285	Midi HDD	Soft	No	453.7	444.8	1.592	1.561
165	610	429	Midi HDD	Hard	No	548.6	311.4	1.279	0.726
166	610	260	Midi HDD	Hard	No	409.2	124.6	1.574	0.479
167	610	303	Midi HDD	Hard	No	486.3	160.1	1.605	0.529
168	610	305	Midi HDD	Soft	No	486.3	206.8	1.595	0.678
169	610	267	Midi HDD	Hard	No	430.0	155.7	1.610	0.583
170	610	273	Maxi HDD	Soft	No	364.8	343.6	1.336	1.259
171	610	1042	Maxi HDD	Hard	Yes	637.6	1014.2	0.612	0.973
172	762	1427	Maxi HDD	Hard	Yes	1533.2	1192.1	1.074	0.835
173	762	766	Maxi HDD	Hard	Yes	860.0	903.0	1.123	1.179
174	914	975	Midi HDD	Hard	No	258.0	338.1	0.265	0.347
175	914	210	Midi HDD	Soft	No	560.5	667.2	2.669	3.177
176	914	275	Midi HDD	Hard	No	154.2	489.3	0.561	1.779
177	914	214	Midi HDD	Soft	No	542.7	889.6	2.536	4.157
178	914	232	Maxi HDD	Soft	No	139.4	462.6	0.601	1.994
179	914	271	Maxi HDD	Soft	No	673.2	462.6	2.484	1.707
180	914	256	Maxi HDD	Soft	No	646.5	716.2	2.525	2.798
181	914	421	Maxi HDD	Soft	No	1052.7	622.8	2.501	1.479
182	914	971	Maxi HDD	Hard	Yes	1301.8	1125.4	1.341	1.159
183	914	647	Midi HDD	Hard	Yes	857.0	649.4	1.325	1.004
184	914	573	Midi HDD	Hard	Yes	779.9	689.5	1.361	1.203
185	914	311	Maxi HDD	Hard	Yes	418.1	467.1	1.344	1.502
186	914	430	Midi HDD	Hard	Yes	593.1	858.5	1.379	1.997
187	914	311	Midi HDD	Soft	Yes	418.1	947.5	1.344	3.047
188	914	328	Midi HDD	Soft	Yes	456.7	858.5	1.392	2.617
189	914	689	Midi HDD	Hard	Yes	969.7	756.2	1.407	1.098
190	914	263	Midi HDD	Soft	Yes	266.9	364.8	1.015	1.387
191	914	228	Midi HDD	Soft	Yes	172.0	364.8	0.754	1.600
192	914	273	Midi HDD	Soft	Yes	347.0	177.9	1.271	0.652
193	914	1370	Maxi HDD	Hard	Yes	1636.9	1067.6	1.195	0.779
194	914	607	Maxi HDD	Soft	Yes	824.4	1321.1	1.358	2.176

195	914	701	Maxi HDD	Hard	Yes	791.8	231.3	1.130	0.330
196	914	524	Maxi HDD	Soft	Yes	708.7	1250.9	1.353	2.387
197	914	400	Midi HDD	Soft	Yes	415.2	333.6	1.038	0.834
198	914	302	Midi HDD	Hard	Yes	302.5	564.9	1.002	1.871
199	914	698	Maxi HDD	Hard	Yes	943.0	1134.3	1.351	1.625
200	1067	998	Maxi HDD	Hard	Yes	2256.7	1294.4	2.261	1.297

[1] Predicted pull forces without any safety factor

Appendix B: Strain Guage Calibration Methodology

In the development of the strain gauge tool, expectations on what the tool would provide required a testing protocol to ensure accuracy and consistent measurement. To address this, a testing procedure was developed to provide a controlled loading condition. The strain gauges were installed into a 219 mm (NPS 8) grade 359 and 3 m long steel pipe. Once the gauges were installed, pull heads were welded on each end of the section, and it was transported to the testing facility. The section was placed in a tensile stress bed and subjected to tensile and bending loading conditions while the data was recorded. The testing procedure apparatus is illustrated in Figure B.1. The loading was increased at an interval of 25,000 lbs. up to a maximum of 100,000 lbs. (due to limitations on the clevis and associated connections). The test recorded strain data in the axial and hoop direction and later was compared with predicted values for the specific pipe section as shown in Figures B.2 and B.3. A bending condition was also introduced on the pipe section, but this was slightly less scientifically applicable because it was difficult to induce a significant pipe deflection on such a short piece of pipe, and the ability to measure the imposed deflection was also quite difficult.

Figure B.1. Axial Strain Gauge Testing Procedure

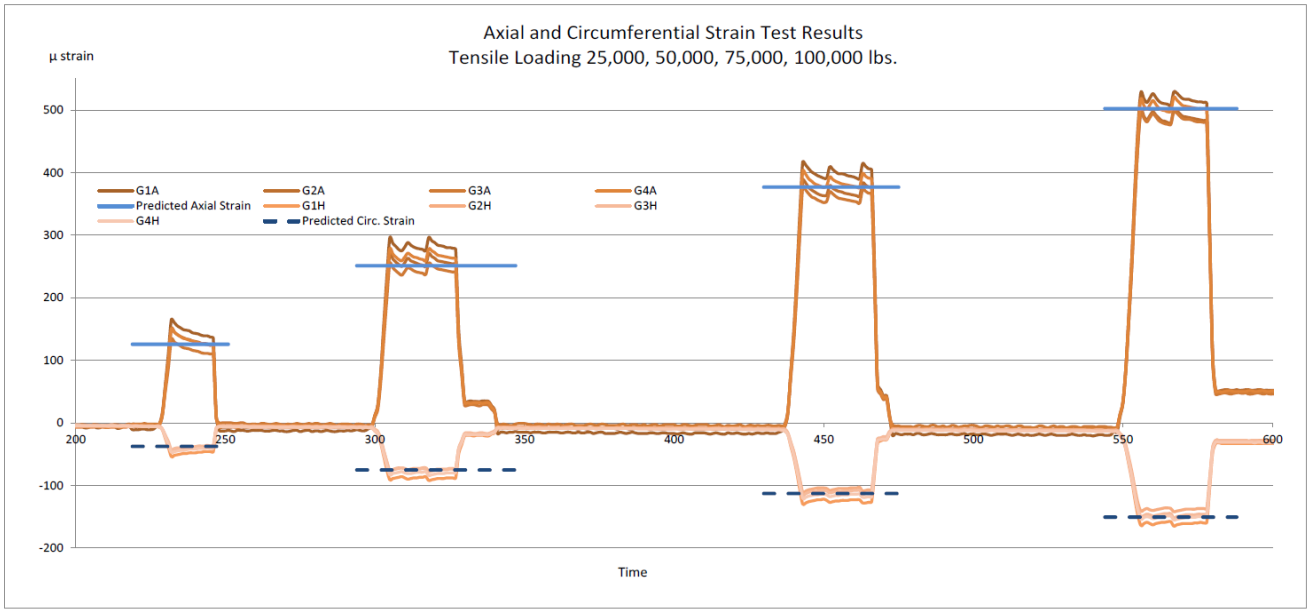

Figure B.2. Measured Axial and Circumferential Strains During Calibration Testing

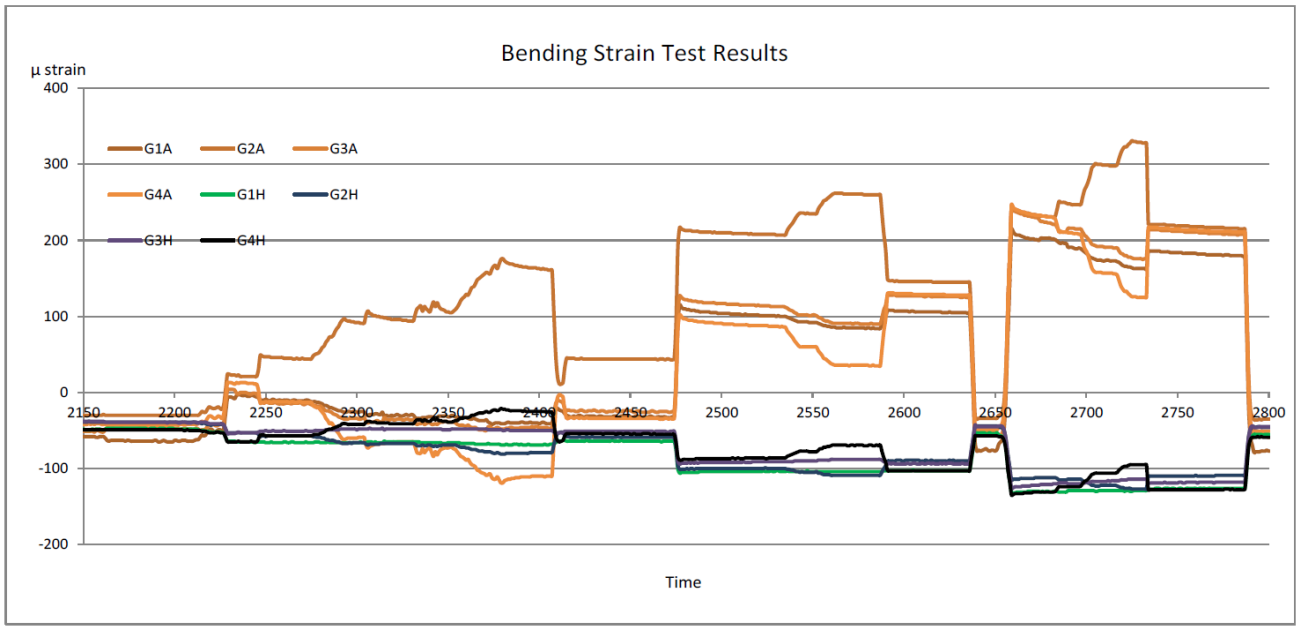

Figure B.3. Measured Axial and Circumferential Strains in Bending During Calibration Testing